ANALYSIS OF MOORING AND STEEL CATENARY RISERS SYSTEM IN ULTRA DEEPWATER

By

Umaru Muhammad Ba

A thesis submitted

in fulfilment of the requirements

for the degree of

Doctor of Philosophy

School of Marine Science and Technology

Newcastle upon Tyne

November 2011

ABSTRACT

With the gradual depletion of oil and gas resources onshore as well as shallow offshore waters, oil exploration is gradually moving deeper into the seas. One of the major means of oil exploration at such locations is by way of Floating Production Storage and offloading (FPSO) system. Because of the ever increasing depths of exploration and the prevailing harsh environmental conditions, there is a need to constantly re-evaluate or develop new methods for mooring system and riser analyses.

There are several methods available which are well tested for the analysis of systems operating in shallow to deepwater using catenary or finite element approach in both frequency and time domain. These have been reviewed and the method considered to be most relevant for the purpose of this research has been identified for further development.

Based on this a methodology a quasi-static and dynamic analyses of single and multi-component mooring and steel catenary risers system in ultra deepwater has been developed. The dynamic equations of motion were formulated based on the modified Lagrange's equation and solved using the fourth order Runge-Kutta method. Because of the dearth of experimental data at such water depth, the developed methodology for line dynamics has been validated using relevant published data for finite water depth.

These techniques are then applied to the analysis of a mooring and steel catenary risers system of an FPSO unit in 2500m of water offshore Nigeria and also the Gulf of Mexico both in the frequency and time domain. The results were found to be practical and compare reasonably very well between the two approaches.

Keywords: FPSO, Mooring system, Steel Catenary Risers, wave induced motions, frequency-domain, low frequency motion, spectral analysis, line dynamics, dynamic analysis

DEDICATION

To my family

ACKNOWLEDGEMENTS

I am thankful to my supervisor Dr Hoi-Sang Chan for his guidance and support throughout the period of the research. I must also thank Professor Atilla Incecik for inspiring the research topic and Professor R. S. Dow for all his advice.

I am grateful to the Petroleum Technology Development Fund (PTDF), Nigeria, for funding the research for the first three years.

I also thank my friends and colleagues here too many to mention, who have been very supportive throughout.

Finally, I wish to thank my mother, brothers and sister, and all my friends back home who have supported me in many ways and encouraged me particularly during my difficult moments.

CONTENTS

APPENDICES

LIST OF FIGURES

LIST OF TABLES

CHAPTER

1 INTRODUCTION AND RATIONALE

1.1. Introduction

With the gradual depletion of oil and gas resources onshore as well as in shallow offshore waters, oil exploration is gradually moving into deeper waters. One of the major means of oil exploration at such locations is by way of Floating Production Storage and Offloading (FPSO) system. In deepwater offshore Nigeria for instance, a couple of FPSOs have so far been installed while many others are under various stages of design and construction. The most recent one, Akpo, which came on stream in 2008 operates at about 1700m water depth. More are still coming and the next in line is Usan and after it Egina.

Even though there are several methods available which are well tested for the analysis of systems operating in shallow to deepwater using catenary or finite element approach in both the frequency domain and the time domain. Most of these methods currently in

use are based on research done in extremely harsh environments such as the Gulf of Mexico (GOM) and the North Sea being the pioneer areas of oil and gas exploration. Using these methods for the analysis of mooring systems and risers in ultra deepwater and benign environments such as West Africa may therefore be unrealistic.

Thus, the main objective of the present study is to develop a methodology for the analysis of mooring and steel catenary risers in ultra deepwater which can be applied for the analysis of mooring systems in benign environments. To achieve this, methodologies for the quasi-static and dynamic analyses of single and multi-component mooring and steel catenary riser systems in ultra deepwater have been developed as discussed in Chapters 2 and 4 respectively. Though some of the formulations are not entirely new, these have been enhanced and solved in a way that has not been done before. This resulted in algorithms that are both easier as well as faster to implement.

For the implementation of the methodologies developed, a FORTRAN program MOOSA has been developed which contains three modules. The first module can be used to compute mooring and SCR pretensions based on the methodology developed in Chapter 2. The second module is for computing the FPSO first and second-order motions as outlined in Chapter 3. The third module is for the mooring system analysis including line dynamics based on the methodology developed in Chapter 4.

These tools were then successfully employed for the analysis of an FPSO mooring and steel catenary riser system in 2500m deep water offshore West Africa as well as the Gulf of Mexico. The analyses were carried out real time without recourse to lookup tables of curve fitting.

1.2. Mooring

The sole purpose of a mooring system is to keep the excursions of the vessel within the allowable tolerances so that drilling or production operations can be performed effectively. These operations are primarily carried out through the risers. Station keeping is therefore a primary function of a mooring line, while the primary function of a riser is the transportation of drilling and/or production fluids. However, in addition to this primary function, risers may also contribute in damping the motions of the vessel particularly when carrying out a fully coupled analysis thereby aiding the mooring system in station keeping of the vessel.

1.2.1. Types and configurations of mooring systems

There are various types of mooring systems which include single point, turret and spread mooring systems, with the most common type being the spread system. Dynamic positioning is also used on a limited number of drilling vessels. The number, arrangement, and spacing of the mooring lines around the drilling/production vessel depends on the type and severity of the environment and the vessel's environmental resistance characteristics. In general, there are two types of mooring patterns which can be used with any particular type of vessel. First is the omni-directional attack pattern, which is arranged to take environmental loads from any attack angle (0 to 360 deg) and can be found in the North Sea and the Gulf of Alaska. This type of pattern is generally implemented using a turret system, which allows the vessel to weather vane. The second type of pattern is the uni-directional attack pattern in which there is a strong

prevailing wave direction as seen in West Africa and the Amazon River off Brazil. This latter type is commonly implemented using a spread system.

The spread mooring system is in reality quite inefficient in that less than half the mooring lines contribute to holding the vessel on location at any given time, with just about one or two of these providing most of the restoring force. In fact, if the leeward lines are not slackened during severe conditions, they actually draw the vessel off location and cause higher mooring line tensions in the windward lines. Therefore, deployment of the proper mooring pattern is a very important factor in reducing mooring line loads and keeping the vessel within desired horizontal displacement tolerances.

In the first of a series of articles Childers (1974a) discussed a number of approaches to deepwater spread mooring particularly in relation to extending mobile rigs for the challenges of deeper water explorations. The design of a spread mooring system like any other type depends on a number of factors which include, the severity of the environment, water depth, and size of vessel and its wind, current and wave resistance characteristics. In addition, the mooring system can be of single or multi-component type. The multi-component is further subdivided into three: the clump weight, the combination chain, and the wire rope-chain combination system shown in Fig. 1.1. The advantages and drawbacks of each type were also presented.

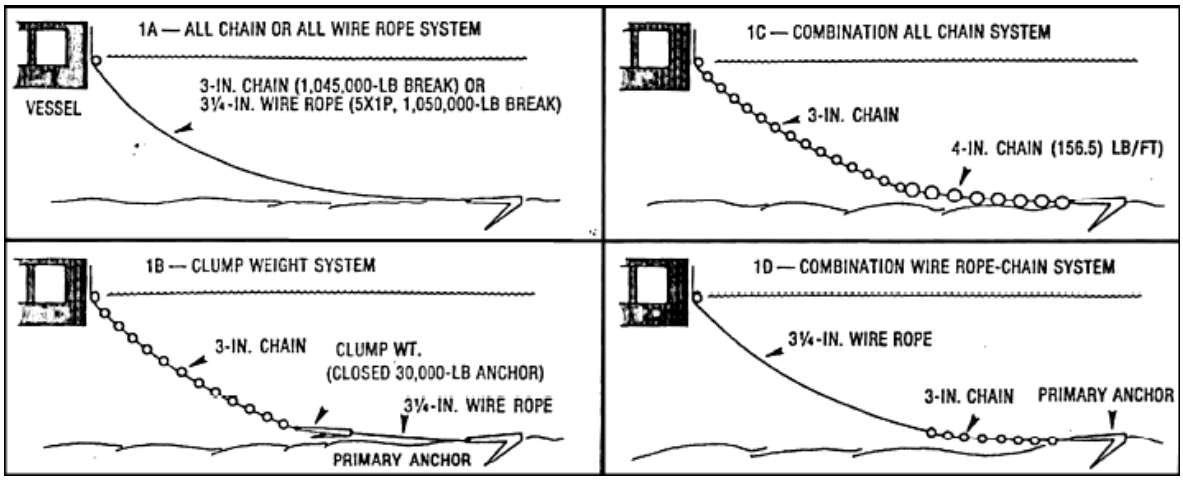

Fig. 1. 1 Mooring line combinations (Childers 1974)

1.2.2. Functional requirements of a mooring system

Typically, a mooring system consists of the mooring lines, anchors, and other equipment such as winches. Its purpose is to maintain the floating drilling or production vessel within certain horizontal excursion tolerances so that drilling or production operations can be carried out without interruption. This excursion limit during actual drilling or production operations is usually held to a maximum of 5 to 6% of water depth; however, most drilling operations are carried out within 2 to 3% of water depth. These limits are controlled by the subsea equipment such as stresses in the marine riser, angle of the lower ball joint, and the nature of the drilling/production operation. During non-operating times when the marine riser is still connected to the blowout preventer (BOP) stack, the mooring system is usually designed to maintain the drilling or production vessel within approximately 8 to 10% of water depth (Childers 1973). When the marine riser is disconnected from the BOP stack in a survival condition, the amount of excursion off the hole or position of zero offset is secondary to relieving high mooring line tensions.

1.2.3. Selection of mooring components

The selection of the appropriate mooring line component(s) depends on factors such as expected mooring line loads, water depth, handling equipment including anchor handling boat in the case of drilling rigs, economics, and storage facilities. The size, strength, and length of the lines also depend upon the size and shape of the vessel, the working water depth, the expected environmental loading conditions, and the allowable horizontal vessel displacement as controlled by the subsea drilling or production equipment.

In general, for a given breaking strength, wire rope provides more restoring force than chain, particularly in water depth of 457m or over (Childers 1973). In addition, wire rope, particularly the spiral strand type commonly employed for floating production system also has greater longitudinal stiffness, torque balance, lower spinning, and ability to be coated in a polyethylene sheath which makes it more suitable for long term installation (Barltrop, 1998). However, chain has shown its durability and versatility in such operations as the Gulf of Mexico where chain life exceeds ten years. Unfortunately, in rough environments such as the North Sea, the chain life is just three to four years due to fatigue (Childers 1973).

In a series of four articles Childers (1973, 1974a, 1974b, 1975) showed that the spread mooring system consisting of several lines with the combination of wire rope and chain as shown in Figure 1.1-1D has a net superiority with substantial station keeping capability even in ultra deepwater (say more than 1219m). He further observed that its water depth capability is probably only limited by economy than station keeping.

The two-component mooring line has an unusual tension-displacement curve (Childers 1974b). When the chain lies on the sea bottom, the line acts primarily like an all wire rope mooring line. The curve has a transition zone when part of the chain is on the sea bed, but it begins to show high strength to weight ratio when the line acts truly like a two-component line. Some of the outstanding capabilities of the system are:

- It has lower pretensions (approximately two-third to one-half) than an all chain system for a required stiffness. This results in much lower operating mooring line tensions even in deep and ultra deepwater with correspondingly longer mooring line life.
- It requires considerably less manual line manipulation for reducing mooring line tensions and maintaining vessel location than does a corresponding all chain system.
- For mobile systems, it requires considerably less anchor handling power (for mobile systems) to deploy than a corresponding all chain system.
- As far as station keeping capability is concerned, it has considerable capability in relation to any known dynamic positioned vessel.

The function of the two-component line is to reduce the catenary length so that the mooring line becomes tangent to the ocean floor at or before the anchor with the maximum anticipated mooring line tension. Thus, the minimum chain size is determined to match the breaking strength of the wire rope. Analysis of the catenary equations show that line tension decreases slightly as the catenary shape moves away from the rig or mean position of the FPSO.

1.2.4. Mooring system pretension

The mooring system pretension should be designed so that no more than a third of the rated breaking strength is reached at a displacement of 5% to 6% water depth off the well bore Childers (1974b) or the mean position of the FPSO. Pretension is defined as the tension in mooring line at zero offset and no environmental loading on the vessel. An equal pretension in all lines is somewhat idealistic since it seldom occurs on location. However, for optimum station keeping, as well as maximum mooring line longevity, the values of the pretensions designed for a specific mooring system should be strived for and maintained.

1.2.5. Anchoring systems

Anchors are another important component of a mooring system and they are of various types. In mobile drilling units, the most commonly used anchors are designated dynamic anchors because they increase their holding power with horizontal pull provided there is no uplifting force. There are basically three types of dynamic anchors: the light weight type, the Stato and the Danforth. Anchor holding power is a function of many parameters such as anchor mass, soil composition, and fluke area and angle. Tests on dynamic anchors have shown that once the line of pull is over 6 deg with the horizontal sea bottom, the holding power starts to decrease rapidly, and after 12 deg., holding power is greatly affected. Hence, enough mooring line length must be deployed such that at maximum design tension the mooring line becomes tangent to the seabed at or just before the anchor (Childers 1974b). For FPSOs the fixed anchoring system is normally used and this is achieved through piles. For this type of anchorage, shorter

mooring lines can be deployed as any uplift force will be absorbed by the piles through skin friction or suction.

1.3. Steel Catenary Risers (SCR)

Conventionally, risers are of rigid or flexible types which are connected to the vessel through jumpers. However, more and more SCRs are now being deployed particularly in deep water. SCRs offer a low cost alternative to conventionally used rigid and flexible risers on floating platforms because they can be suspended in longer lengths, eliminating the need for mid-depth arches or buoys. SCRs are cheaper alternatives and can be used at pressures, temperatures and diameters which cannot be achieved by flexible pipes, allowing use of a smaller number of larger diameter lines. Furthermore, steel pipes are more adaptable for design purposes and are more readily available than flexible pipes (Hugh 1995).

The first SCRs were 12 inch export SCRs installed in 1994 on the Auger tension leg platform (TLP) in Garden Bank block 426 in 2860’ water depth. Since then, SCRs have been widely used around the world in various water depths for both production and export. Depending on operating water depth, type of vessel, product properties and the environment, typical SCR design challenges include: fatigue, strength, clashing with other installations, coating and cathodic protection, thermal insulation and interface with the floater. The SCR cross section configuration is generally determined based on flow assurance requirements and can be either a single pipe with or without external

coating or, a pipe-in-pipe (PIP) arrangement where a smaller pipe is fitted into a larger pipe with sufficient insulation clearance (Mansour et.al 2007).

When risers are modelled as SCRs they are assumed to behave like common catenaries, which is quite a reasonable assumption especially in ultra deepwater where the riser diameter is very small compared to its length. In that case the SCRs are then modelled and analysed in the same way as the mooring lines either as single or multi-component to accommodate changes in diameter or buoyancy modules. The axial and bending stresses in the riser especially at or close to the touchdown point are then calculated from relevant catenary equations. The equation of curvature, as a function of the horizontal tension, Young's modulus, distance from neutral axis to extreme fibres, and the hang-off angle is then applied to calculate the bending stress.

1.4. Criteria for Deepwater Mooring System and SCR Analyses

Mooring and riser system analysis is a complex subject due to inherent material and geometrical nonlinearities. This is further complicated by the ever increasing operating depths of the moored platforms which directly affect the number, size, length and footprint of mooring cables, thereby complicating handling operations and increasing cost. Effective station keeping therefore requires among other things, the ability to strike a balance between cost, handling and size of footprint in order to minimise interference such as clashing with neighbouring installations.

This requires the choice of an appropriate mooring system pattern (turret or spread, equally spaced or grouped) and line configuration (single or multi-component), riser type and configuration (rigid, flexible or steel catenary), depending on; the environment such as directionality and severity, vessel characteristics such as type, size and shape, water depth, and product type for risers. For ultra deepwater, multi-component mooring lines and steel catenary risers are generally employed. Also required is a good analysis methodology which can account for wave frequency and low frequency second-order motion of the FPSO, coupling between its motion and those of mooring/risers, and the geometrical as well as drag nonlinearities. Similarly, the chosen methodology should also combine speed and accuracy of results in order to be effective. In ultra deepwater, line (mooring and SCR) dynamics is quite important, therefore fully coupled time-domain analysis should be aimed for particularly in the final stages of the riser/mooring system design.

Furthermore, fatigue assessment for both mooring and SCR lines is equally important for ultra deepwater systems. Fatigue sources include: first and second-order vessel motions due to wave and wind loading, line motions due to direct wave loading, vortex induced vibration (VIV) of risers due to current loading, thermal and pressure induced stresses, and residual stresses due to fabrication and installation loads, etc. Fatigue prone areas of the SCRs are mostly the touchdown section, the topmost section close to the flex joint and other joints and connections in between. In calculating the damage along the length of the SCR, input from all the sources mentioned above should be considered. The fatigue life calculations should take into account all the relevant uncertainties associated with it such as, the statistical distribution of the S-N curve, eccentricities induced during

welding, modelling errors leading to errors in stress calculations, uncertainties in the cumulative damage calculation using Miner's rule.

1.5. Approach to Analysis

In the analysis and design of mooring systems, it is first necessary to determine the environment conditions to which the FPSO and mooring system must be subjected. Field experience has shown that the maximum working load of a chain is approximately one-third of its breaking strength or approximately half of its proof load which are approximately the same (Childers 1973).

The next step is to determine the mooring pattern in order to select the type, size and number of mooring lines and then analyse the line tensions and restoring forces of the system. There are two classes of forces which the system must resist;

1. Steady forces such as current, wind, and wave drift
2. Dynamic loads induced by the FPSO motions in surge, sway, heave, roll, pitch, and yaw modes. For mooring systems, surge, sway and yaw motion are usually more important than the other three.

One of the critical aspects of the analytical model of a mooring line is the inclusion of the hydrodynamic loading acting on it. A review of the various modelling methods and their capabilities particularly for two-dimensional steady-state and dynamic analysis of cable systems has been carried out by Casarella and Parsons (1970). They observed that the effectiveness of two-dimensional steady-state analysis of cable systems depends on the validity of the hydrodynamic force model with respect to full-scale test data and the

accurate modelling of boundary conditions. The effectiveness of the dynamic model on the other hand, will be affected by the coupled vessel-mooring line motions due to random wave excitations which are an extremely important practical problem in towing, buoy and mooring application.

There are basically three different approaches to analysis usually adopted; the frequency domain, the time domain and the hybrid method which is a combination of the frequency and time domain approaches. The fundamentals of these approaches are briefly discussed below.

1.5.1. The Frequency Domain

The frequency domain approach which is inherently linear (Barltrop, 1998 and Law and Langley, 2006) is both simple and efficient, and the formulation as well as interpretation of the response process is easy in relation to the time domain. The statistics associated with frequency domain are based on the established principle that Gaussian input produces Gaussian output (Barltrop, 1998 and Price and Bishop, 1975). Hence all the statistical properties of the response process can be derived from the response spectrum. In addition, if the response is both Gaussian and narrow banded then Rayleigh statistics may be applied to the response spectrum. Therefore, since it is generally accepted that the random sea is a zero mean Gaussian process characterised by the associated energy spectrum which can be obtained directly from the incident wave spectrum and the RAO, frequency domain approach can be used for the analysis of offshore structures such as FPSO and its mooring system. The frequency domain method

is described in great detail in Barltrop and Adams (1991), DNV (1996) and Barltrop (1998).

To apply frequency domain to the solution of a nonlinear process such as hydrodynamic analysis, all nonlinearities such as geometric nonlinearities arising from large deflection and drag forces in Morison's equation must be linearized. This can be achieved either locally about an appropriate mean position or by separating the nonlinear effects into different orders. The first type is usually applied in treating nonlinearities in mooring system, while the second is applicable in treating nonlinearities associated with wave forces. It is important to check the validity of the linearization in a chain of dynamic systems such as waves, wave loading and structural response to ensure the validity of the analysis (Barltrop, 1998).

Geometric nonlinearities in mooring and steel catenary riser lines can be linearized by calculating the stiffness tangential to the line at equilibrium position which allow for large static deflections but assume that the dynamic deflections around the static position are small enough to be neglected. In ultradeep water, the motions of the vessel compared to the dimensions of the lines can be quite small, hence this type of nonlinearity can be assumed to be negligible.

On the other hand, the drag force which normally depends on the square of the relative velocity can be linearized by replacing the full vector form by an approximate one in which the drag is computed in two orthogonal directions normal to the line. Details of this type of linearization can be found in Law and Langley (2006). In addition to these,

linear wave theory and the use of small amplitude waves can be considered in order to avoid nonlinear immersion as suggested by Barltrop (1998).

1.5.2. The Time Domain

Although the frequency domain approach is predominantly used for the dynamic analysis of floating structures, there are cases where a time domain solution is necessary (Barltrop, 1998) or even desirable. The comparison of the two approaches is shown in Table 1.1. Time domain approach (also known as time history) analysis is desirable because of its resemblance to what is physical and real. The appeal to time domain lies mainly in its ability to accommodate the complications of a dynamic system beyond what frequency domain can handle, such as nonlinear effects due to quadratic damping, drag, nonlinear mooring stiffness, Barltrop (1998).

Since the sea environment is a random and non-stationary real process, it is also both nonlinear and non-Gaussian, this means that the principle of superposition by which regular wave solutions are combined to represent the random sea does not apply. This is because the coefficients of interest in the equation of motion are no longer constant throughout the duration of interest as is the assumption in frequency domain. In time domain, such coefficients must be calculated at each time stem. This will however involve lengthy numerical calculations at each time step and also make the interpretation of the results difficult. Furthermore, each solution represents only a realisation of just one response of the process. Therefore, reliable estimates of the extreme values can only be achieved with a number of runs. In addition, care must be

taken to adequately represent statistical properties such as the significant wave height, zero crossing periods and other characteristics like wave grouping. The solution time step as well as integration algorithms must be carefully selected to enhance computational efficiency, numerical stability and convergence. Typical step size to achieve this is usually in the range of $1/20^{th}$ to 18^{th} of the shortest natural period or loading period of the system (Barltrop, 1998). The wave exciting period for an FPSO is of the order of 3 seconds and the horizontal motion periods are of the order of 100 seconds. Therefore typical time steps required for motion analysis in waves is around 10,000 depending on the level of accuracy required.

Table 1. 1 Comparison of frequency and time domain methods (Barltrop, 1998)

Frequency Domain Methods	Time Domain Methods
Assumptions:	
Linear or quadratic dynamic system	Linear or non-linear dynamic system
Stationary process	Stationary or non-stationary process
Gaussian process	Gaussian or non-Gaussian processes
Results from:	
Mean, standard deviation, zero crossing period and probability density function	Sampling of the random process time history

1.5.3. The Third Alternative

An alternative to a full time domain approach can however be achieved by adopting a frequency domain solution for a series of time interval or snapshots each representing a stationary phase within the duration of interest (Barltrop, 1998).

1.6. State-of-Art Review

Mooring lines and SCRs are generally treated as cable structures. The analysis of cable structures has been of interest for a very long time such that investigators had begun to consider the dynamic response of a cable system since the early fifties. At the time, research was concerned mostly with the violent motion of towed speed measuring bodies in air and the effects of surface motion on ocean moorings. Since then, the rapid growth of ocean and offshore engineering applications has led to further development of steady-state dynamic cable system analysis methods (Casarella and Parsons 1970). Most recent application relate to the use of multi-component mooring systems in ultra deepwater to secure FPSOs as oil and gas exploration moves deeper into the seas. These applications require the ability to accurately predict the static and dynamic forces in the cable system resulting from loads imposed by gravity, current, and waves (Berteaux 1970) to insure that a cost effective cable system with adequate strength of minimum size and weight is achieved. Several techniques and methodologies have as a result, been developed over the years to achieve this.

In reviewing the literature one finds a great variety of approaches used for the analysis of cable and cable like systems such as mooring lines and risers. A number of numerical modelling and analysis tools ranging from the catenary shape formulations to the finite element method (FEM) have been introduced. For cable structures having small displacements and a well defined geometry such as guyed towers or suspension bridges, it is common to replace the cables by a series of short truss links and apply nonlinear finite element programs developed for solid structures to determine their tension displacement characteristics. However, for other types of cable structures such as

mooring lines, catenary formulations are often applied to first obtain their static configurations before using either the FEM or the lumped mass method (LMM) to determine their final tension displacement characteristics. Most of the literature reviewed fall into either of these with only a few exceptions as discussed in the following paragraphs.

Skop and O'hara (1970) presented a method of imaginary reactions which is globally convergent for the analysis of loaded cable array. The technique does not require the evaluation of derivatives and converges rapidly. There are two drawbacks to this method; the first is the requirement that the user makes a reasonable engineering guess as to the components of reaction at the redundant anchor, and the second is the requirement that there are no internal loops or cable segments with zero tension condition. Therefore, this method, like the FEM is more suitable to structures with small displacements and having a well defined geometry before the start of the analysis.

Mooring lines and risers are subject to displacements of the same order of magnitude as the size of the structures themselves and their configurations are not known before the start of the analysis. Usually a static analysis is conducted to find the static equilibrium configuration before carrying out a quasi-static or dynamic analysis. The dynamic analysis can be complicated by the occurrence of singular behaviour such as line snapping and slacking. For these types of structures the numerical method developed by Pevrot and Goulois (1979) may be more appropriate, since from given loads and positions of the ends of a cable, the program can determine the complete geometry of the cable, its end forces, and its tangent stiffness matrix.

An analysis tool to determine the static stiffness characteristics of a multi-component cable including a clump weight and the effects of line stretch was developed by Ansari (1980) using catenary equations. He went further to discuss in detail the various mooring line components available for use. His methodology addresses the dynamics of the mooring system in a static manner ignoring line inertia. This is valid only on the assumption that the response of the moored vessel is normally outside the frequency range of the mooring lines.

Van den Boom (1985) presented a lumped mass method (LMM) for the dynamic analysis of mooring lines. The mathematical model used was a modification of the lumped mass method by Nakajima et al (1982). Results from the study show the importance of dynamic analysis for various mooring configurations and how dynamic tension amplification is strongly influenced by geometrical, material and drag nonlinearities.

Khan and Ansari (1986) derived the equations of motion including the allowance for anchor motion for a multi-component mooring line using the modified Lagrange's equation. They also presented a numerical solution for different mooring configurations that can occur using the static configuration obtained from the catenary equations (Ansari 1980) as the starting point. The whole mass of the vessel as well as half of the mass of the topmost segment of the line was lumped at the attachment point of one line. This can create problems in the analysis since in practice the vessel is connected to several mooring lines from different directions. In addition only external force due to current drag was considered on both line and vessel which will lead to underestimating the exciting force on the vessel.

Hugh (1995) reviewed the advances in steel catenary risers design and concluded that steel catenaries offer economical design configurations for flowline/platform interfaces across a broad spectrum of platform types and environmental conditions. He argued that catenaries can be used as an alternative to conventional arrangements for both rigid and flexible pipes to predict response satisfactorily, provided that sufficient care is taken in the modelling and analysis. He further noted that in difficult conditions, such as high temperature and high pressure applications, steel catenaries possibly offer the only viable design solution available.

Barltrop (1998) co-authored a two volume guide for the design and analysis of floating structures which is an excellent reference for practical design and analysis mooring systems for both rigs and floating production systems.

Ormberg and Larsen (1998) presented a finite element (FE) model for the coupled motion analysis of a turret-moored ship operating in 150m, 330m and 2000m water depths. The results showed that the traditional uncoupled approach may be severely inaccurate, especially for floating structures operating in deep waters.

Huang (2000) discussed in detail the mooring system design considerations for FPSOs from the designer's point of view. These include the selection of vessel size, design pretension, turret location, mooring pattern, line configuration and anchoring point.

Chaudhury (2001) developed a methodology in the form of a Fortran computer program, NICDAF to perform non-linear integrated coupled dynamic analysis of SCRs

and pointed out that motion analysis results from NICDAF showed excellent agreement on the motions of a platform and mean line tension when compared to results obtained from a rigorous and fully coupled analysis performed in ABAQUS. However, dynamic amplitudes of tensions based on full dynamic equilibrium were not in good agreement, with the NICDAF solution being considerably higher compared to those predicted by ABAQUS.

Chai et al. (2002) presented a three-dimensional Lump-Mass formulation of a catenary riser capable of handling irregular seabed interaction with bending and torsional stiffness. The formulation permits static and dynamic analyses of a wide range of offshore-related slender structure systems such as mooring cables, rigid and flexible risers as well as submarine pipelines.

Hogg et al. (2004) presented a design methodology for a combined riser mooring (CRM) system for application in deepwater developments offshore of West Africa. They found that CRM offers significant benefits over the independent riser and mooring systems, such as reduced riser dynamics, reduced vessel offsets, a smaller seafloor footprint, and system installation prior to the arrival of the FPSO. In this system the mooring lines are attached to the stern and the SCRs are connected to a subsea buoy with flexible jumpers located between the buoy and the vessel at the bow. The risers of the CRM are analyzed using the finite element program, Flexcom-3D from MCS International, and the mooring of the full system is analyzed using the mooring analysis program, Ariane from Bureau Veritas.

Braskoro et.al (2004) discussed a number of issues which need to be taken into account in the design of pipelines in deepwater such as external pressure, material grade, fatigue, geo-hazards and design code selection. They observed that because of the large unsupported pipe section between the touchdown point and the last support on the vessel both in length and time, a quasi static approach to the solution for maximum stress during installation is no longer valid and a dynamic installation analysis is therefore required.

Garrett (2005) demonstrated that most of the available mooring system analysis tools are limited to the time domain procedure, with the exception of RAMS and COSMOS, which have the ability to solve coupled problems by either time domain or the frequency domain methods.

Kim et al (2005) have also developed a vessel/mooring/riser coupled dynamic analysis program in the time domain for the global motion simulation of a turret-moored, tanker based FPSO designed for 6000-ft (1829m) water depth.

Low and Langley (2006a, 2006b, 2007) compared time domain and frequency domain methods for the coupled dynamic analysis of a floating vessel-mooring-riser system using the rigorous fully coupled time domain analysis as a benchmark for accuracy. They observed that the highly efficient approach of frequency domain coupled analysis can provide highly accurate response predictions for an ultra-deepwater floating system because of the minimal geometric nonlinearity displayed by the mooring lines in deepwater. The method was however found to be less accurate for intermediate water depths where the geometric nonlinearity of the moorings/risers is significant.

A review of the state-of-the-art in coupled analysis was also presented in Tahar and Kim (2003) and Ormberg et al. (2005). Other references on the numerical modelling and analysis of floating production system include Garrett (1982), Garrett et al (2002), Wichers and Devlin (2001), and Jun-Bumn et al (2007).

Chan and Ha (2008) employed a frequency-domain method and a fast time-domain technique to estimate wave-induced extreme excursions and the resulting tensions on the mooring lines due to both the first-order and second-order motions. The calculated results of wave frequency and low frequency motions of the FPSO and the corresponding maximum line tensions by the two methods were compared and discussed. Based on the assumption that the response of the moored vessel is normally outside the frequency range of the mooring lines, the method did not include line dynamics.

Liang (2009) reviewed recent research on interaction between deepwater catenary risers and soft clay seabed including STRIDE (steel risers in deepwater environments), CARISIMA (catenary riser soil interaction model for global riser analysis) and information from published papers. He found that current development of SCR technology has been focused on better understanding of the touch-down-point (TDP) and the SCR interaction with the seabed. This involves a lot of complexities such as nonlinear soil behaviour, soil yielding and softening under cyclic loading, variable trenching width and depth, wide range of riser displacement amplitudes and conditions where the riser completely pulls out of contact with soil.

In almost all the reviewed literature, the analysis and design methodology was concentrated on the oil producing areas with severe environmental conditions such as the Gulf of Mexico, the North Sea, the West of Shetland Islands, the South China Sea, and to a lesser extent offshore Brazil as seen in Connaire et al.(1999) and Huang (2000). The water depth too has been limited to shallow and deep water development. Not much was found to have been done on the benign waters of West Africa despite the percentage of world crude located in the area or areas of water depths in the region of 2500m and above.

In this thesis numerical modelling and analysis techniques were developed in a compact form suitable for the static and dynamic analysis of multi-component mooring systems and steel catenary risers in any water depth and for any pattern. The approach used by Ansari and Khan (1986) together with the practical design considerations suggested by Childers has been adopted with relevant modifications where appropriate. Some of these modifications include the provision for any number of clump weights up to the number of mooring line components. A FORTRAN program incorporating these modifications has been developed to implement the numerical techniques and applied to the analysis of a mooring system in 2500m water depth offshore Nigeria and the Gulf of Mexico as case studies.

1.7. Aims and Objectives

The aim of this research is to investigate the static and dynamic behaviour of a FPSO/ riser/ mooring system operating in ultra deepwater offshore West Africa. The objectives include;

1. To develop suitable analysis methodologies taking into account the interactions between risers, mooring lines and the FPSO system in terms of the following:
    i. non-linear geometric and drag damping effects on steel catenary risers and mooring lines
    ii. Effects of non-linear second-order difference frequency wave force on FPSO motions
    iii. Steel catenary risers and mooring lines end conditions
2. To develop suitable analysis tools for the analysis of a mooring system operating in ultra deepwater.
3. To compare analysis results obtained in frequency and time domain with and without line dynamics

1.8. Layout of Thesis

The thesis is divided into seven chapters including reference and bibliography. Chapter 1 is the introduction to the research area giving the background, rationale and the objectives as well as expected outcome from it.

Static mooring system and steel catenary riser (SCR) analysis methodology is covered in Chapter 2 along with validation.

In Chapter 3 the implementation of the methodology developed in Chapter 2 for the analysis of a multi-component mooring and SCR in both frequency and time domain is presented.

Chapter 4 presents the dynamic analysis methodology for multi-component mooring and SCR systems using the modified Lagrange's equation validated using experimental and numerical results from Nakajima et al (1982).

Chapter 5 presents the conclusions reached and recommendations for future work.

CHAPTER

2 RISER/MOORING SYSTEM STATIC ANALYSIS METHODOLOGY

2.1. Introduction

In order to successfully analyse a mooring system, suitable mathematical and numerical techniques are required to assess its integrity and station-keeping capability. Mooring analysis may be performed by means of a static, quasi-static or dynamic approach either in frequency or time domain. When the motion responses of a moored vessel are outside the wave exciting frequency range of the mooring system, the dynamic behaviour of the lines is negligible. Hence, the mooring lines will only respond statically to the motions of the vessel. The static method applies the total steady environmental force due to wind and current to the load-excursion curve of the mooring system in order to find the static offset of the vessel. The resultant of the static and dynamic offset

caused by the first-order and second-order waves on the line-excursion curve of the most loaded line is then used to find the corresponding maximum tension. The dynamic offset may be estimated statically from coarse estimation of wave forces and the system stiffness. Irrespective of the type of analysis and approach however, it is necessary to first and foremost determine the load-excursion characteristics of the mooring system at the initial static configuration. The initial horizontal tensions and stiffness of the lines are then used as inputs to determine the motion response of the vessel. The initial static configuration also provides the starting values for the dynamic analysis parameters.

The evaluation of environmental loads on a FPSO due to steady wind and current are covered in Section 2.2. The formulae for the calculations of the mooring lines' horizontal tensions and restoring forces at the initial static equilibrium are derived in Section 2.3. The analysis methodology is covered in Section 2.4. The validation of the methodology is covered in Section 2.6. Section 2.7 concerns the evaluation of horizontal tensions and restoring forces due to steel catenary risers on the system. The implementation of the methods developed in sections 2.3 and 2.7 for the analysis of a multi-component mooring and steel catenary riser system in ultra deepwater for both frequency and time domain without line dynamics is the subject of Chapter 3.

2.2. Current and Wind Loads on FPSO Structures

2.2.1. Current loads

Current loads on ships and FPSOs are usually calculated using empirical formulae. For a moored FPSO, the current loads induce principally surge and sway forces, and yaw moment on her hull structure.

The surge current force F_1^c is the drag force in the longitudinal direction and is mainly due to friction. The force can be estimated using the procedures normally followed for estimating ship resistance in still water, since the Froude number $Fn = U_c \big/ (Lg)^{\frac{1}{2}}$ is so small that wave resistance can be totally neglected relative to viscous resistance (Faltinsen 1990).

$$F_1^c = \frac{1}{2}\rho S U_c^2 C_F \cos\beta|\cos\beta| \qquad (2.1)$$

where ρ is the density of the water

S is the wetted surface area of the FPSO

β is the angle between current velocity and the longitudinal axis of the FPSO

C_F is the skin friction coefficient (ITTC 1957), $C_F = \dfrac{0.075}{(\log_{10} Rn - 2)^2}$

Rn is the Reynolds's number given by, $Rn = \dfrac{U_c L|\cos\beta|}{\nu}$

ν is the kinematic viscosity of water; $\nu = 1.19 \cdot 10^{-6} m^2 s^{-1}$ in $15^0 C$ water temperature

L is the length of the ship

U_c is the current velocity

The sway current force, F_2^c in the transverse direction is obtained by integrating the drag force on a cross-section over the whole length of the FPSO using the principle of cross-flow and is given by.

$$F_2^c = \frac{1}{2}\rho U_c^2 \sin\beta|\sin\beta|\left[\int_L C_D(x)D(x)dx\right] \tag{2.2}$$

where $C_D(x)$ is the drag coefficient for the cross-flow past an infinitely long cylinder with the cross-sectional area of the FPSO at the longitudinal coordinate x and $D(x)$ is the sectional draught.

The yaw moment due to current, F_6^c is given by the sum of the Munk moment and the viscous yaw moment due to cross-flow as shown below (Faltinsen 1990).

$$F_6^c = \frac{1}{2}\rho U_c^2 \sin\beta|\sin\beta|\left[\int_L C_D(x)D(x)xdx\right] + \underbrace{\frac{1}{2}U_c^2(A_{22}-A_{11})\sin 2\beta}_{Munk\ moment} \tag{2.3}$$

where A_{11} *and* A_{22} are, the added mass in surge and sway directions respectively.

The Munk moment can be derived from non-separated potential theory and is valid for any body shape.

2.2.2. Wind loads

Wind loads on FPSOs can also be estimated in a similar manner as the current loads using empirical or experimental data. The following formulae can be used to determine the steady mean wind loads F_1^w and F_2^w in x and y directions respectively on an FPSO

structure. The wind forces can also be estimated using the OCIMF second edition (1994) approach as

$$F_1^w = \frac{1}{2}\rho_{air} C_{XW} A_T V_Z^{\ 2}$$

$$F_2^w = \frac{1}{2}\rho_{air} C_{YW} A_L V_Z^{\ 2} \quad (2.4)$$

$$F_6^W = \frac{1}{2}\rho_{air} C_{XYW} A_L V_Z^{\ 2} L_{pp} \quad (2.5)$$

where ρ_{air} is the air density; $1.23 \cdot 10^{-3} t \cdot m^{-3}$ in $15^0 C$ air temperature

C_{XW} , C_{YW} , C_{XYW} are the lateral, longitudinal and yaw moment coefficients which varies with type of vessel

A_T and A_L are the exposed projected areas in m^2 in x and y direction

V_Z is the undisturbed mean hourly wind speed in $m \cdot s^{-1}$ at the force centre

$$V_Z = V_{Z_R}\left(\frac{Z}{Z_R}\right)^{0.125}$$

where Z is the height of force centre above the reference surface

Z_R is the reference height

V_{Z_R} is the wind velocity at the reference height

β is the angle between x-axis of the FPSO and the wind direction

where A_{p_L} is the exposed longitudinal projected area of the FPSO

L_{pp} is the length between perpendiculars

2.3. Derivation of the Multi-component Mooring Line Equations

Fig. 2.1 below shows a typical multi-component mooring line connecting a vessel at the attachment point $n+1$ to the anchor/pilehead at point 1 on the seabed. The line between points 1 and $n+1$ is suspended in the X, Z plane. The coordinate system XZ is chosen such that the origin O is at the free water surface and directly above point 1 on the seabed.

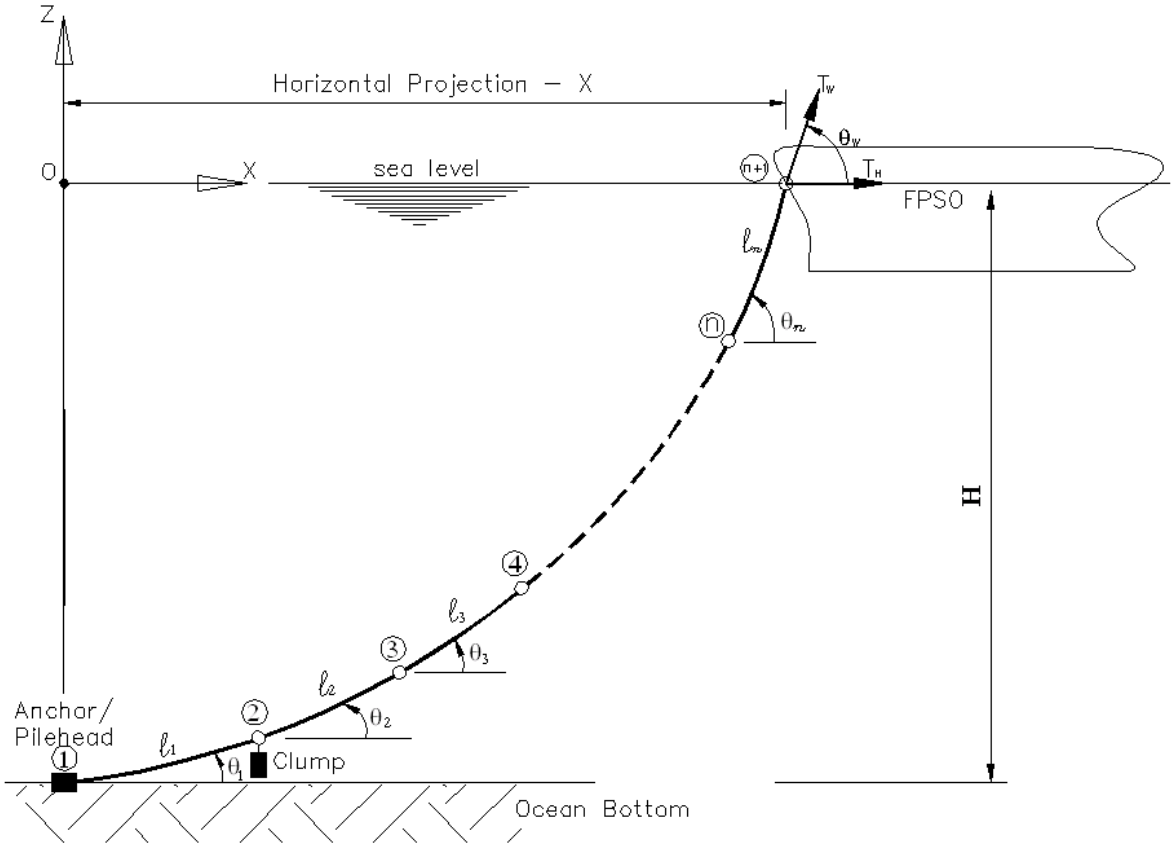

Fig. 2. 1 A typical multi-component mooring line

Fig. 2.2a shows the ith component of the mooring line having a cross-sectional area A_x and elastic modulus E. The tension, T in the line component at any arbitrary point $P(x, z)$ along its length a distance s from the lower end acts at an angle θ to the

horizontal (Chakrabarti 1990). Now consider a small element of this component having a length, ds from P as shown in Fig. 2.2b, the forces acting on the element are;

1. Its own weight $w' = w - \rho g A_x$ per unit length in water. w is the unit weight of the element in air and $\rho g A_x$ is it's buoyancy in water.
2. Mean hydrodynamic forces, $D \text{and} F$ per unit length in the normal and tangential direction respectively
3. The tension, T in the line

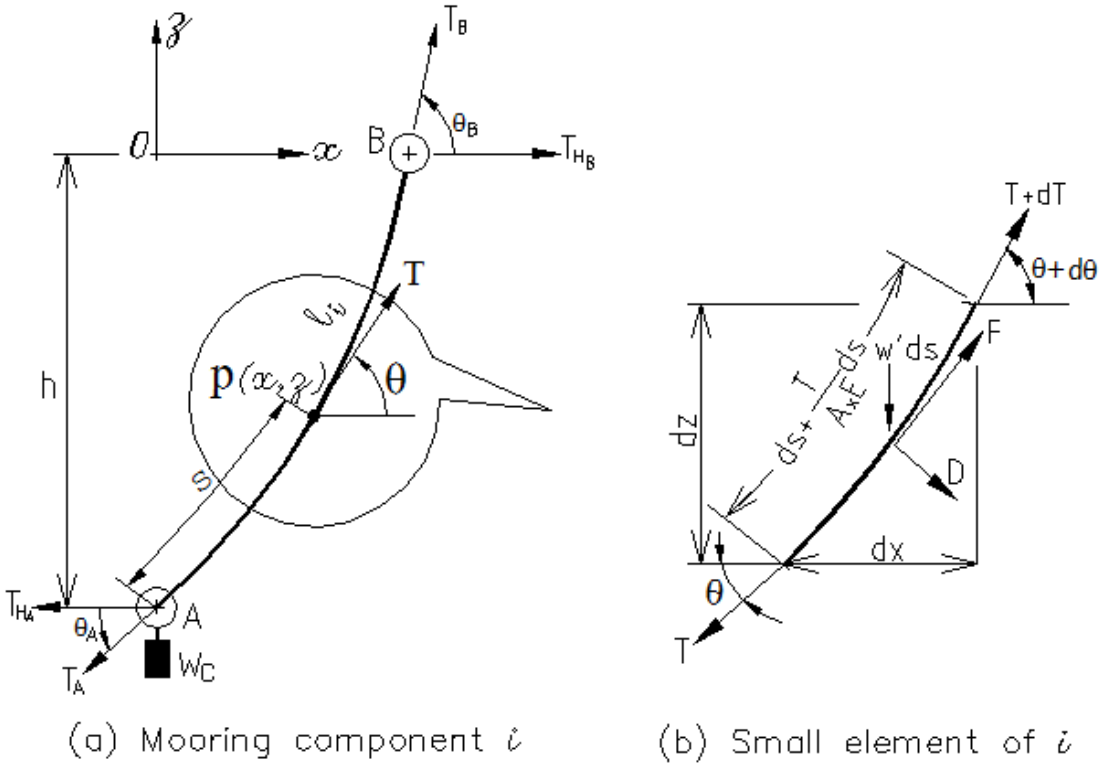

Fig. 2. 2 Forces acting on an element of a uniform mooring line component

Taking equilibrium of forces normal and tangential to the small element, ds gives

$$\sum F_T = 0 : -T + F\left(1 + \frac{T}{A_x E}\right)ds - w'ds\sin\theta + T\cos d\theta + dT\cos d\theta = 0 \qquad (2.6)$$

$$\sum F_N = 0 : -D\left(1+\frac{T}{A_x E}\right)ds - w'ds\cos\theta + T\sin d\theta + dT\sin d\theta = 0$$

For a very small element ds, $d\theta$ is correspondingly small, hence $\cos d\theta = 1 \; and \; \sin d\theta \approx d\theta$. Furthermore, the product, $dTd\theta$ is negligible compared to the rest of the terms. Therefore, the above equations reduce to

$$dT = \left[w'\sin\theta - F\left(1+\frac{T}{A_x E}\right)\right]ds \tag{2.7}$$

$$Td\theta = \left[w'\cos\theta + D\left(1+\frac{T}{A_x E}\right)\right]ds \tag{2.8}$$

Eq. 2.7 and 2.8 are nonlinear and it is in general not possible to find an explicit solution. However, for many operations it is good approximation to neglect the effect of the current forces, $F \; and \; D$, (Faltinsen 1990).

2.3.1. General catenary equations for inelastic mooring line

In normal conditions, the catenary line can be assumed to be inelastic, so that Eqns. 2.7 and 2.8 become

$$dT = w'\sin\theta ds \tag{2.9}$$

$$Td\theta = w'\cos\theta ds \tag{2.10}$$

Dividing Eq. 2.9 by Eq. 2.10 gives

$$\frac{dT}{T} = \tan\theta\, d\theta \tag{2.11}$$

$$\int_{T_A}^{T} T^{-1} dT = \int_{\theta_A}^{\theta} \tan\theta d\theta$$

$$\ln T \Big|_{T_A}^{T} = \ln\left|\sec\theta\right| \Big|_{\theta_A}^{\theta}$$

$$\ln T - \ln T_A = \ln\left|\sec\theta\right| - \ln\left|\sec\theta_A\right|$$

$$\ln\frac{T}{T_A} = \ln\left|\frac{\sec\theta}{\sec\theta_A}\right|$$

$$\frac{T}{T_A} = \frac{\sec\theta}{\sec\theta_A}$$

Therefore,

$$T = \frac{T_A \cdot \cos\theta_A}{\cos\theta} \tag{2.12}$$

Putting Eq. 2.12 into Eq. 2.10 and making ds the subject of formula gives,

$$ds = \frac{T}{w'\cos\theta}d\theta$$

$$ds = \frac{T_A}{w'}\cdot\frac{\cos\theta_A}{\cos^2\theta}d\theta \tag{2.13}$$

$$\int_{s_A}^{s} ds = \frac{T_A}{w'}\cos\theta_A \int_{\theta_A}^{\theta} \sec^2\theta d\theta$$

$$s - s_A = \frac{T_A}{w'}\cos\theta_A \cdot \left[\tan\theta - \tan\theta_A\right]$$

At the lower point, A of the mooring component, the following boundary conditions apply;

$x_A = 0,\ s_A = 0$ *and* $z_A = -h$

Therefore,

$$s = \frac{T_A}{w'}\cdot\cos\theta_A\left[\tan\theta - \tan\theta_A\right] \tag{2.14}$$

Substituting $\cos\theta ds = dx$ into Eq. 2.13 for *ds* results in

$$dx = \frac{T_A}{w'}\cdot\frac{\cos\theta_A}{\cos\theta}d\theta$$

$$\int_{x_A}^{x} dx = \frac{T_A}{w'}\cos\theta_A \int_{\theta_A}^{\theta} \sec\theta d\theta$$

$$x - x_A = \frac{T_A}{w'}\cos\theta_A \cdot \left[\ln(\sec\theta + \tan\theta) - \ln(\sec\theta_A + \tan\theta_A)\right]$$

Applying the boundary conditions at point A to this equation also results into

$$x = \frac{T_A}{w'} \cdot \cos\theta_A\left[\ln(\sec\theta + \tan\theta) - \ln(\sec\theta_A + \tan\theta_A)\right] \qquad (2.15)$$

Finally, substituting $\sin\theta ds = dz$ into Eq. 2.13 for *ds* results in

$$dz = \frac{T_A}{w'} \cdot \cos\theta_A \frac{\sin\theta}{\cos^2\theta}$$

$$\int_{z_A}^{z} dz = \frac{T_A}{w'}\cos\theta_A \int_{\theta_A}^{\theta} \sec\theta\tan\theta d\theta$$

$$z - z_A = \frac{T_A}{w'} \cdot \cos\theta_A\left[\sec\theta - \sec\theta_A\right]$$

Applying the boundary conditions at point A as before yields

$$z + h = \frac{T_A}{w'} \cdot \cos\theta_A\left[\sec\theta - \sec\theta_A\right] \qquad (2.15)$$

From Fig. 2.2a, the horizontal component of the tension at point B is

$$T_{H_B} = T_B\cos\theta_B \qquad (2.16)$$

Eq. 2.12 could also be rewritten as,

$$T_{H_A} = T_A\cos\theta_A = T\cos\theta = T_H \qquad (2.17)$$

where T_H is the horizontal tension component at the point $P(x, z)$ of the line segment.

For global equilibrium of force in the mooring component, $T_{H_A} = T_{H_B}$

Hence, $T_{H_A} = T_{H_B} = T_H$ (constant)

Therefore, substituting $T_A\cos\theta_A = T_H$ into Eq. 2.15 and rearranging gives

$$\frac{w'x}{T_H} = \left[\ln(\sec\theta + \tan\theta) - \ln(\sec\theta_A + \tan\theta_A)\right]$$

Similarly, let T_{V_A} *and* T_V be the vertical components of the line tension at points A and $P(x,z)$ of the mooring line component respectively. Hence

$$\tan\theta = \frac{T_V}{T_H};\ \sec\theta = \frac{T}{T_H};\ \tan\theta_A = \frac{T_{V_A}}{T_H};\ \sec\theta_A = \frac{T_A}{T_H};\ T = \sqrt{T_H^2 + T_V^2};\ T_A = \sqrt{T_H^2 + T_{V_A}^2}$$

Therefore,

$$\frac{w'x}{T_H} = \left[\ln\left(\frac{T_V}{T_H} + \sqrt{\left(\frac{T_V}{T_H}\right)^2 + 1}\right) - \ln\left(\frac{T_{V_A}}{T_H} + \sqrt{\left(\frac{T_{V_A}}{T_H}\right)^2 + 1}\right)\right]$$

Recall from standard hyperbolic functions that

$$\sinh^{-1}(x) = \ln\left|x + \sqrt{1+x^2}\right|,\ and\ \ \cosh^{-1}(x) = \ln\left|x + \sqrt{x^2 - 1}\right|$$

$$\frac{w'x}{T_H} = \left[\sinh^{-1}\left(\frac{T_V}{T_H}\right) - \sinh^{-1}\left(\frac{T_{V_A}}{T_H}\right)\right]$$

It is noted that $T_V = w's + T_{V_A}$ for equilibrium of force in *z* direction but from Fig. 2.2a it can be shown T_{V_A} has two values:

1. When there is no clump weight W_C at A, $T_{V_A} = T_{V_S}$ where T_{V_S} is the weight of the mooring components below A.
2. When the clump weight is present at A, $T_{V_A} = T_{V_S} + W_C$

Hence, $T_V = T_{V_S} + W_C + w's$ and the above equation can be rewritten in general as:

$$x = \frac{T_H}{w'}\left[\sinh^{-1}\left(\frac{w's + T_{V_S} + W_C}{T_H}\right) - \sinh^{-1}\left(\frac{T_{V_S} + W_C}{T_H}\right)\right] \qquad (2.18)$$

When there is no clump weight or the weight is still inactive (when lying on seabed) W_C is dropped from Eq. 2.18.

The general expression for the curved length of the catenary line component s can also be obtained by rearranging Eq. 2.18 and making s the subject of formula as follows:

$$\frac{w'x}{T_H}+\sinh^{-1}\left(\frac{T_{V_S}+W_C}{T_H}\right)=\sinh^{-1}\left(\frac{T_{V_S}+W_C+w's}{T_H}\right)$$

$$\sinh\left(\frac{w'x}{T_H}+\sinh^{-1}\left(\frac{T_{V_S}+W_C}{T_H}\right)\right)=\frac{T_{V_S}+W_C+w's}{T_H}$$

$$s=\frac{T_H}{w'}\left(\sinh\left(\frac{w'x}{T_H}+\sinh^{-1}\left(\frac{T_{V_S}+W_C}{T_H}\right)\right)-\frac{T_{V_S}+W_C}{T_H}\right) \tag{2.19}$$

Similarly, from Eq. 2.16 it is noted that,

$$(z+h)\frac{w'}{T_H}=\left[\sec\theta-\sec\theta_A\right]=\frac{T}{T_H}-\frac{T_A}{T_H}$$

Or

$$(z+h)\frac{w'}{T_H}=\sqrt{\frac{T_V^2+T_H^2}{T_H^2}}-\sqrt{\frac{T_{V_A}^2+T_H^2}{T_H^2}}$$

$$=\sqrt{\left(\frac{T_V}{T_H}\right)^2+1}-\sqrt{\left(\frac{T_{V_A}}{T_H}\right)^2+1}$$

Recall that, $\sinh^{-1}(x)=\ln\left|x+\sqrt{1+x^2}\right|$, *or* $e^{\sinh^{-1}(x)}-x=\sqrt{1+x^2}$

Therefore

$$(z+h)\frac{w'}{T_H}=e^{\sinh^{-1}\left(\frac{T_V}{T_H}\right)}-\left(\frac{T_V}{T_H}\right)-e^{\sinh^{-1}\left(\frac{T_{V_A}}{T_H}\right)}-\left(\frac{T_{V_A}}{T_H}\right)$$

But $e^{(x)}=\cosh(x)+\sinh(x)$ *and* $e^{-(x)}=\cosh(x)-\sinh(x)$

Hence,

$$(z+h)\frac{w'}{T_H}=\cosh\left(\sinh^{-1}\left(\frac{T_V}{T_H}\right)\right)+\sinh\left(\sinh^{-1}\left(\frac{T_V}{T_H}\right)\right)-\left(\frac{T_V}{T_H}\right)-\cosh\left(\sinh^{-1}\left(\frac{T_{V_A}}{T_H}\right)\right)$$
$$+\sinh\left(\sinh^{-1}\left(\frac{T_{V_A}}{T_H}\right)\right)-\left(\frac{T_{V_A}}{T_H}\right)$$

$$(z+h)\frac{w'}{T_H} = \cosh\left(\sinh^{-1}\left(\frac{T_V}{T_H}\right)\right) + \left(\frac{T_V}{T_H}\right) - \left(\frac{T_V}{T_H}\right) - \cosh\left(\sinh^{-1}\left(\frac{T_{V_A}}{T_H}\right)\right) + \left(\frac{T_{V_A}}{T_H}\right) - \left(\frac{T_{V_A}}{T_H}\right)$$

$$(z+h) = \frac{T_H}{w'}\left(\cosh\left(\sinh^{-1}\left(\frac{T_{V_S} + W_C + w's}{T_H}\right)\right) - \cosh\left(\sinh^{-1}\left(\frac{T_{V_S} + W_C}{T_H}\right)\right)\right)$$

Substituting Eq.2.19 into the foregoing equation gives

$$(z+h) = \frac{T_H}{w'}\left(\cosh\left(\frac{w'x}{T_H} + \sinh^{-1}\left(\frac{T_{V_S} + W_C}{T_H}\right)\right) - \cosh\left(\sinh^{-1}\left(\frac{T_{V_S} + W_C}{T_H}\right)\right)\right) \qquad (2.20)$$

Eq. 2.20 is the general expression for the elevation of the attachment point of the mooring line.

2.3.2. The general multi-component mooring line equations

Using Eqns. 2.18 and 2.20 the governing system equations for an n-component mooring line shown in Fig. 2.1can be written in general as

$$\begin{aligned} x_i &= a_i\left[\sinh^{-1}\left(\frac{s_i}{a_i} + \tan(\theta_i)\right) - \sinh^{-1}(\tan(\theta_i))\right] \\ h_i &= a_i\left[\cosh\left(\frac{x_i}{a_i} + \sinh^{-1}(\tan(\theta_i))\right) - \cosh\left(\sinh^{-1}(\tan(\theta_i))\right)\right] \end{aligned} \quad \text{for } i = 1,2,\cdots,n \qquad (2.21)$$

where

$$s_i = a_i\left(\sinh\left(\frac{x_i}{a_i} + \sinh^{-1}(\tan\theta_i)\right) - \tan\theta_i\right)$$

$$\tan(\theta_i) = \begin{cases} \tan(\theta_{s_i}) \text{ ; Inactive or no } W_C \text{ at joint i} \\ \tan(\theta_{s_i}) + \dfrac{W_{C_i}}{T_H} \text{ ; } W_C \text{ present and active at joint i} \end{cases}$$

$$\tan(\theta_{i+1}) = \tan(\theta_i) + \frac{s_i}{a_i}$$

$$a_i = \frac{T_H}{w'_i}$$

$$\theta_i = \tan^{-1}\left(\frac{T_{V_i}}{T_H}\right)$$

$$T_{V_i} = \begin{cases} T_{V_{S_i}} \; ; & \text{Inactive or no } W_C \text{ at joint i} \\ T_{V_{S_i}} + W_{C_i} \; ; & W_C \text{ present and active at joint i} \end{cases}$$

$T_{V_{S_i}}$ = vertical reaction at joint i due mooring component only

W_{C_i} = Clump weight

Subscript *si* refers to suspended part of line segment *i*, $i = 1,2,3,...,n$

The total horizontal distance, X between the attachment point and the anchor point is the sum of mooring components lengths lying on the seabed, x_b and the projected lengths of the hanging n components in the horizontal direction x_i. Similarly, the elevation H of the attachment point above the seabed is the sum of the projected lengths of the hanging *n* components in the vertical direction h_i as shown in Eq. 2.21.

It can be shown that $x_b = L - \sum_{i=1}^{n} s_i$, therefore,

$$\begin{aligned} X &= L - \sum_{i=1}^{n} s_i + \sum_{i=1}^{n} x_i \\ H &= \sum_{i=1}^{n} h_i \end{aligned} \qquad (2.22)$$

where L= total length of mooring line

Eq. 2.22 is the general catenary equations for an n-component mooring line.

2.4. Analysis Methodology

A multi-component mooring line as shown in Fig. 2.1 can assume different configurations during its service life. The number of configurations depends on:

- The number of components making up the mooring line
- Type of anchoring system; fixed or mobile, and
- Whether or not there is a clump weight(s) or a buoy(s) attached to the mooring line

On the other hand, each of the multi-component mooring line components can only be in one of following three states in any given configuration:

1. Completely lying on the seabed whereby all its length, l_i is part of x_b. In this condition the mooring line component does not contribute to the station keeping of the FPSO.
2. Partly lying on the seabed and partly suspended with zero slope at the point of contact with the seabed. In this case it will have a suspended length, s_i with projected lengths x_i and h_i to the horizontal and vertical respectively, and the rest of its length lying on the seabed will be part of x_b
3. Completely suspended, making an angle θ_i, with the seabed. In this case, its suspended length s_i is equal to its total length l_i having projected lengths of x_i and h_i.

The analysis methodology adopted in this study is to subject each of the mooring line components to the three possible states in the order outlined above, except the topmost one which will only be subjected to the last two of the three states. The sequence of the analysis is as follows;

1. Starting with a small elevation h such that $n-1$ components (starting from the anchor point) and substantial part of the nth component will be on the seabed, analyse the mooring line for the horizontal tension T_H at the attachment point.
2. Keep increasing the elevation by ΔH (in the order of small fraction of a meter) and running the analysis to calculate T_H until all the components are completely suspended in water or the maximum water depth reached.

Repeat the above procedure for each of the mooring lines in the system.

2.4.1. Four-component mooring line

To demonstrate the above methodology, a multi-component mooring system consisting of mooring lines having four components is discussed in the following sections. The four components of the mooring lines are: a chain at the bottom which connects the mooring line to the anchor pile, a wire rope at the middle and a chain at the top. In between the lower chain and the wire rope is a clump weight which provides additional anchorage, especially useful for mooring mobile platforms. This type of multi-component catenary line can assume any one of the five configurations suggested by Ansari (1980). The five configurations are discussed in the following subsections in a more detail but in a way that is easier to implement.

2.4.1.1. *Multi-Component Mooring System configuration one*

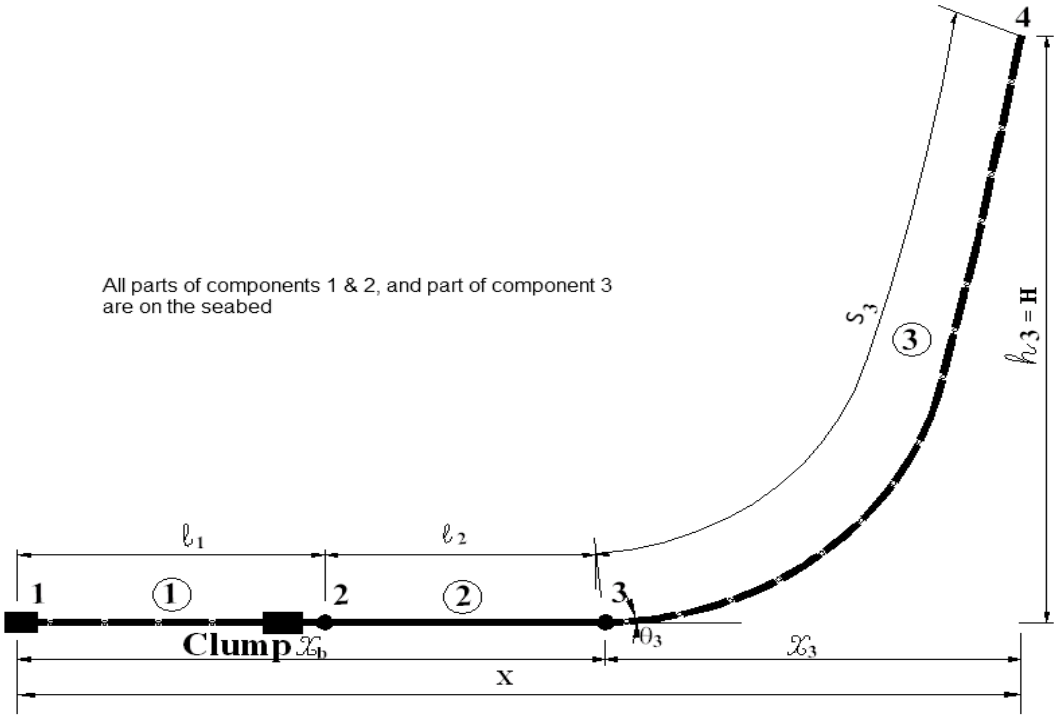

Fig. 2. 3 Multi-component catenary line configuration one

In this configuration,

$$s_1 = s_2 = \theta_1 = \theta_2 = \theta_3 = T_{V_1} = T_{V_2} = T_{V_3} = 0$$
$$x_b = l_1 + l_2 + l_3 - s_3$$

Thus, Eq. 2.21 reduces to

$$x_3 = a_3 \sinh^{-1}\left(\frac{s_3}{a_3}\right)$$
$$H = h_3 = a_3\left[\cosh\left(\frac{x_3}{a_3}\right) - 1\right] \tag{2.23}$$

From Eq. 2.23 it can be shown that

$$s_3 = h_3\left(1 + \frac{2a_3}{h_3}\right)^{\frac{1}{2}} \tag{2.24}$$

The expression for the horizontal distance, X between the anchor and the mooring attachment points is shown in Eq. 2.25 below. In order to find the mean position of the

FPSO in wind, waves and current, the horizontal force, T_H, from the cable must be expressed as a function of X (Faltinsen 1990).

$$X = L - s_3 + x_3 \tag{2.25}$$

where

$L = l_1 + l_2 + l_3$, is the total length of the mooring line,

$s_3 =$ Curved length of the cable segment between joints 3 and 4 given in Eq. 2.24,

$x_3 =$ The horizontal projection of s_3.

From Eq. 2.23 we have

$$x_3 = a_3 \cosh^{-1}\left(1 + \frac{h_3}{a_3}\right)$$

Hence,

$$X = L - h_3\left(1 + \frac{2a_3}{h_3}\right)^{\frac{1}{2}} + a_3 \cosh^{-1}\left(1 + \frac{h_3}{a_3}\right) \tag{2.26}$$

The horizontal restoring coefficient, k_{11} due to mooring line is obtained by differentiating Eq. 2.26 with respect to T_H and is given by

$$k_{11} = \frac{dT_H}{dX} = w'_3 \left[\frac{-2}{\left(1 + \frac{2a_3}{h_3}\right)^{\frac{1}{2}}} + \cosh^{-1}\left(1 + \frac{h_3}{a_3}\right) \right]^{-1} \tag{2.27}$$

The expression for the vertical mooring line force at the attachment point is given by

$$T_{V4} = s_3 \cdot w'_3$$

$$T_{V4} = h_3\left(1 + \frac{2a_3}{h_3}\right)^{\frac{1}{2}} \cdot w'_3 \tag{2.28}$$

The vertical restoring coefficient k_{33} due to the mooring line is obtained by differentiating Eq. 2.28 with respect to h_3 as follows

$$k_{33} = \frac{dT_{V4}}{dh_3} = w'_3\left(1+\frac{2a_3}{h_3}\right)^{\frac{1}{2}} - \frac{T_H}{h_3\left(1+\frac{2a_3}{h_3}\right)^{\frac{1}{2}}} \tag{2.29}$$

2.4.1.2. *Multi-Component Mooring System configuration two*

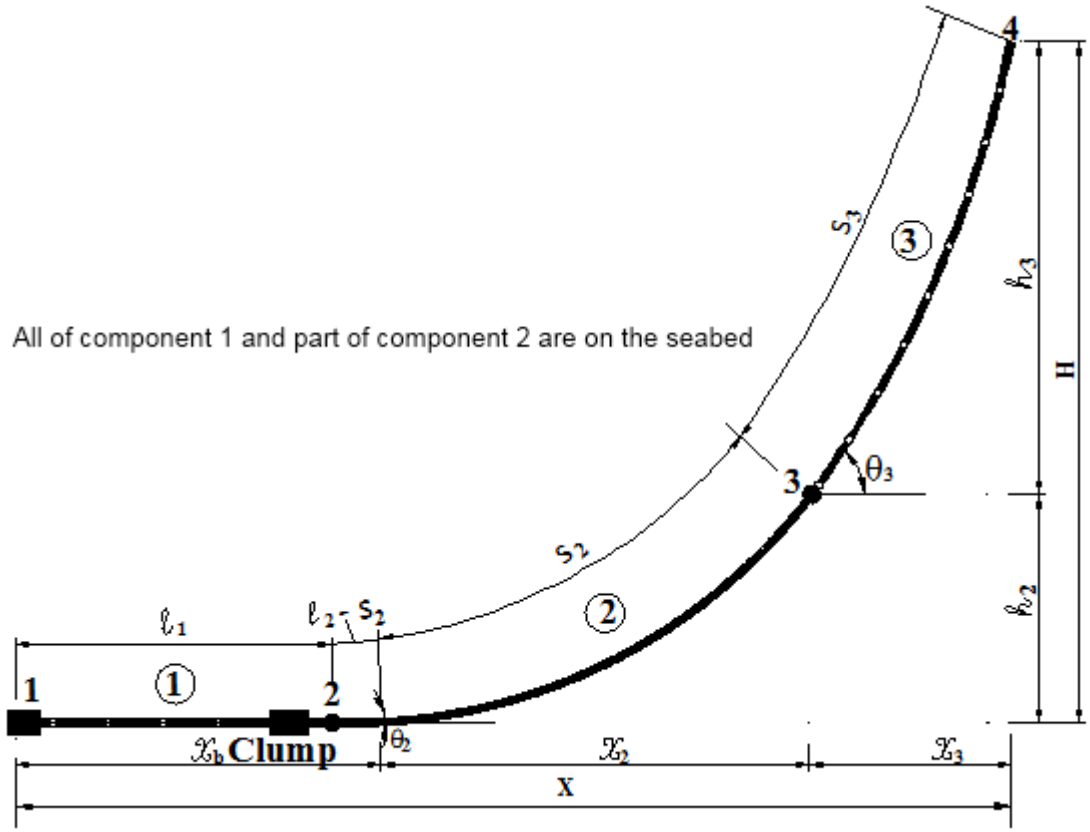

Fig. 2. 4 Multi-component catenary line configuration two

In configuration two,

$$s_1 = \theta_1 = \theta_2 = T_{V_1} = T_{V_2} = 0$$

$$s_2 = l_1 + l_2 - x_b,\ \ s_3 = l_3 \ \ and \ \ \tan(\theta_3) = \tan(\theta_2) + \frac{s_2}{a_2}$$

Hence Eq. 2.21 reduces to :

$$
\begin{aligned}
x_2 &= a_2 \sinh^{-1}\left(\frac{s_2}{a_2}\right) \\
h_2 &= a_2\left[\cosh\left(\frac{x_2}{a_2}\right)-1\right] \\
x_3 &= a_3\left[\sinh^{-1}\left(\frac{L_3}{a_3}+\frac{s_2}{a_2}\right)-\sinh^{-1}\left(\frac{s_2}{a_2}\right)\right] \\
h_3 &= a_3\left[\cosh\left(\frac{x_3}{a_3}+\sinh^{-1}\left(\frac{s_2}{a_2}\right)\right)-\cosh\left(\sinh^{-1}\left(\frac{s_2}{a_2}\right)\right)\right]
\end{aligned}
\tag{2.30}
$$

From Eq. 2.30 it could be shown that

$$
s_2 = h_2\left(1+\frac{2a_2}{h_2}\right)^{\frac{1}{2}}, \text{ and } x_2 = a_2\cosh^{-1}\left(1+\frac{h_2}{a_2}\right) \tag{2.31}
$$

To evaluate T_H for this configuration, the expressions for the elevation H of the attachment point above the seabed and the horizontal distance, X between the anchor and the mooring points are required as given respectively by

$$
H = h_2 + h_3 \tag{2.32}
$$

$$
X = L - l_3 - s_2 + x_2 + x_3 \tag{2.33}
$$

where

L is the total length of the cable,

l_3 is the length of the cable between joints 3 and 4,

s_2 is the curved length of the cable between joints 2 and 3,

x_2 and x_3 are the projected horizontal length of $s_2, and\, l_3$ respectively.

Using equations Eq. 2.30 and Eq. 2.31, Eq. 2.32 and Eq. 2.33 could be further simplified in terms of variables T_H and h_2 which will then be solved simultaneously.

The horizontal stiffness, k_{11} of the mooring line is obtained from the differentiation of Eq. 2.33 with respect to X , and is given by

$k_{11} = \frac{dT_H}{dX}$ (see Appendix A for the expression)

The expression for the vertical mooring line force at the attachment point is given by

$$T_{V4} = s_2 \cdot w'_2 + l_3 \cdot w'_3$$

$$T_{V4} = h_2\left(1+\frac{2a_2}{h_2}\right)^{\frac{1}{2}} \cdot w'_2 + l_3 w'_3 \qquad (2.34)$$

The vertical stiffness, k_{33} of the mooring line is obtained by differentiating Eq. 2.34 with respect to H as follows

$$k_{33} = \frac{dT_{V4}}{dH} \text{ (see Appendix A for the full expression)} \qquad (2.35)$$

2.4.1.3. ***Multi-Component Mooring System configuration three***

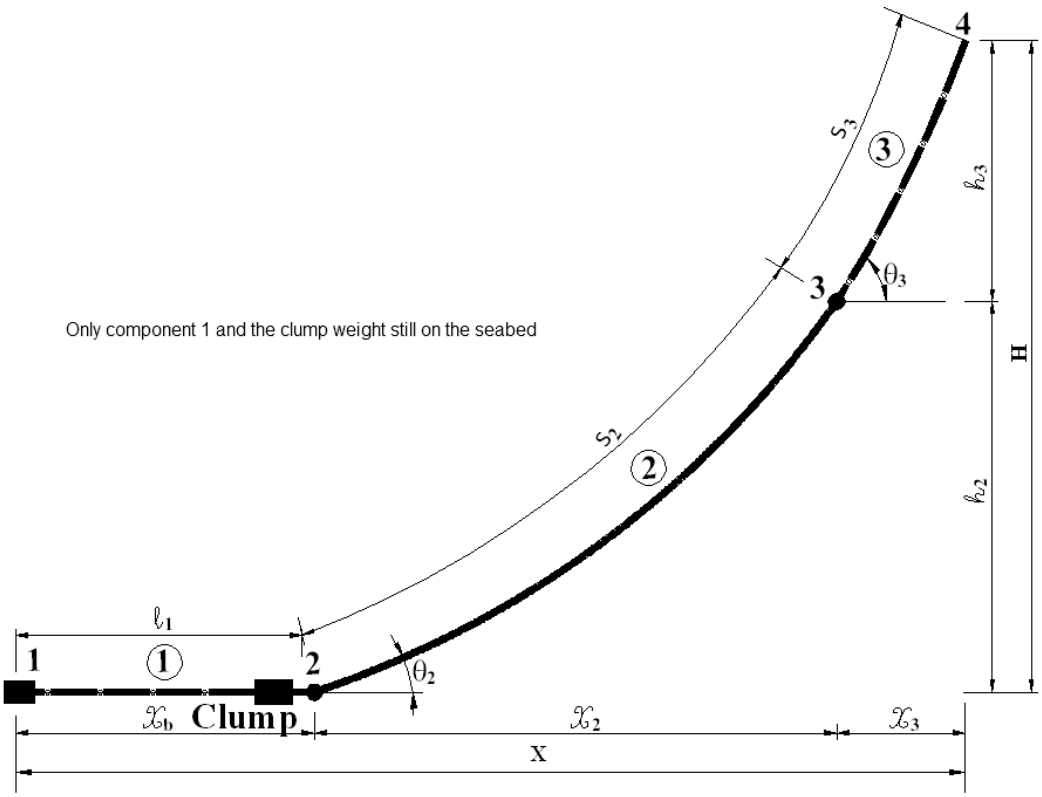

Fig. 2. 5 Multi-component catenary line configuration three

In this configuration,

$s_1 = \theta_1 = T_{V_1} = 0, \quad s_2 = l_2$

$s_3 = l_3, \ x_b = l_1, \ T_{V_2} = T_H \tan\theta_2$

Hence Eq. 2.21 becomes:

$$
\begin{aligned}
x_2 &= a_2\left[\sinh^{-1}\left(\frac{l_2}{a_2}+\tan(\theta_2)\right)-\sinh^{-1}(\tan(\theta_2))\right] \\
h_2 &= a_2\left[\cosh\left(\frac{x_2}{a_2}+\sinh^{-1}(\tan(\theta_2))\right)-\cosh\left(\sinh^{-1}(\tan(\theta_2))\right)\right] \\
x_3 &= a_3\left[\sinh^{-1}\left(\frac{l_3}{a_3}+\tan\theta_3\right)-\sinh^{-1}(\tan\theta_3)\right] \\
h_3 &= a_3\left[\cosh\left(\frac{x_3}{a_3}+\sinh^{-1}(\tan\theta_3)\right)-\cosh\left(\sinh^{-1}(\tan\theta_3)\right)\right]
\end{aligned}
\tag{2.36}
$$

where

$$\tan\theta_3 = \tan\theta_2 + \frac{l_2}{a_2}.$$

The expressions for the elevation H of the attachment point above the seabed and the horizontal distance, X between the anchor and the mooring points are required as given respectively by

$$H = h_2 + h_3 \tag{2.37}$$

$$X = l_1 + x_2 + x_3 \tag{2.38}$$

where

l_1 is the length of the cable segment between joints 1 and 2; x_2 and x_3 are the projected horizontal length of $l_2, and\, l_3$ respectively.

Therefore,

$$H = a_2\left[\cosh\left(\sinh^{-1}\left(\frac{l_2}{a_2}+\tan(\theta_2)\right)\right)-\cosh\left(\sinh^{-1}(\tan(\theta_2))\right)\right]+ a_3\left[\cosh\left(\sinh^{-1}\left(\frac{l_3}{a_3}+\tan(\theta_2)+\frac{l_2}{a_2}\right)\right)-\cosh\left(\sinh^{-1}\left(\tan(\theta_2)+\frac{l_2}{a_2}\right)\right)\right] \quad (2.39)$$

$$X = l_1 + a_2\left[\sinh^{-1}\left(\frac{l_2}{a_2}+\tan(\theta_2)\right)-\sinh^{-1}(\tan(\theta_2))\right]+ a_3\left[\sinh^{-1}\left(\frac{l_3}{a_3}+\tan(\theta_2)+\frac{l_2}{a_2}\right)-\sinh^{-1}\left(\tan(\theta_2)+\frac{l_2}{a_2}\right)\right] \quad (2.40)$$

Equations Eq. 2.39 and Eq. 2.40 will be solved simultaneously for $\theta_2 and\ T_H$ .The horizontal stiffness, k_{11} of the mooring line is obtained from differentiating Eq. 2.40 with respect to X and is given by

$k_{11} = \frac{dT_H}{dX}$ (See Appendix A for the full expression)

The expression for the vertical mooring line force at the attachment point is given by

$$T_{V4} = T_H\tan(\theta_2)+l_2\cdot w'_2+l_3\cdot w'_3 \quad (2.41)$$

The vertical stiffness, k_{33} of the mooring line is obtained by differentiating Eq. 2.41 with respect to H as follows

$$k_{33} = \frac{dT_{V4}}{d\theta_2}\cdot\frac{d\theta_2}{dH} \text{ (see Appendix A for the full expression)} \quad (2.42)$$

2.4.1.4. *Multi-Component Mooring System configuration four*

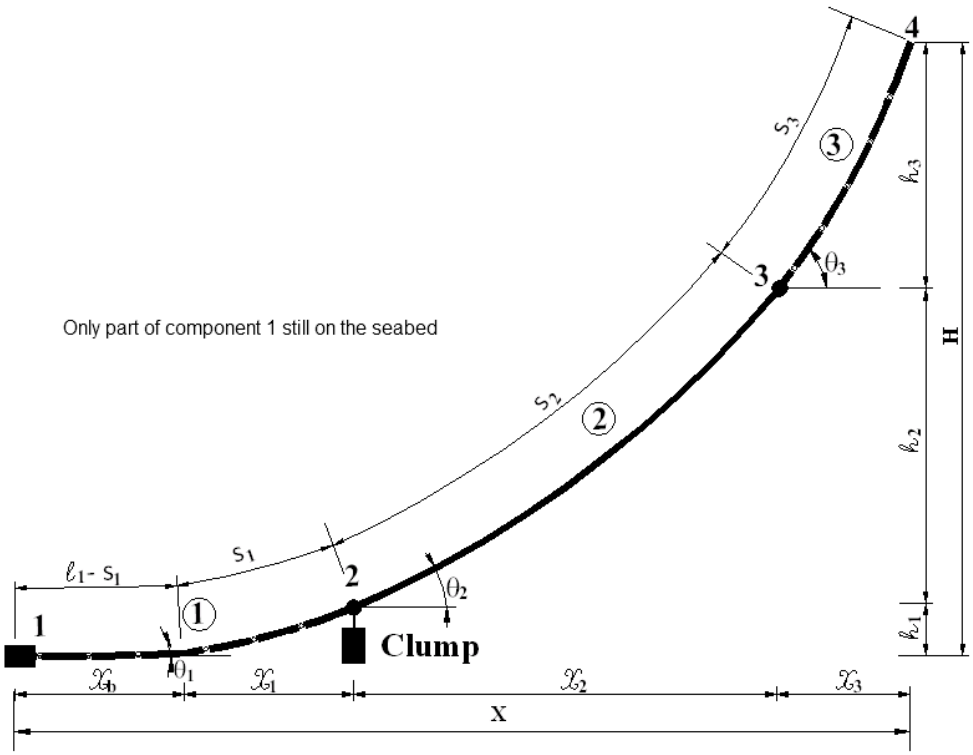

Fig. 2. 6 Multi-component catenary line configuration four

In this configuration, $\theta_1 = T_{V_1} = 0;\ s_1 = l_1 - x_b;\ s_2 = l_2,\ s_3 = l_3$. HenceEq.2.21reduces to

$$
\begin{aligned}
x_1 &= a_1 \sinh^{-1}\left(\frac{s_1}{a_1}\right) \\
h_1 &= a_1\left[\cosh\left(\frac{x_1}{a_1}\right) - 1\right] \\
x_2 &= a_2\left[\sinh^{-1}\left(\frac{l_2}{a_2} + \tan\theta_2\right) - \sinh^{-1}\left(\tan\theta_2\right)\right] \\
h_2 &= a_2\left[\cosh\left(\frac{x_2}{a_2} + \sinh^{-1}\left(\tan\theta_2\right)\right) - \cosh\left(\sinh^{-1}\left(\tan\theta_2\right)\right)\right] \\
x_3 &= a_3\left[\sinh^{-1}\left(\frac{l_3}{a_3} + \tan\theta_3\right) - \sinh^{-1}\left(\tan\theta_3\right)\right] \\
h_3 &= a_3\left[\cosh\left(\frac{x_3}{a_3} + \sinh^{-1}\left(\tan\theta_3\right)\right) - \cosh\left(\sinh^{-1}\left(\tan\theta_3\right)\right)\right]
\end{aligned}
\tag{2.43}
$$

where

$$\tan\theta_2 = \frac{s_1}{a_1} + \frac{W_C}{T_H} \; and \;\; \tan\theta_3 = \frac{s_1}{a_1} + \frac{W_C}{T_H} + \frac{l_2}{a_2}$$

From Eq. 2.43 it could be shown that

$$s_1 = h_1\left(1+\frac{2a_1}{h_1}\right)^{\frac{1}{2}}, \text{ and } x_1 = a_1\cosh^{-1}\left(1+\frac{h_1}{a_1}\right) \tag{2.44}$$

The expressions for the elevation, H of the attachment point above the seabed, and the horizontal distance, X between the anchor and the mooring points are required as given respectively by

$$H = h_1 + h_2 + h_3 \tag{2.45}$$

$$X = l_1 - s_1 + x_1 + x_2 + x_3 \tag{2.46}$$

where

l_1, l_2 and l_3 are the lengths of the cable segments,

s_1 is the curved length of the cable between joints 1 and 2,

x_1, x_2 and x_3 are the projected horizontal length of s_1, $l_2 and l_3$ respectively.

Therefore,

$$H = h_1 + a_2\left[\cosh\left(\sinh^{-1}\left(\frac{l_2}{a_2}+\frac{s_1}{a_1}+\frac{W_C}{T_H}\right)\right)-\cosh\left(\sinh^{-1}\left(\frac{s_1}{a_1}+\frac{W_C}{T_H}\right)\right)\right]+ a_3\left[\cosh\left(\sinh^{-1}\left(\frac{l_3}{a_3}+\frac{s_1}{a_1}+\frac{W_C}{T_H}+\frac{l_2}{a_2}\right)\right)-\cosh\left(\sinh^{-1}\left(\frac{s_1}{a_1}+\frac{W_C}{T_H}+\frac{l_2}{a_2}\right)\right)\right] \tag{2.47}$$

$$X = l_1 - h_1\left(1+\frac{2a_1}{h_1}\right)^{\frac{1}{2}} + a_1\cosh^{-1}\left(1+\frac{h_1}{a_1}\right)+ a_2\left[\sinh^{-1}\left(\frac{l_2}{a_2}+\frac{s_1}{a_1}+\frac{W_C}{T_H}\right)-\sinh^{-1}\left(\frac{s_1}{a_1}+\frac{W_C}{T_H}\right)\right]+ a_3\left[\sinh^{-1}\left(\frac{l_3}{a_3}+\frac{s_1}{a_1}+\frac{W_C}{T_H}+\frac{l_2}{a_2}\right)-\sinh^{-1}\left(\frac{s_1}{a_1}+\frac{W_C}{T_H}+\frac{l_2}{a_2}\right)\right] \tag{2.48}$$

Eqns. 2.47 and 2.48 will be solved simultaneously for T_H and h_1. The horizontal restoring coefficient, k_{11} due to mooring line is obtained by differentiating Eq. 2.48 with respect to X and is given by

$k_{11} = \frac{dT_H}{dX}$ (see Appendix A for the full expression),

The expression for the vertical mooring line force at the attachment point is given by

$$T_{V4} = s_1 \cdot w'_1 + W_c + l_2 \cdot w'_2 + l_3 \cdot w'_3$$

$$T_{V4} = h_1\left(1+\frac{2a_1}{h_1}\right)^{\frac{1}{2}} \cdot w'_2 + W_c + l_2 w'_2 + l_3 w'_3 \qquad (2.49)$$

The vertical restoring coefficient, k_{33} due the mooring line is obtained by differentiating 2.3.42 with respect to H as

$$k_{33} = \frac{dT_{V4}}{dH} = \frac{dT_{V4}}{dh_1} \cdot \frac{dh_1}{dH} \text{ (see Appendix A for the full expression)} \qquad (2.50)$$

2.4.1.5. *Multi-Component Mooring System configuration five*

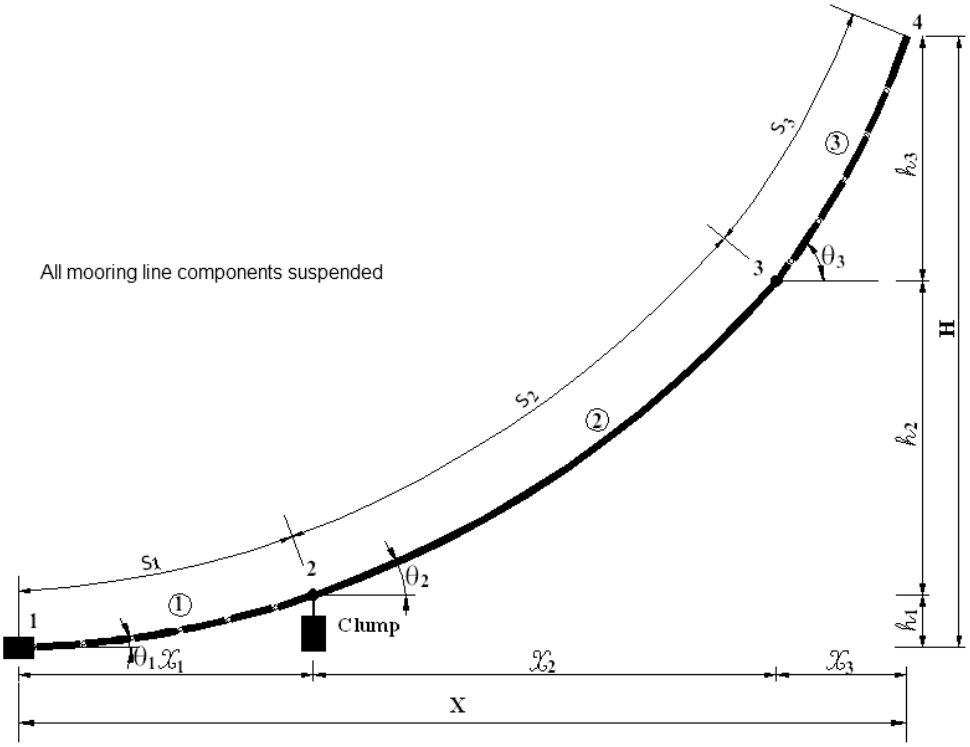

Fig. 2. 7 Multi-component catenary line configuration five

Finally, in configuration 5,

$s_1 = l_1,\ s_2 = l_2,\ s_3 = l_3,\ x_b = 0.$ HenceEq.2.21reducesto

$$
\begin{aligned}
x_1 &= a_1\left[\sinh^{-1}\left(\frac{l_1}{a_1}+\tan\theta_1\right)-\sinh^{-1}\left(\tan\theta_1\right)\right]\\
h_1 &= a_1\left[\cosh\left(\frac{x_1}{a_1}+\sinh^{-1}\left(\tan\theta_1\right)\right)-\cosh\left(\sinh^{-1}\left(\tan\theta_1\right)\right)\right]\\
x_2 &= a_2\left[\sinh^{-1}\left(\frac{l_2}{a_2}+\tan\theta_2\right)-\sinh^{-1}\left(\tan\theta_2\right)\right]\\
h_2 &= a_2\left[\cosh\left(\frac{x_2}{a_2}+\sinh^{-1}\left(\tan\theta_2\right)\right)-\cosh\left(\sinh^{-1}\left(\tan\theta_2\right)\right)\right]\\
x_3 &= a_3\left[\sinh^{-1}\left(\frac{l_3}{a_3}+\tan\theta_3\right)-\sinh^{-1}\left(\tan\theta_3\right)\right]\\
h_3 &= a_3\left[\cosh\left(\frac{x_3}{a_3}+\sinh^{-1}\left(\tan\theta_3\right)\right)-\cosh\left(\sinh^{-1}\left(\tan\theta_3\right)\right)\right]
\end{aligned}
\qquad (2.51)
$$

where

$$\tan\theta_2 = \tan\theta_1 + \frac{W_C}{T_H} + \frac{l_1}{a_1} and \quad \tan\theta_3 = \tan\theta_1 + \frac{W_C}{T_H} + \frac{l_1}{a_1} + \frac{l_2}{a_2}$$

The expressions for the elevation, H of the attachment point above the seabed and the horizontal distance, X between the anchor and the mooring points are required as given respectively by

$$H = h_1 + h_2 + h_3 \tag{2.52}$$

$$X = x_1 + x_2 + x_3 \tag{2.53}$$

where

x_1, x_2 and x_3 are the projected horizontal length of l_1, $l_2 and l_3$ respectively.

Therefore,

$$\begin{aligned} H = a_1\left[\cosh\left(\sinh^{-1}\left(\frac{l_1}{a_1} + \tan\theta_1\right)\right) - \cosh\left(\sinh^{-1}\left(\tan\theta_1\right)\right)\right] + \\ a_2\left[\cosh\left(\sinh^{-1}\left(\frac{l_2}{a_2} + \tan\theta_2\right)\right) - \cosh\left(\sinh^{-1}\left(\tan\theta_2\right)\right)\right] + \\ a_3\left[\cosh\left(\sinh^{-1}\left(\frac{l_3}{a_3} + \tan\theta_3\right)\right) - \cosh\left(\sinh^{-1}\left(\tan\theta_3\right)\right)\right] \end{aligned} \tag{2.54}$$

$$\begin{aligned} X = a_1\left[\sinh^{-1}\left(\frac{l_1}{a_1} + \tan\theta_1\right) - \sinh^{-1}\left(\tan\theta_1\right)\right] + \\ a_2\left[\sinh^{-1}\left(\frac{l_2}{a_2} + \tan\theta_2\right) - \sinh^{-1}\left(\tan\theta_2\right)\right] + \\ a_3\left[\sinh^{-1}\left(\frac{l_3}{a_3} + \tan\theta_3\right) - \sinh^{-1}\left(\tan\theta_3\right)\right] \end{aligned} \tag{2.55}$$

Eqns. 2.54 and 2.55 will be solved simultaneously for the unknown values of θ_1 and T_H .

The horizontal restoring coefficient, k_{11} due to mooring line is the obtained from the

differentiation of Eq. 2.55 with respect to X , and is given by $k_{11} = \frac{dT_H}{dX}$ (see Appendix A for the full expression)

The expression for the vertical mooring line force at the attachment point is given by

$$T_{V4} = T_H \tan(\theta_1) + l_1 w'_1 + W_C + l_2 \cdot w'_2 + l_3 \cdot w'_3 \quad (2.56)$$

The vertical restoring coefficient, k_{33} due the mooring line is obtained by differentiating Eq. 2.56 with respect to H as

$$k_{33} = \frac{dT_{V4}}{d\theta_1} \cdot \frac{d\theta_1}{dH} \text{ (see Appendix A for the expression)} \quad (2.57)$$

2.5. Numerical Solution Technique

To obtain the horizontal tension, T_H and the angle between the line and the seabed at the touchdown point, θ where necessary for each configuration, the governing equation(s) applicable to that configuration must be solved numerically. These equations are highly non-linear with no direct solution available. In this study therefore, the globally convergent Newton-Raphson Method has been applied to find the solutions iteratively. The algorithm combines the rapid local convergence of Newton's method with a globally convergent strategy that will guarantee some progress towards the solution with each iteration using the Line Search technique (Press et al., 1996). Once the horizontal tension in the mooring line is found, other parameters such as the axial tension, the vertical tension and the slope of the line at any point along each component of the line can easily be calculated.

2.6. Comparison of Results with those from Similar Techniques

The mooring line catenary formulations derived and the numerical technique outlined above were used for the static analysis of a multi-component mooring cable presented by Ansari (1980) for shallow water depth for comparison. The total length of the mooring line is 500 ft (152.4 m) length. It is a chain 2-1/8 in (54 mm) in diameter with a 10 kip (44.4 kN) clump weight positioned 150 ft (45.7 m) from an anchor pile. The chain forward of the clump weight is broken up into two equal segments of 53.35m each. The horizontal tension-displacement characteristics obtained using the current methodology is shown in Fig. 2.8. Also shown in the figure is the result from Ansari (1980) for comparison.

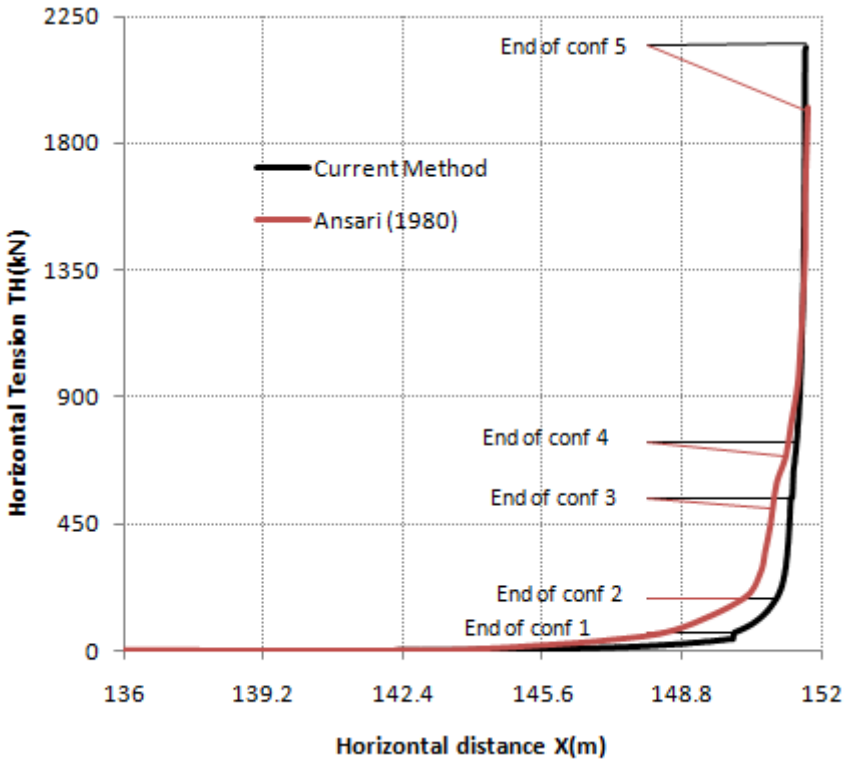

Fig. 2. 8 Multi-component mooring line tension-displacement characteristics

It is observed that Ansari's results tend to be more conservative for configurations 2, 3 and 4 even though the shapes of the two curves are quite similar. The beginning and end

of each configuration in the current method lag behind those of Ansari by up to about 1.5m but have higher end horizontal tension values. This may be as a result of different convergence criteria used by the two methods.

2.7. Derivation of the Steel Catenary Riser (SCR) Equations

Steel catenary risers are different from mooring lines in several ways. The bending stiffness, EI, axial stiffness, EA, and torsional stiffness, GJ of mooring lines are quite small compared to those of SCRs. Due to their outer diameters being larger than those of the mooring lines, SCRs also have greater buoyancy. Also because of the fluid flow inside them, SCRs may be subjected to thermal stresses in addition. For these reasons, the SCR formulations are slightly different from those of the mooring lines.

However, for deep and ultra deepwater applications, the lengths of the SCRs are much greater than their diameters. At such water depth, the SCRs behave as perfectly flexible strings and assume a catenary shape. Hence, it is common practice to model the SCRs just like mooring lines by neglecting their axial, bending and torsional stiffness. After computing the horizontal tension, the maximum bending stresses in the SCRs can then be calculated using the standard equation of curvature for large deflection beams as shown in Eq. 2.64. This section discusses the SCRs formulations in detail.

Fig. 2. 9 below shows a typical steel catenary riser connected to a vessel at the flex joint 2 to the touch down point 1 on the seabed. The line between points 1 and 2 is suspended in a 2D X, Z system. The coordinate system is chosen such that the origin O

is at the free water surface and directly above point 1 on the seabed. At any arbitrary point $P(x,z)$ on the riser with a distance s from 1, the tension, T in the riser acts at an angle, θ with the horizontal.

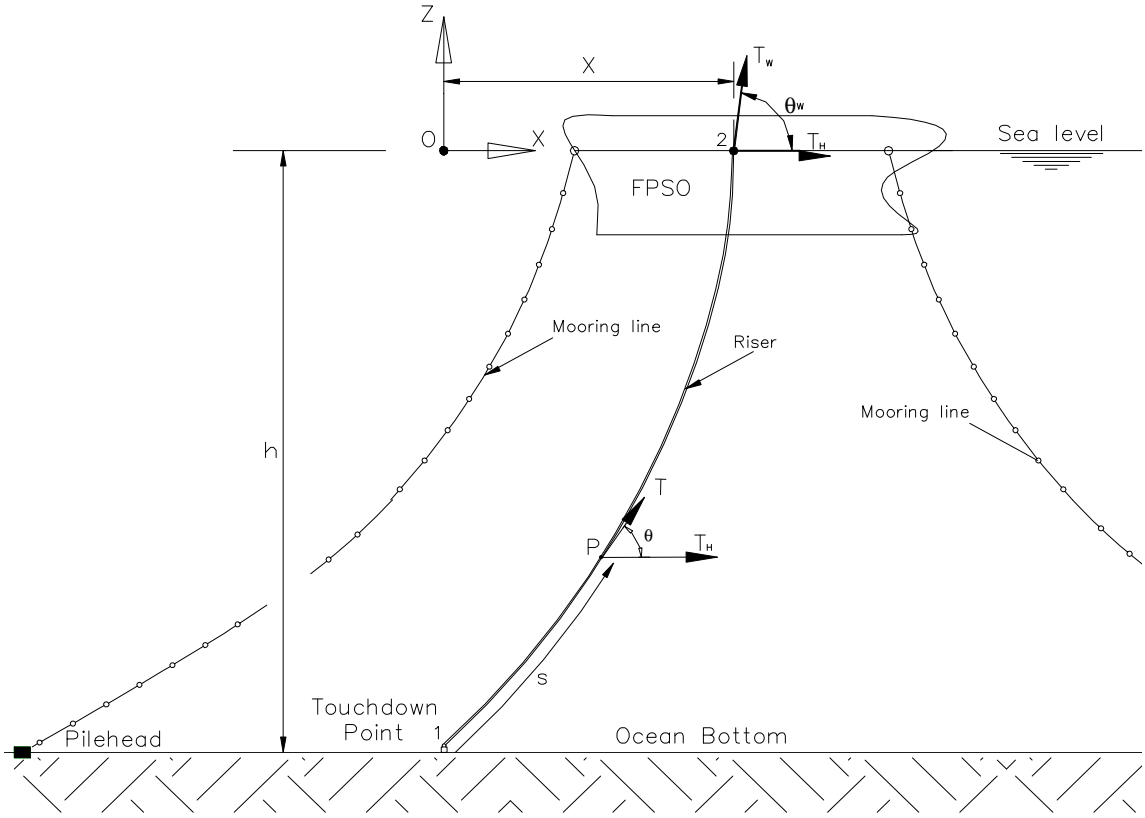

Fig. 2. 9 A typical mooring system with Steel Catenary Riser

Fig. 2. 10 shows a small element of the riser. The forces acting on the element as shown in the figure are:

1. Its own weight $W_e = W_R - B + W_C$ per unit length in water.
2. The mean hydrodynamic forces, F_t *and* F_n per unit length acting tangentially and normally on the element respectively.
3. The equivalent axial tension, $T_e = T - \rho_w g\pi \frac{D_o^2}{4}(h-z) + \rho_c g\pi \frac{D_i^2}{4}(h_c - z)$
4. The internal structural reactions at the ends of the element (Bernitsas 1982) are:

a. The axial tension T

b. The normal in-plane shear force Q, and

c. The in-plane moment M

where

W_R = the weight of the riser element in air,

B = the buoyancy of the riser element,

W_C = the weight of the riser contents,

ρ_w = the density of sea water,

$h \, and \, h_c$ = the water depth and height of contents free surface,

$D_o \, and \, D_i$ = the outer and inner diameters of the riser,

z = the z-coordinate of the point under consideration,

ρ_c = the density of riser contents and

θ = the angle between T and the horizontal at P(x,z).

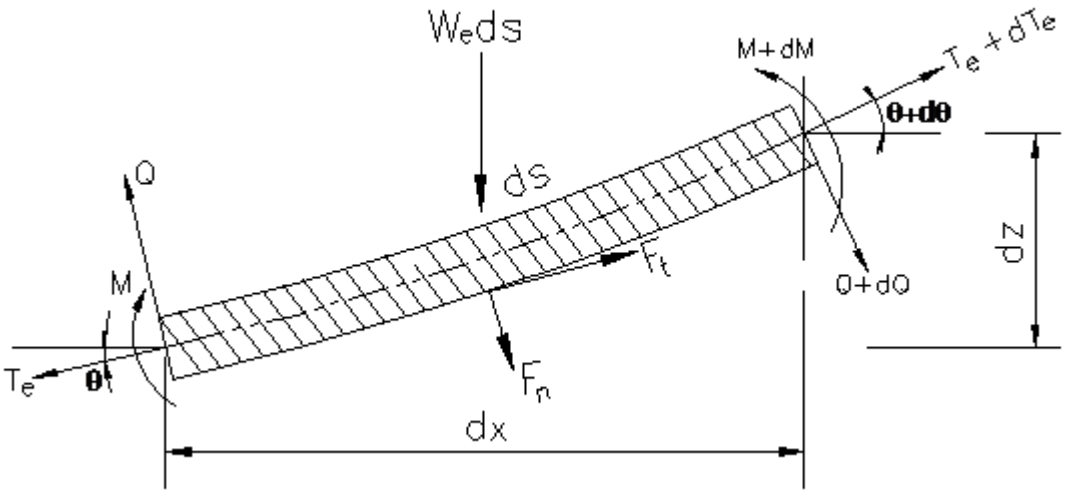

Fig. 2. 10 Forces acting on the deformed riser element

Taking equilibrium of forces and moments on a small element of the riser as shown in Fig. 2. 10 results in

$$\begin{aligned}\sum F_X = & -T_e\cos\theta - Q\sin\theta + (T_e + dT_e)\cos(\theta + d\theta) + (Q + dQ)\sin(\theta + d\theta) + \\ & F_t ds\cdot\cos\theta + F_n ds\cdot\sin\theta = 0 \\ \sum F_Z = & -T_e\sin\theta + Q\cos\theta + (T_e + dT_e)\sin(\theta + d\theta) - (Q + dQ)\cos(\theta + d\theta) - \\ & F_n ds\cdot\cos\theta + F_t ds\cdot\sin\theta - W_e ds = 0 \\ \sum M = & -M + (M + dM) + W_e ds\cdot\frac{dx}{2} + (F_n\cos\theta ds - F_t\sin\theta ds)\cdot\frac{dx}{2} + \\ & (F_t\cos\theta ds + F_n\sin\theta ds)\cdot\frac{dz}{2} + (T_e\sin\theta - Q\cos\theta)dx - \\ & (T_e\cos\theta + Q\sin\theta)dz = 0\end{aligned} \tag{2.58}$$

Expanding and neglecting higher terms and products of two infinitesimals from Eq. 2.58 results in the following:

$$\begin{aligned}\sum F_X = & dT_e\cos\theta - T_e\sin\theta d\theta + dQ\sin\theta + Q\cos\theta d\theta + F_t ds\cdot\cos\theta + \\ & F_n ds\cdot\sin\theta = 0 \\ \sum F_Z = & dT_e\sin\theta + T_e\cos\theta d\theta - dQ\cos\theta + Q\sin\theta d\theta - F_n ds\cdot\cos\theta + \\ & F_t ds\cdot\sin\theta - W_e ds = 0 \\ \sum M = & dM - Qds = 0\end{aligned} \tag{2.59}$$

Eq. 2.59 reduces to

$$d(T_e\cos\theta + Q\sin\theta) + (F_t\cos\theta + F_n\sin\theta)ds = 0 \tag{2.60}$$

$$d(T_e\sin\theta - Q\cos\theta) - W_e ds - (F_n\cos\theta - F_t\sin\theta)ds = 0 \tag{2.61}$$

$$dM - Qds = 0 \tag{2.62}$$

From bending theory, the in-plane moment on the differential element of the riser in Eq. 2.62 can be written as

$$M = E\cdot I\cdot K \tag{2.63}$$

where

$E =$ Young modulus of the riser material

$I =$ Second moment of cross sectional area of the riser about its neutral axis

$K =$ local curvature of the riser given by

$$K = \frac{d^2z}{dx^2} \Bigg/ \left[1 + \left(\frac{dz}{dx}\right)^2\right]^{\frac{3}{2}} \tag{2.64}$$

From Eqns. 2.62 and 2.63, $Q = \frac{dM}{ds} = EI \cdot \frac{dK}{ds}$

Eqns. 2.60 and 2.61 (neglecting the hydrodynamic force) can be rewritten as

$$\frac{d}{ds}\left(T_e \cos\theta + Q \sin\theta\right) = 0 \tag{2.65}$$

$$\frac{d}{ds}\left(T_e \sin\theta - Q \cos\theta\right) = W_e \tag{2.66}$$

Eq. 2.65 implies that

$$T_e \cos\theta + Q\sin\theta = \text{Constant} = T_H \tag{2.67}$$

$$T_e = T_H \sec\theta - Q\tan\theta$$

Substituting the foregoing equation into Eq.2.66, noting that $\cos\theta = \frac{dx}{ds}$ and $\sin\theta = \frac{dz}{ds}$,

results in:

$$d\left[T_H \tan\theta - Q\tan\theta\sin\theta - Q\cos\theta\right] = W_e ds$$

$$d\left[T_H \frac{dz}{dx} - Q\frac{dz}{dx}\cdot\frac{dz}{ds} - Q\frac{dx}{ds}\right] = W_e ds$$

Dividing both sides by dx results in

$$\frac{d}{dx}\left[T_H \frac{dz}{dx} - Q\frac{dz}{dx}\cdot\frac{dz}{ds} - Q\frac{dx}{ds}\right] = W_e \frac{ds}{dx}$$

$$\frac{dT_H}{dx}\cdot\frac{dz}{dx} + T_H\frac{d^2z}{dx^2} - \frac{dQ}{dx}\cdot\frac{dz}{dx}\cdot\frac{dz}{ds} - Q\frac{d^2z}{dx^2}\cdot\frac{dz}{ds} - Q\frac{dz}{dx}\cdot\frac{d^2z}{dxds} - \frac{dQ}{dx}\cdot\frac{dx}{ds} - Q\frac{d^2x}{dxds} = W_e\frac{ds}{dx}$$

Neglecting the products of two and three infinitesimals will result into

$$T_H \frac{d^2z}{dx^2} - W_e \frac{ds}{dx} = Q\left(\frac{d^2z}{dx^2}\cdot\frac{dz}{ds} + \frac{dz}{dx}\cdot\frac{d^2z}{dxds} + \frac{d^2x}{dxds}\right) \tag{2.68}$$

2.7.1. Basic Catenary Equations of an SCR

As a typical ultra deepwater riser has a length that is much greater than its diameter, the greatest deformation will be caused by bending (Hibbeler 1998). For this and the fact that this study is concerned with catenary risers which are assumed to be almost perfectly flexible, the effects of the shear force in Eq. 2.68 will be neglected in the formulation of the catenary equations that follow. Hence,

$$T_H \frac{d^2z}{dx^2} - W_e \frac{ds}{dx} = 0 \tag{2.69}$$

Rearranging Eq. 2.69 gives

$$\frac{d^2z}{dx^2} = \frac{W_e}{T_H}\cdot\frac{ds}{dx} \tag{2.70}$$

Since $ds^2 = dx^2 + dz^2$, we have

$$\frac{ds}{dx} = \sqrt{1+\left(\frac{dz}{dx}\right)^2} \tag{2.71}$$

Hence,

$$\frac{d^2z}{dx^2} = \frac{W_e}{T_H}\cdot\sqrt{1+\left(\frac{dz}{dx}\right)^2} \tag{2.72}$$

Integrating Eq. 2.72 with respect to x gives

$$\sinh^{-1}\left(\frac{dz}{dx}\right)=\frac{W_e}{T_H}x+C \tag{2.73}$$

$$\frac{dz}{dx}=\sinh\left(\frac{W_e}{T_H}x+C\right) \tag{2.74}$$

Again, integrating Eq. 2.74 with respect to x gives

$$z=\frac{T_H}{W_e}\cosh\left(\frac{W_e}{T_H}x+C\right)+C_1 \tag{2.75}$$

When $x=0,\ z=-h$, we have

$$-h=\frac{T_H}{W_e}\cosh(C)+C_1 \ \ or$$

$$C_1=-h-\frac{T_H}{W_e}\cosh(C)$$

Hence, Eq. 2.75 becomes

$$z+h=\frac{T_H}{W_e}\left[\cosh\left(\frac{W_e}{T_H}x+C\right)-\cosh(C)\right] \tag{2.76}$$

C is obtained by applying the boundary condition at the seabed to Eq. 2.73. For non-zero slope, the boundary condition at $x=0$ and $z=-h$ is $\frac{dz}{dx}=\tan\theta_1$, so that

$$C=\sinh^{-1}(\tan\theta_1) \tag{2.77}$$

In this study, it is assumed that the riser attachment point is at $x=\overline{X}$ and $z=0$. It is also noted that for a touchdown point on the seabed with non-zero slope, $\tan\theta_1=\frac{T_{V_1}}{T_H}$. Eq. 2.76 then becomes

$$h=a\left[\cosh\left(\frac{\overline{X}}{a}+\sinh^{-1}\left(\frac{T_{V_1}}{T_H}\right)\right)-\cosh\left(\sinh^{-1}\left(\frac{T_{V_1}}{T_H}\right)\right)\right] \tag{2.78}$$

where

$$a = \frac{T_H}{W_e}$$

$h =$ water depth,

$T_{V_1} =$ vertical component of the riser tension at the seabed,

$T_H =$ horizontal component of the riser tension which is a constant,

$\theta_1 =$ angle of the riser at the touchdown point from the horizontal seabed.

Eq. 2.78 is the well known general equation of a simple catenary with non-zero slope at the seabed (Dingwall 1997) and is the same as the second equation in Eq. 2.21.

The equation for the curved length of the SCR can be obtained by substituting Eq. 2.74 into Eq. 2.71 as follows

$$\frac{ds}{dx} = \cosh\left(\frac{W_e}{T_H}x + C\right) \tag{2.79}$$

$$ds = \cosh\left(\frac{W_e}{T_H}x + C\right)dx$$

$$s = a\sinh\left(\frac{x}{a} + C\right) + C_1$$

Since $s = 0$ at $x = 0$, we have $C_1 = -a\sinh(C)$. From Eq. 2.77, it can be shown that

$$s = a\left[\sinh\left(\frac{x}{a} + \sinh^{-1}\left(\frac{T_{V_1}}{T_H}\right)\right) - \frac{T_{V_1}}{T_H}\right] \tag{2.80}$$

The equation for the horizontal projection, x of the SCR curved length, s at any point can be obtained from Eq. 2.80 as

$$x = a\left[\sinh^{-1}\left(\frac{s}{a} + \frac{T_{V_1}}{T_H}\right) - \sinh^{-1}\left(\frac{T_{V_1}}{T_H}\right)\right] \tag{2.81}$$

Eqns. 2.80 and 2.81 are equivalent to Eq. 2.21. The riser tension T_e can be obtained from Eq. 2.67 neglecting the shear component as

$$T_e = T_H \sec\theta = T_H \frac{ds}{dx}$$

$$T_e = T_H \cosh\left(\frac{x}{a} + \sinh^{-1}\left(\frac{T_{V_1}}{T_H}\right)\right) \tag{2.82}$$

The riser vertical tension component, T_V can be found from Eq. 2.74 and the following relationship

$$\frac{T_V}{T_H} = \frac{dz}{dx}$$

$$T_V = T_H \frac{dz}{dx}$$

$$T_V = T_H \sinh\left(\frac{W_e}{T_H} x + \sinh^{-1}\left(\frac{T_{V_1}}{T_H}\right)\right) \tag{2.83}$$

Based on Eqn. 2.64 and 2.74, the curvature K of the SCR is given by

$$K = \left[a\cosh^2\left(\frac{x}{a} + \sinh^{-1}\left(\frac{T_{V_1}}{T_H}\right)\right)\right]^{-1} \tag{2.84}$$

Substituting Eq. 2.84 into Eq. 2.63 gives the expression for the bending moment M as

$$M = EI \cdot \left[a\cosh^2\left(\frac{x}{a} + \sinh^{-1}\left(\frac{T_{V_1}}{T_H}\right)\right)\right]^{-1} \tag{2.85}$$

From Eqns. 2.62 and 2.63, the shear force Q is written as

$$Q = \frac{dM}{ds} = EI \cdot \frac{dK}{ds} \text{ (see Appendix B for the full expression)} \tag{2.86}$$

Finally, the expression for the bending stress σ_b may be obtained from

$$\sigma_b = \frac{M}{I} y \tag{2.87}$$

Substitution Eq. 2.85 into Eq. 2.87 gives

$$\sigma_b = \pm Ey \cdot \left[a \cosh^2 \left(\frac{x}{a} + C \right) \right]^{-1} \tag{2.88}$$

where y is the transverse distance of the point under consideration from the neutral axis of the cross section of the SCR.

Eqns. 2.78, 2.80 and 2.81 are the standard equations of a catenary with non-zero slope at the seabed as seen before in Section 2.3.

2.8. Riser Configurations

Just like mooring lines, the SCRs can also be of single or multi-component and will therefore have different configurations during their service life. When modelled as a multi-component SCR line, the methodology outlined in Section 2.3 will apply. However, when modelled as a single component, the SCR will basically have only two configurations; zero and non-zero slope at seabed. In this case only the first and the last configurations described in Section 2.3 apply as discussed below.

2.8.1.1. *Configuration one: Part of SCR lying on seabed*

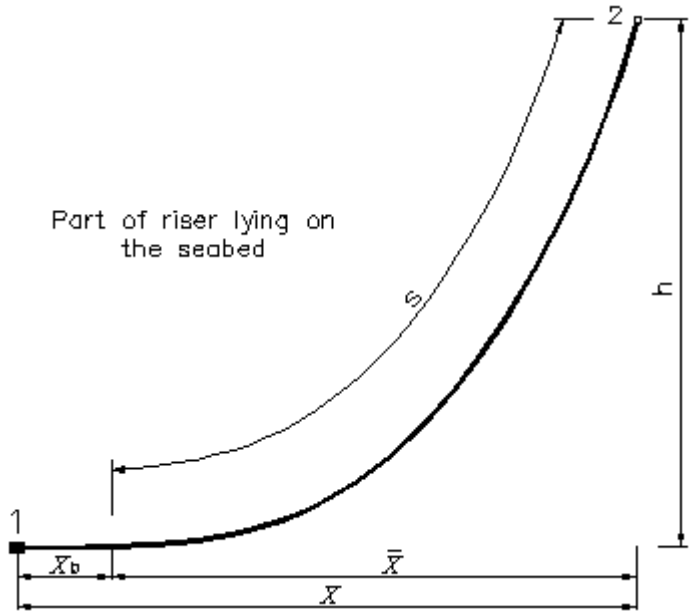

Fig. 2. 11 Steel catenary riser configuration one

In this configuration Eqns. 2.78 and 2.80 are applied with $T_V = \theta_o = C = 0$ and the total horizontal distance, X of the riser attachment point is given by

$$X = \overline{X} + X_b = \overline{X} + L - S \tag{2.89}$$

where

L is the total length of the SCR

S is the curved length of the riser

$\overline{X}$ is the projected horizontal length of S on the seabed

Therefore Eqn. 2.78 and 2.80 reduce to

$$h = a\left[\cosh\left(\frac{\overline{X}}{a}\right) - 1\right] \tag{2.90}$$

$$S = a \cdot \sinh\left(\frac{\overline{X}}{a}\right) \tag{2.91}$$

From Eqns. 2.90 and 2.91 it can be shown that

$$S = h\left(1+\frac{2a}{h}\right)^{\frac{1}{2}}, \text{ and } \overline{X} = a\cdot\cosh^{-1}\left(1+\frac{h}{a}\right)$$

Hence, Eq. 2.89 becomes

$$X = L - h\left(1+\frac{2a}{h}\right)^{\frac{1}{2}} + a\cosh^{-1}\left(1+\frac{h}{a}\right) \tag{2.92}$$

Eqns. 2.89 to 2.92 are similar to those in Eqns. 2.23 to 2.26. Thus, the horizontal and vertical components of SCR stiffness of the SCR may be obtained from Eqns. 2.27 and 2.29 respectively.

2.8.1.2. ***Configuration Two: No part of SCR lying on the seabed***

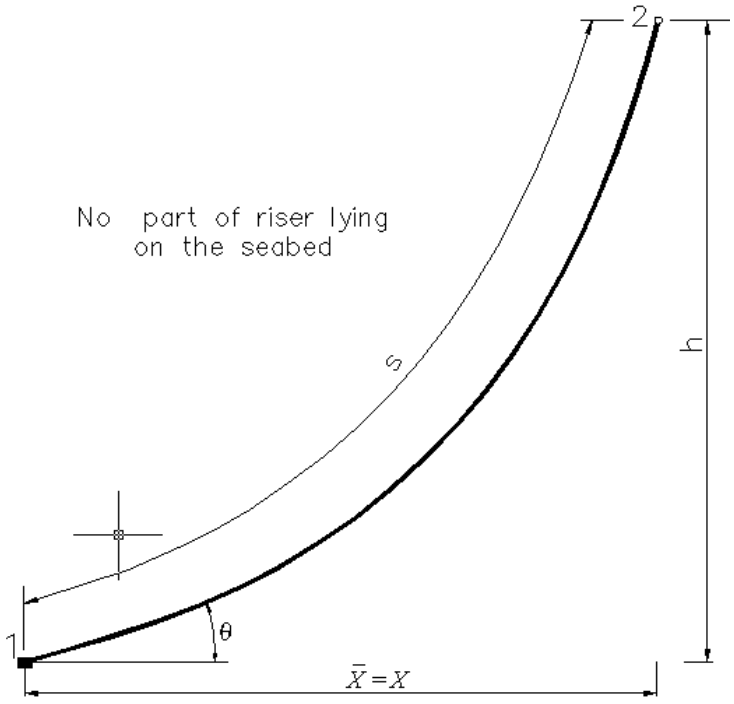

Fig. 2. 12 Steel catenary riser configuration two

In this configuration Eqns 2.77 to 2.88 can be applied. At $x = X = \overline{X}$, $s = L$ and we have

$$h = a\left[\cosh\left(\frac{X}{a}+\sinh^{-1}\left(\tan\left(\theta_1\right)\right)\right)-\cosh\left(\sinh^{-1}\left(\tan\left(\theta_1\right)\right)\right)\right] \tag{2.93}$$

$$X = a\left[\sinh^{-1}\left(\frac{L}{a}+\tan(\theta_1)\right)-\sinh^{-1}(\tan(\theta_1))\right] \tag{2.94}$$

Putting Eq. 2.98 into Eq. 2.97 results in

$$h = a\cdot\left[\cosh\left(\sinh^{-1}\left(\frac{L}{a}+\tan(\theta_1)\right)\right)-\cosh\left(\sinh^{-1}(\tan(\theta_1))\right)\right] \tag{2.95}$$

The horizontal restoring coefficient, k_{11} due to the SCR is then obtained from the differentiation of Eq. 2.94 with respect to T_H as

$k_{11} = \left(\frac{dX}{dT_H}\right)^{-1}$ (see Appendix B for the full expression)

From Eq. 2.87, the riser vertical tension component, T_{V_2} at attachment point is given by

$$T_{V_2} = T_H \sinh\left(\frac{W_e}{T_H}X+\sinh^{-1}\left(\frac{T_{V_1}}{T_H}\right)\right) \tag{2.96}$$

The vertical restoring coefficient, k_{33} due the SCR is obtained by differentiating Eq. 2.96 with respect to h as follows

$$k_{33} = \frac{dT_{V_2}}{dh} \text{(see Appendix B for the full expression)} \tag{2.97}$$

2.9. Summary

Catenary equations for the analysis of multi-component mooring and steel catenary risers have been discussed in detail along with implementation methodology. Though based on existing methodologies, it has been modified and presented in a way which is both easier to understand and efficient compared to existing ones. An algorithm for a step by step implementation is shown in Fig. 2.13 below.

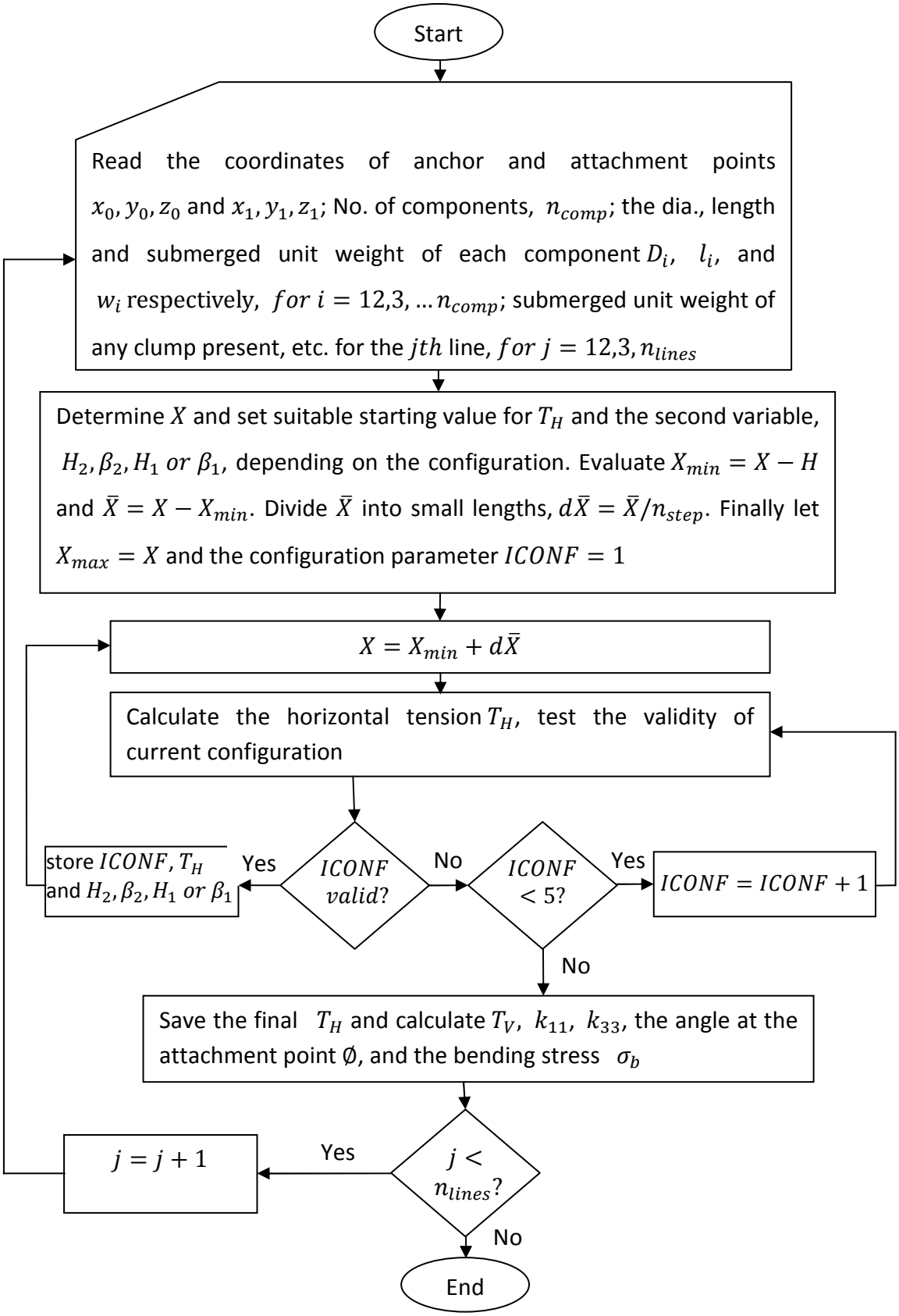

Fig. 2. 13 Algorithm for a step by step implementation of static mooring/SCR analysis

2.10. Conclusions

Methodologies have been presented for the static analysis of multi-component mooring lines and steel catenary risers for any number of line components and clump weights including an algorithm for implementation. A four component mooring line has been used to demonstrate how the basic catenary equations for the different components can be combined into one or two nonlinear equations depending on the instantaneous configuration of the line. These equations can then be solved simultaneously using iterative techniques as described above for the horizontal tension, T_H and the restoring coefficients, k_{11} and k_{33} at the attachment points of the lines.

Comparison of results obtained using the methodology developed here to published results has been carried out using the multi-component mooring line data in Ansari (1980). The analysis was carried out at incremental horizontal distance of 0.01m. The analysis time was four seconds and the results were found to generally agree with those of Ansari (1980) as shown in Fig. 2. 8

CHAPTER

3 QUASI-STATIC ANALYSIS OF MOORING AND STEEL CATENARY RISERS

3.1. Introduction

FPSOs have become the favourite platform for oil and gas exploration as the depth of exploration keeps increasing. At such deep locations in the seas, the FPSO vessel is subjected to extremely hostile environmental conditions. The vessel's position is maintained within operational limits through a mooring system. It is therefore, important to determine the range of all the possible vessel excursions and the corresponding mooring line and riser tensions. It is also vital to determine all the possible failure modes such as mooring line failure. Several methods have been developed in the past for the analysis of mooring systems in shallow and deepwater employing static, quasi-static or dynamic approach. These approaches to mooring system analysis have been described by Ansari and Khan (1986).

Static method is usually carried out at an initial stage of mooring system design and has a disadvantage that the important features of FPSO dynamics such as the effects of added mass, damping and wave excitations are absent. Hence, large safety factors are required for taking uncertainties into account. The method applies the total steady environmental force to the load-excursion curve of the mooring system to find the static offset of the vessel and then use the resultant of the static offset and dynamic offset caused by the first-order and second-order waves on the line excursion curve of the most loaded line to find the corresponding maximum tension. The dynamic offset may be estimated statically from coarse estimation of wave forces and the system stiffness (Chan and Ha 2008).

The quasi-static method is used when the motion responses of a moored vessel are outside the wave exciting frequency range of the mooring system. This means that the dynamic behaviour of the lines is negligible and the mooring lines will only respond statically to the motions of the vessel. The dynamic motion responses of the vessel coupled with the static catenary riser/mooring system can then be used to find the resulting maximum line tension (Ansari 1979; Schellin et al. 1982; Tahar and Kim 2003). Quasi-static analysis may be carried out in either the frequency domain or the time domain. The weakness of this method is that the effects of line dynamics which may be significant if the line inertia is important are ignored.

In the dynamic approach, the equations of motion of line dynamics are formulated and numerically solved to develop tension-displacement characteristics, which is then used as non-linear restoring forces in the motion response analysis of the moored vessel

(Ansari and Khan 1986). This kind of analysis is usually performed in the time domain and is time consuming. Time-domain simulations of motion responses of a moored vessel in irregular seas are computationally intensive even in quasi-static mooring analysis since the equations of motion are integrated in the time domain and a number of test cases must be considered due to the random nature of the seastates (Chan and Ha 2008). It is therefore common practice to carry out the analysis in frequency domain combined with spectral analysis to predict the extreme motions of the system with reasonable engineering accuracy. However the combination of the extreme first-order wave-induced motion and second-order slow-drift motion in the frequency domain analysis is an engineering approximation for design purpose only and is uncertain. In this chapter, the analysis of a multi-component mooring lines and steel catenary risers system based on the formulations developed in chapter two is presented in both the time- as well as frequency-domain.

3.2. The FPSO, mooring lines and steel catenary risers (SCR)

The FPSO hull, mooring and risers used in this research are based on a similar FPSO operating in the Atlantic Ocean about 200km offshore Nigeria in West Africa referred to here as the ARDO FPSO. It is moored in a mean water depth of 2500m with a spread mooring.

3.2.1. ARDO FPSO Particulars

The main particulars of the FPSO are shown in Table 3. 1. The panel model of the wetted hull surface discretised with 1750 panels is shown in Fig. 3. 1.

Table 3.1 FPSO Details

Description	Parameter	Value
Length over all	LOA	330.00m
Length between perpendiculars	L_{PP}	316.00m
Beam	B	61.00m
Depth	D	31.00m
Draught	T	25.50m
Block coefficient	C_B	0.96
Displacement	Δ	478034.42T
Long. Center of gravity from amidships, +ve aft	L_{CG}	3.115m
Vertical center of gravity from baseline	V_{CG}	24.16m
Pitch / yaw radii of gyration	r_{yy}/r_{zz}	79.20m
Roll radius of gyration	r_{xx}	24.40m

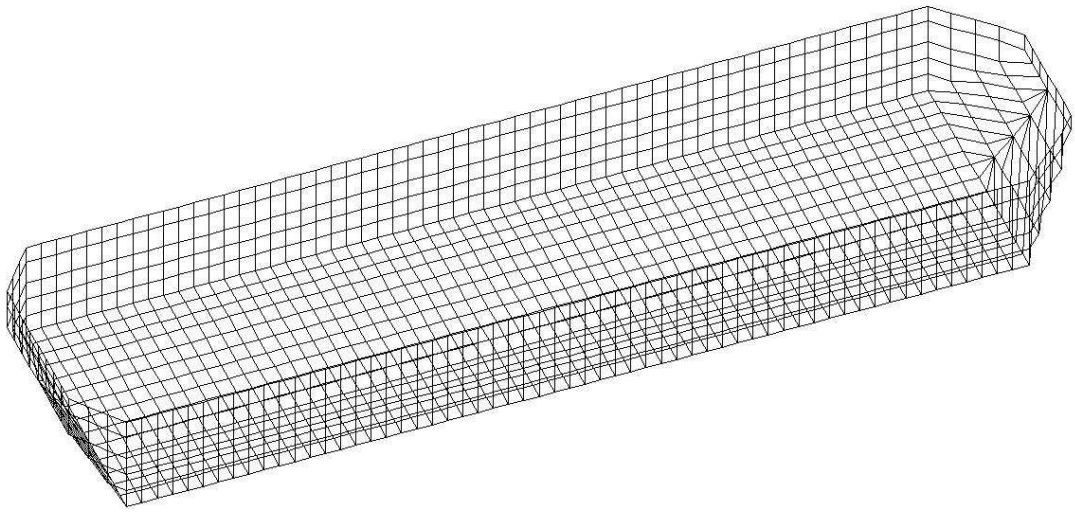

Fig. 3.1 Panel model of FPSO wetted surface

3.2.2. Mooring lines Particulars

The mooring system is a spread and semi-taut with 16 lines consisting of 4 sets of 4 lines each as shown in Fig. 3.3. Each mooring line consists of 3 segments in the form: Studless chain – Spiral strand wires – Studless chain respectively with a total length of 4552m. Details of the mooring line components are shown in Table 3.2. The mooring lines are

anchored to the seabed by means of suction piles. The maximum allowable FPSO horizontal excursions are ±5% of water depth in intact conditions and ±8% of water depth in damage (one line broken) conditions (Childers 1973). The nominal anchor radius is 3670m. A typical multi-component mooring line of three segments is shown in Fig. 3.2.

Table 3.2 Mooring Line Details

Item	Dia. (mm)	MBL (T)	L (m)	Submerged Weight (N/m)
Top Chain	142	1670	200	3475.3
Spiral Strand Wire	122	1427	3993	548.9
Bottom Chain	142	1670	359	3475.3

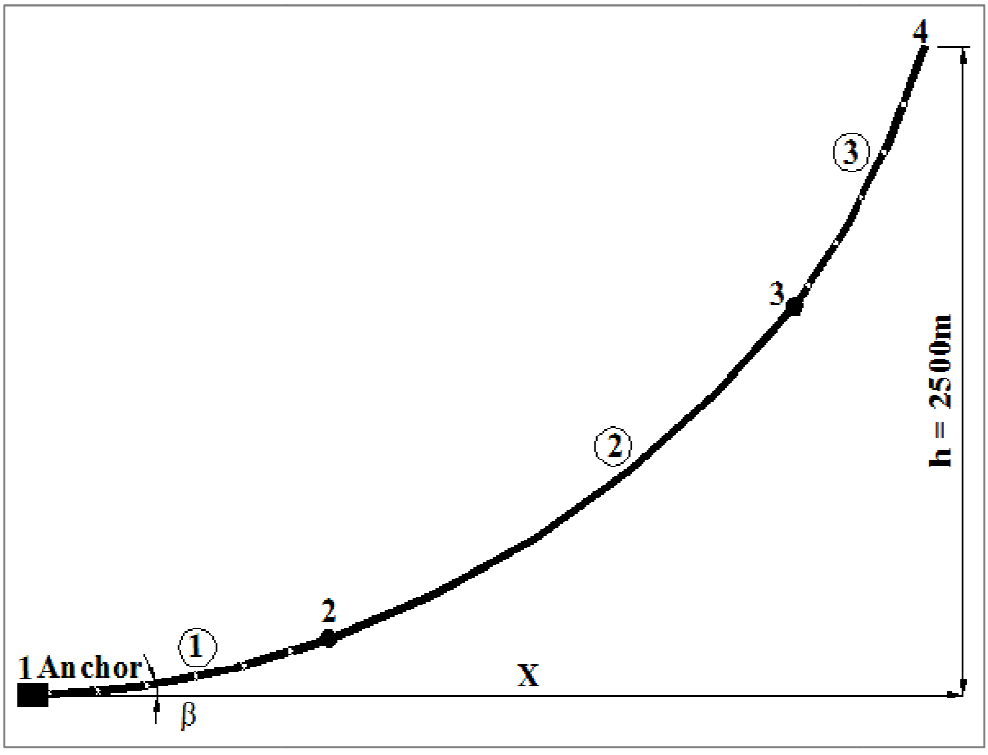

Fig. 3. 2 A typical multi-component mooring line

3.2.3. Steel Catenary Risers (SCR) particulars

There are 12 steel catenary risers (SCRs) with flex joints and top spools connected to the FPSO. Eight of these are production lines of 10in internal diameter plus 100mm thermal insulation, and four water injection lines of 10in internal diameter. There is no information regarding the actual arrangement or pattern of the risers around, and how they are connected to the FSPO. Therefore in this study the risers are equally distributed – 6 each on port and starboard as shown in Fig. 3.3. The riser details are shown in Table 3.3.

Table 3.3 Steel catenary riser details

Item	Units	8 x 10" PFL	4 x 10" WFL
Weight in air	N/m	278.3	194.9
weight in water	N/m	85	134.85
Buoyancy	N/m	193.3	60.05
EI	MT-m2	2261.0	3123.2
EA	MT	274100.0	402940.5

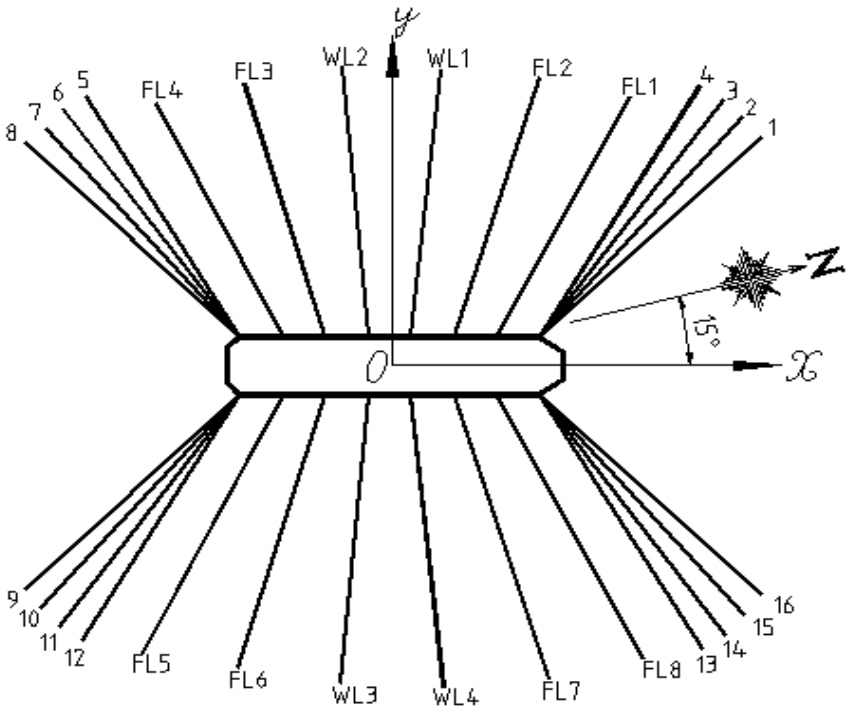

Fig. 3. 3 Mooring and SCRs Layout of ARDO FPSO

3.2.4. Met-Ocean Data

The environmental forces in West Africa are predominantly unidirectional. Hence, in this study the extreme 100 year environmental conditions are considered as follows: 3 seconds sustained gust wind of 36m/s from the east-north east direction (127.5^{o}); wave of 3.6m significant height and peak period of 15.9s due to swell from the south - south west direction (352.5^{o}) and associated inline current of 2.0m/s. In addition to these mild conditions, the severe environmental conditions in the Gulf of Mexico with significant wave height of 15.8m and peak period of 16.9s have also been considered to test the mooring and riser system.

3.2.5. Coordinate system and sign convention

The coordinate system and sign convention used in the study is shown in Figure 3. 4 below.

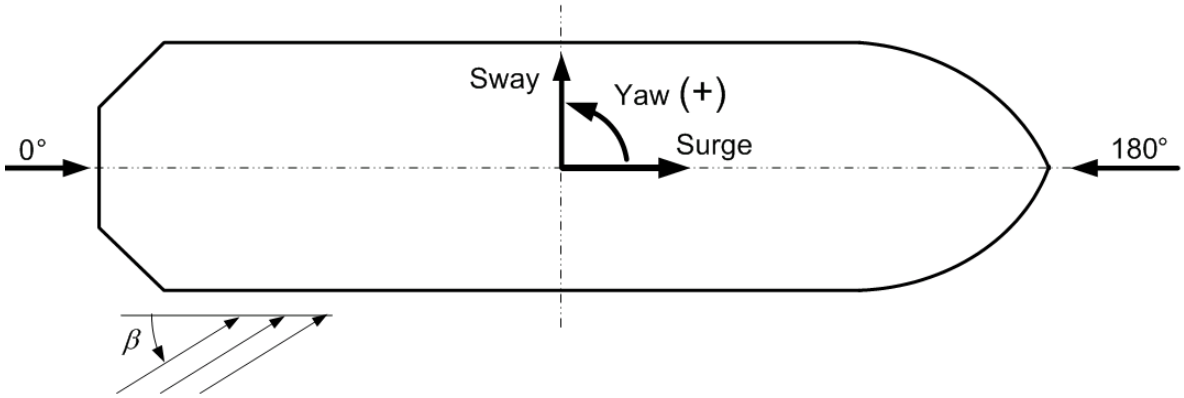

Fig. 3. 4 Coordinate system and sign convention

3.3. Static tension and bending stress characteristics

The static tension in each mooring cable and steel catenary riser line at a given horizontal distance X from its anchor point for mooring line or from its bottom joint for SCR line can be obtained through their load-excursion characteristics. For a multi-component line the load-excursion characteristics of the line is obtained by solving the nonlinear catenary equations simultaneously presented in Chapter 2.

Based on the formulations of a mulit-component catenary line, a custom mooring system analysis FORTRAN program MOOSA has been developed and used to calculate the line tension with a given horizontal distance X. The variations of the horizontal component of line tension with horizontal distance X for the mooring and SCR lines are

shown in Fig. 3.5 while the touchdown point (TDP) bending stress characteristics of the SCR lines against the distance from the bottom joint are shown in Fig. 3.6.

It can be observed from Fig. 3.5 that the horizontal tension $\mathrm{T_H}$ in the mooring line is zero when$0 \leq \mathrm{X} \leq \mathrm{L} - \mathrm{H}$, where X is the horizontal distance between the anchor and attachment points, L is the total length of the line, H is the elevation of the attachment point above the seabed. $\mathrm{T_H}$, then begun the increase fairly linearly through the different line configurations until X approaches its maximum value towards the beginning of configuration five. At this point it is observed that any small increase X results in a disproportionate increase in$\mathrm{T_H}$, that is the analysis becomes highly nonlinear. Similarly, it is evident from Fig. 3.6 that the bending stress at the touch point of the SCRs increases with the attachment point moves from maximum X towards $X_{min} = \mathrm{L} - \mathrm{H}$.

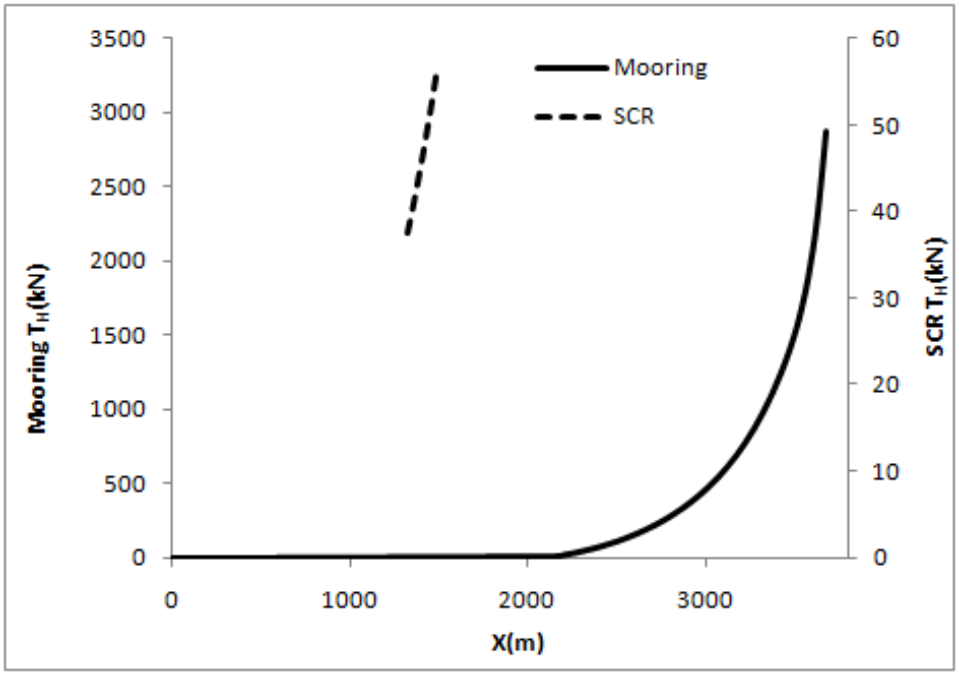

Fig. 3. 5 Tension displacement characteristics

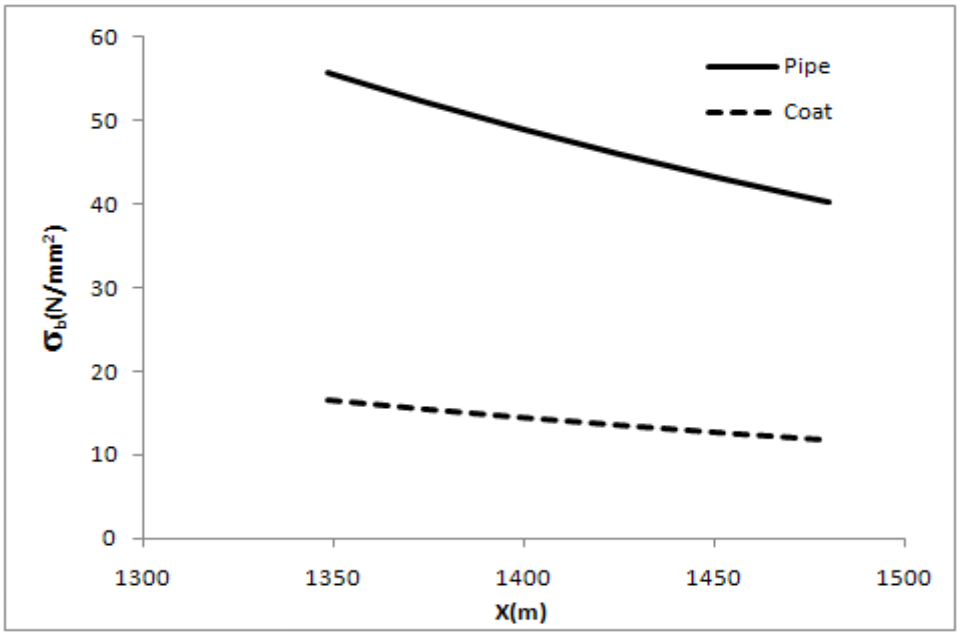

Fig. 3. 6 SCR Touchdown point bending stress characteristics

3.4. Motion Response Analysis of FPSO

For a moored FPSO oscillating as a rigid body in six degrees of freedom about its mean position with complex amplitudes ξ_k, where $k = 1, 2, 3, 4, 5, 6$, refer to surge, sway, heave, roll, pitch and yaw modes of motion respectively, the coupled linear motions of a moored FPSO can be expressed by Eq. 3.1. These motions are with respect to the rectangular co-ordinate system $o - xyz$ as shown in Fig. 3.4. The z-axis is vertically upward through the centre of gravity of the body with the origin o on the mean free surface and the x-axis is longitudinally pointing to the bow.

$$\sum_{k=1}^{6}\left[\left(M_{jk} + A_{jk}\right)\ddot{\xi}_k + B_{jk}\dot{\xi}_k + \left(C_{jk} + K_{jk}\right)\xi_k\right] = F_j^W + F_j^V \text{ for } j = 1, 2, \ldots 6 \qquad (3.1)$$

where $\ddot{\xi}_k$ and $\dot{\xi}_k$ are the motion acceleration and velocity respectively. M_{jk} and A_{jk} are the elements of mass and added mass matrices respectively, B_{jk} is the damping, C_{jk} is the restoring coefficient due to change in buoyancy, K_{jk} is the stiffness due to mooring

system, F_j^W is the wave exciting force (or moment) and F_j^V is the viscous excitation force. The indices j and k indicate the direction of the fluid force and the mode of motion respectively. The hydrodynamic coefficients in the equations of motion may be considered as linear dependence of fluid forces due to non-lift potential flow and viscous flow such that $B_{jk} = b_{jk} + \hat{b}_{jk}$, etc. where b_{jk} is the wave damping coefficient and $\hat{b}_{jk}$ is the viscous damping coefficient.

The viscous effects on damping, restoring and excitation forces may be found using the Froude-Krylov approach together with the cross-flow and the pseudo-steady state assumptions (Chan 1992). It is noted that the viscous effects terms in the equations of motion depend upon the amplitudes of motion responses. Thus, the equations of motion are solved iteratively until a reasonable convergence of motion amplitudes is obtained.

The unsteady motions of the stationary FPSO and the fluid are assumed to be small so that the unsteady body boundary and free surface conditions can be linearised. The solution of the linearised unsteady motion problem is constructed by means of the three-dimensional Green's function integral equation method. Thus the domain of the problem is reduced from the infinite fluid domain to the hull surface on which oscillating source singularities are distributed. The Green's function satisfies the three-dimensional Laplace's equation, the linearised free surface condition, the sea bottom condition and the far-field radiation condition. Hydrodynamic coefficients and wave exciting forces given in Eq. 3.1 can be obtained after solving the integral equation which satisfies the linearised body boundary conditions (Chan 1992). This is accomplished by the

discretisation of the mean wetted body surface into a finite but large number of flat panels (Hess and Smith 1962). The mooring stiffness is obtained from the solution of the non-linear catenary equations at initial static equilibrium position of the vessel.

Numerical computations were carried out to predict the first-order motion responses of the FPSO to regular waves at different wave frequencies for the main wave heading angle of 352.5^{o} and the resulting mean second-order forces and moment in the frequency domain. For a unidirectional environment such as West Africa it is enough to cover the prevailing direction of the environmental loads only.

The motion response amplitude operators (RAOs) of surge, sway and yaw modes are shown in Fig. 3.7. The corresponding phase angles at different wave frequencies are shown in Fig. 3.8. The RAOs are non-dimensionalised by wave amplitude ζ and wave number κ. The surge and sway mean second-order forces and yaw moments on the FPSO can be calculated by means of near-field method (Pinkster 1979) or far-field method (Maruo 1960; Newman 1967). In the present study, the mean second-order surge force $\overline{\mathrm{F}}_1^{(2)}$, sway force $\overline{\mathrm{F}}_2^{(2)}$ and yaw moment $\overline{\mathrm{F}}_6^{(2)}$ were calculated by integrating the first-order hydrodynamic pressures as explained in Chan and Ha (2008).

The calculated surge and sway drift forces and mean second-order yaw moments on the FPSO at different wave frequencies for the prevailing wave heading are shown in Fig. 3.9. A negative value of surge drift force indicates that the force is in negative x direction, while a positive value of sway drift force means that the force is in positive y direction. The positive yaw moment indicates that the vessel yaws anti-clockwise. The

spikes in the drift forces and yaw moment may be caused by irregular frequency phenomenon where no unique solution exists.

Fig. 3. 7 Surge, sway and yaw motion amplitudes

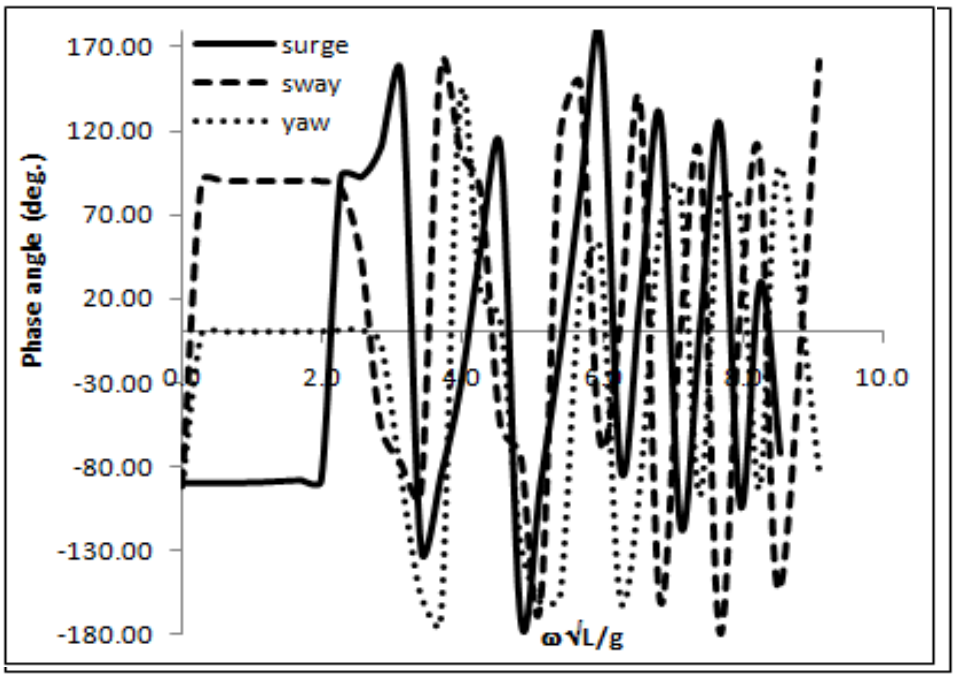

Fig. 3. 8 Surge, sway and yaw motion phase angles

The value of sway drift force is larger than that of surge drift force as shown in Fig. 3.9. This is because the lateral area of a vessel is greater than the frontal area. The mean second-order yaw moment on the FPSO is negligible in the 352.5^{o} head waves.

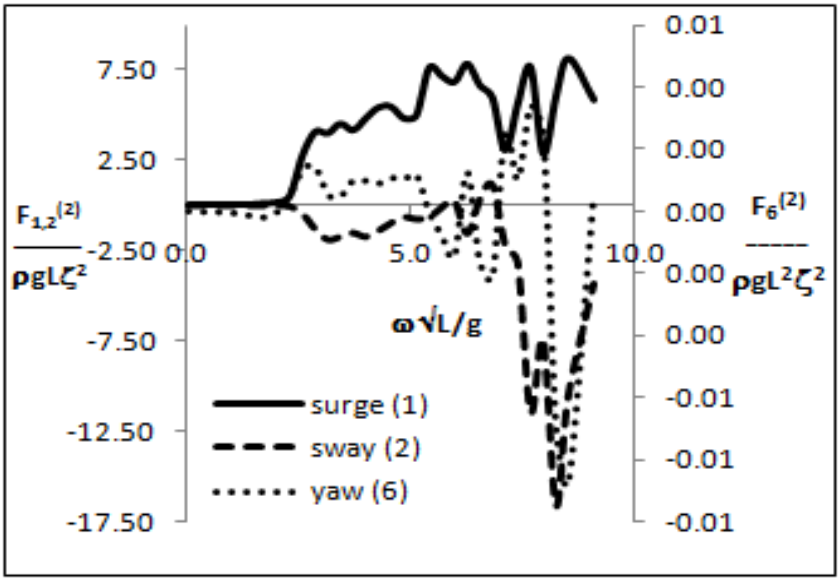

Fig. 3. 9 Mean second order forces and yaw moment

3.5. Quasi-Static Analysis in Frequency Domain

Because of the constantly changing environment of the sea, motion response and mooring analysis require a large number of variations covering all possible wave directions not only in regular waves but also in irregular waves. However, when the environmental loads are considered to be unidirectional only one wave direction needs to be considered. Within the framework of linearization discussed in Section 1.5, the responses of a floating body to irregular waves can be considered as the summation of the responses to regular waves of all frequencies. Thus, stochastic analysis can be carried out to predict the various statistical characteristics of dynamic motion responses.

The statistical properties such as the maximum and significant values of the first-order and second order wave-induced motions at the attachment points of the mooring lines are presented below.

The maximum excursion of the attachment point $(\mathrm{x},\mathrm{y},\mathrm{z})$ of a mooring line in the $\mathrm{j}-\mathrm{th}$ mode of motion may be obtained by combining the first-order wave-induced motion with second-order motion in accordance with the empirical equations in (DNV 1996):

$$\begin{aligned}\chi_j &= \bar{\xi}_j + \hat{\xi}_j^{(2)} + \xi_{j1/3}^{(1)};\ when\ \hat{\xi}_j^{(2)} > \hat{\xi}_j^{(1)} \\ \chi_j &= \bar{\xi}_j + \hat{\xi}_j^{(1)} + \xi_{j1/3}^{(2)};\ when\ \hat{\xi}_j^{(2)} < \hat{\xi}_j^{(1)}\end{aligned} \tag{3. 2}$$

where $\bar{\xi}_j = \bar{\xi}_j^W + \bar{\xi}_j^C + \bar{\xi}_j^{(2)}$ is the mean offset due to steady wind force $\overline{\mathrm{F}}_{\mathrm{j}}^{\mathrm{W}}$, current force $\overline{\mathrm{F}}_{\mathrm{j}}^{\mathrm{C}}$ and mean second-order force $\overline{\mathrm{F}}_{\mathrm{j}}^{(2)}$ respectively. $\bar{\xi}_j^W$ and $\bar{\xi}_j^C$ are obtained from the static equilibrium of the FPSO subject to steady wind and current forces only, while $\bar{\xi}_j^{(2)}$ can be obtained from Eq. 3.3. $\hat{\xi}_j^{(1)}$ and $\xi_{j1/3}^{(1)}$ are the most probable maximum and significant values of the first-order motion in the $\mathrm{j}-\mathrm{th}$ mode of motion respectively while $\hat{\xi}_j^{(2)}$ and $\xi_{j1/3}^{(2)}$ are the most probable maximum and the significant values of the second-order motion in the $\mathrm{j}-\mathrm{th}$ mode of motion. These values may be obtained by means of spectral analysis with the applications of the following equations:

$$\bar{\xi}_j^{(2)} = \frac{2\int_0^\infty \bar{F}_j^{(2)} S(\omega) d\omega}{K_{jj}} \tag{3. 3}$$

$$\xi_{j1/3}^{(1)} = 2\sqrt{m_0} \tag{3. 4}$$

$$\hat{\xi}_j^{(1)} = \sqrt{2m_0 \ln(N)} \tag{3. 5}$$

$$\xi_{j1/3}^{(2)} = 2\sigma_j \tag{3. 6}$$

$$\hat{\xi}_j^{(2)} = \sqrt{2\ln\left(3600\,T/T_{jn}\right)} \tag{3. 7}$$

$$m_0 = \int_0^\infty \left|\xi_j(x,y,z,\omega,\beta)\right|^2 S(\omega) d\omega \tag{3. 8}$$

$$m_2 = \int_0^{\infty} \omega^2 \left|\xi_j(x, y, z, \omega, \beta)\right|^2 S(\omega) d\omega \tag{3. 9}$$

$$\sigma_j^2 = \int_0^{\infty} \frac{S_{Fj}(\mu)}{\left\{K_{jj} - \left(M + A_{jj}\right)\mu^2\right\}^2 + B_{jj}^2 \mu^2} d\mu \tag{3. 10}$$

$$S_{Fj}(\mu) = 8\int_0^{\infty} S(\omega) S(\omega + \mu)\left[\overline{F}_j^{(2)}(\omega + \mu/2)\right]^2 d\omega \tag{3. 11}$$

$$N = 3600 T n' \tag{3. 12}$$

$$n' = \frac{1}{2\pi}\sqrt{\frac{m_2}{m_0}} \tag{3. 13}$$

where m_0 and m_2 are respectively the area and second moment of area of the first-order motion response spectrum, $\left|\xi_j(x, y, z, \omega, \beta)\right|$ is the first-order wave-induced motion amplitude operator of the attachment point $(\mathrm{x}, \mathrm{y}, \mathrm{z})$ at wave frequency ω and heading angle β, $S(\omega)$ is the wave spectral density, S_{Fj} is the spectral density of the low frequency drift force and σ_j is the root-mean-square value of the second-order motion in the single degree of freedom in the $\mathrm{j-th}$ mode (Pinkster 1979), A_{jj} and B_{jj} are respectively the added mass and damping at the natural frequency of the $\mathrm{j-th}$ mode motion, T is the duration of storm in hours and n' is the average number of a motion response per unit time. N is the number of responses in a given storm, T_{jn} and ω_{jn} are the natural period and frequency of the FPSO in the $\mathrm{j-th}$ mode respectively.

Once the values of surge excursion X_1 and sway excursion X_2 from the initial equilibrium are obtained from Eq. 3.2, the maximum horizontal distance X can be calculated and input to the nonlinear catenary equations which will then be solved simultaneously to get the maximum horizontal tension component T_H in the mooring line. It should be noted that this quasi-static approach is conservative since the maximum surge and sway excursion may not occur simultaneously.

3.5.1. Frequency domain analysis results

Based on the forgoing formulations and the results of the first-order motion responses and mean second-order forces on the Ardo FPSO obtained in the frequency domain, a spectral analysis was performed to predict the extreme excursions of the mooring attachment points and resulting maximum tensions in the mooring lines and bending stress in the SCRs in a design extreme sea state of significant wave height 3.6m and zero-crossing period 11.5 seconds in West Africa, and 100 year design sea state of significant wave height 7.3m and zero-crossing period 8.68 seconds for winter storm (DNV, 1996) in the Gulf of Mexico (GoM). The Two-parameter ITTC wave spectrum was used. The results showed that mooring line 9 is the most loaded while fluid line 8 and water line 4 had the least tensions and therefore correspondingly higher bending stresses.

3.5.1.1. *West Africa (WA) condition*

The maximum values of surge and sway motions based on Eq. 3.2 are shown in Table 3.4 for the West Africa condition.

Table 3.4 Maximum excursions of the FPSO attachment point 9 for WA

Parameter	Moorings only		Moorings + SCRs	
	Surge X_1(m)	Sway X_2(m)	Surge X_1(m)	Sway X_2(m)
$\bar{\xi}_j$	9.259	-1.599	9.324	-1.515
$\xi_{j1/3}^{(1)}$	0.409	0.063	0.409	0.063
$\xi_{j1/3}^{(2)}$	13.305	2.547	13.178	2.402
$\hat{\xi}_j^{(1)}$	0.733	0.133	0.733	0.133
$\hat{\xi}_j^{(2)}$	37.914	7.259	37.545	6.840
Maximum (see Eq.2)	**47.583**	**5.724**	**47.279**	**5.388**

Table 3. 5 Maximum mooring and Minimum SCR line tensions for WA

Line	T (kN)	Case
Mooring line 9	5656.17	Mooring only
Mooring line 9 Fluid line 8 Water line 4	5644.22 264.21 421.22	Mooring + SCR

Table 3. 6 Maximum bending stress of the SCR lines at the touchdown point for WA

Description	σ_b (N/mm^2)	
	Pipe	Coating
Fluid line 8	43.24	12.78
Water line 4	42.14	N/A

It is observed in Table 3.4 that the maximum tensions in the lines are caused by the maximum surge excursion in the West Africa condition because the direction of the environment is almost wholly in that direction. It is evident from Tables 3.4 and 3.5 that

the SCRs do not contribute significantly in limiting the excursions of the vessel. A decrease in the maximum excursions in both surge and sway directions has been observed in Table 3.4 when both mooring lines and SCRs were modeled instead of just the mooring lines. These differences were also observed in the line tensions for the two case studies as can be seen in Table 3.5. It is remarkable that both the significant and most probable values of the first-order motions are quite negligible compared to the corresponding values of the slow-drift motions of the Ardo FPSO as demonstrated in Table 3.4. The maximum bending stress at the extreme fibres of both steel and concrete coating as shown in Tabel 3.6 for the West Africa condition are found to be small and within their design strength limits. For high strength concrete grades 30 and above, the design strength according to Eurocode 2 is 17N/mm^2 and above (Bamforth, P. et al. 2008). The allowable bending stress in steel is 0.6Fy, where Fy is the yield strength for a particular grade of steel. For a 248N/mm^2 grade of steel the allowable bending stress is 148N/mm^2.

3.5.1.2. *Gulf of Mexico (GoM) condition*

The maximum values of surge and sway motions based on Eq. 3.2 are shown in for the Gulf of Mexico condition is shown in Table 3.7.

Table 3.7 Maximum excursions of the FPSO attachment point 9 for GoM

Parameter	Moorings only		Moorings + SCRs	
	Surge X_1(m)	Sway X_2(m)	Surge X_1(m)	Sway X_2(m)
$\bar{\xi}_j$	60.835	-11.138	60.015	-10.555
$\xi_{j1/3}^{(1)}$	0.325	0.058	0.325	0.058
$\xi_{j1/3}^{(2)}$	76.428	16.260	75.697	15.333
$\hat{\xi}_j^{(1)}$	0.713	0.079	0.639	0.078
$\hat{\xi}_j^{(2)}$	217.781	46.338	215.670	43.660
Maximum (see Eq.2)	**278.942**	**35.258**	**276.010**	**33.163**

Table 3. 8 Maximum mooring and Minimum SCR line tensions for GoM

Line	T (kN)	Case
Mooring line 9	7754.84	Mooring only
Mooring line 9 Fluid line 8 Water line 4	7754.84 257.78 420.31	Mooring + SCR

Table 3. 9 Maximum bending stress of the SCR lines at the touchdown point for GoM

Description	σ_b (N/mm^2)	
	Pipe	Coating
Fluid line 8	49.29	14.57
Water line 4	42.52	N/A

It can be shown from Table 3.7 that resultant maximum excursion for the Gulf of Mexico (winter storm) condition for the same mooring system is 279 when only mooring lines were modeled and 276m when both mooring and SCR lines were modeled. This is way above the allowable excursions, which for in the intact condition is 125m. Therefore, the analysis for tensions and bending stresses in the lines has been limited to the allowable excursions only. Again as in the case of West Africa condition, the presence of the SCRs has impacted on the magnitude of attachment point excursions as well as the line tensions and bending stresses as is evident from Tables 3.6, 3.8 and 3.9 respectively.

3.6. Quasi-Static Analysis in Time Domain

Although the frequency domain method is practical to some degrees of engineering accuracy, the combination of the extreme first-order wave-induced motion and second-order slow-drift motion in the frequency domain analysis is an engineering approximation for a design purpose only of mooring systems and is conservative. In order to design an optimum mooring system, a time-domain coupled motion and mooring analysis is required. In general, the equations of motion for the six degrees of freedom of a floating vessel are integrated in the time domain and the effects of added mass, damping and non-linear restoring forces due to mooring lines on the motions are included. It is computationally intensive to run this kind of time domain simulation in an irregular sea with storm duration of at least three hours.

In the present study, an alternative time-domain method developed by Chan and Ha (2008) which integrates motion responses to regular waves of all frequencies is adopted and used for a quasi-static analysis of the ARDO FPSO mooring system. Based on

linearization assumption, the wave elevation ζ at the origin of the co-ordinate system and the corresponding first-order motion $\xi_j^{(1)}$at a point (x, y, z) on the floating vessel are the summation of their amplitude components of all frequencies as given by Eqns. 3.14 and 3.15 respectively.

$$\zeta(\mathrm{x},\mathrm{y},\mathrm{t}) = \sum_{\mathrm{m}=1}^{\mathrm{N}} \mathrm{a_m cos}[\omega_\mathrm{m}\mathrm{t} \mp \epsilon_\mathrm{m}] \tag{3. 14}$$

$$\xi_j^{(1)}(x,y,\mathrm{z},t) = \sum_{m=1}^{N} \left|\xi_\mathrm{j}(\mathrm{x},\mathrm{y},\mathrm{z},\omega,\beta)\right| a_m cos\left[\omega_m t \mp \epsilon_m - \theta_{jm}\right] \tag{3. 15}$$

$$a_m = \sqrt{2\mathrm{S}(\omega_\mathrm{m})\delta\omega} \tag{3. 16}$$

where a_m is the wave amplitude component at wave frequency ω_m and ϵ_m is the random phase. θ_{jm} is the corresponding phase angle of the first-order motion RAO$\left|\xi_\mathrm{j}(\mathrm{x},\mathrm{y},\mathrm{z},\omega,\beta)\right|$. N is the number of wave frequency components.

Since the first-order excitations hardly induce the slowly-varying drift motion of a moored vessel and vice versa, the displacement $\xi_j(x,y,\mathrm{z},t)$ of the point in the j-th mode can be assumed to be the resultant of the first-order motion $\xi_j^{(1)}$ at that point and the slowly-varying drift motion $\xi_j^{(2)}$ of the vessel as

$$\xi_j(x,y,\mathrm{z},t) = \xi_j^{(1)}(x,y,\mathrm{z},t) + \xi_j^{(2)}(t) \tag{3. 17}$$

The second-order motion in the j-th mode $\xi_j^{(2)}(t)$ can be found by solving the following slow-drift motion equation:

$$\left(M + A_{jj}\right)\ddot{\xi}_j^{(2)} + B_{jj}\dot{\xi}_j^{(2)}\left|\dot{\xi}_j^{(2)}\right| + K_{jj}\dot{\xi}_j^{(2)} = F_j^{(2)}(t) \tag{3. 18}$$

Using Newman's approximation for the second-order force (Newman 1974), the slow-drift exciting force may be written as

$$F_j^{(2)}(t) = \sum_{\mathrm{m}=1}^{\mathrm{N}} \sum_{m=1}^{N} a_m a_{\mathrm{n}} \bar{F}_j^{(2)}(\omega_m, \beta) cos[(\omega_m - \omega_n)\mathrm{t} + \epsilon_{\mathrm{m}} - \epsilon_{\mathrm{n}}] \quad (3.\ 19)$$

There are a number of contributions to the damping $\mathrm{B_{jj}}$ of an FPSO-mooring-riser system. These include viscous drag on the vessel and mooring lines, wave drift damping due to vessel drift velocity, line internal damping, and soil-line frictional damping. In the present study, only wave drift damping was considered and is estimated by:

$$\mathrm{B_{jj}} = 2\int_0^{\infty} \mathrm{S}(\omega).\mathrm{B_{jj}^{(2)}}\mathrm{d}\omega \quad (3.\ 20)$$

where $\mathrm{B_{jj}^{(2)}} = -\frac{\partial \bar{\mathrm{F}}_{\mathrm{j}}^{(2)}}{\partial \mathrm{U}}(\omega)\Big|_{\mathrm{U}=0}$ Wichers (1982), U is the forward speed of the FPSO vessel. The mean second-order force $\bar{\mathrm{F}}_{\mathrm{j}}^{(2)}(\omega)$ was evaluated at four different values of U: 0.0, 0.01, 0.02 and 0.03 m/s. These were then plotted against the forward speed values for each frequency and the slope at zero forward speed obtained.

Once the displacements of the attachment points are traced in the time domain, the corresponding maximum horizontal tensions T_H on the mooring lines can also be obtained from the nonlinear catenary equations.

The analysis was carried for two case scenarios. In the first case only the mooring lines were considered while in the second case both mooring and risers were taken into account in calculating surge and sway excursions. The analysis results are presented and discussed in the following sections.

3.6.1. Time domain analysis results

Based on the foregoing method, a fast time-domain analysis was carried out to obtain the time series of undisturbed wave profile, the displacements of the mooring and risers attachment points due to the first and second-order motions in surge and sway, and the corresponding maximum mooring and SCR line tensions in two design extreme irregular sea states with a duration of 3 hours respectively for the West Africa and the Gulf of Mexico conditions as described in Section 3.2.4. The results showed that mooring line 9 is the most loaded while fluid line 8 and water line 4 had the least tensions and therefore correspondingly higher bending stresses.

3.6.1.1. *West Africa (WA) condition*

Fig. 3.10 demonstrates the time series of instantaneous wave elevation at attachment point 9 in the West Africa condition and Figs. 3.11 and 3.12 show the corresponding time series of displacements in surge and sway respectively without the stiffness effect of SCRs. Figs. 3.13 to 3.15 illustrate the time histories of the maximum mooring, steel catenary riser (fluid and water) lines tensions respectively for the West Africa condition.

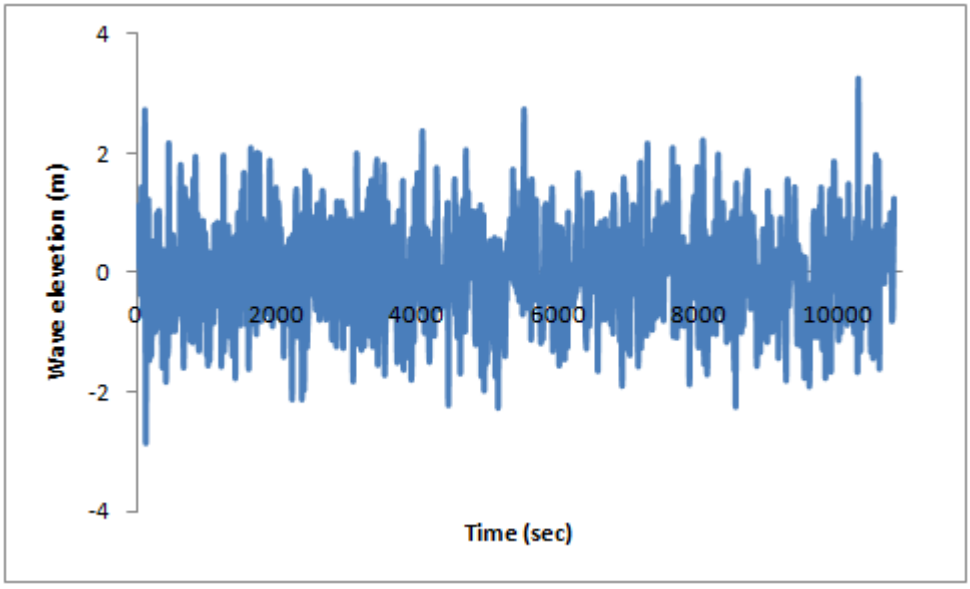

Fig. 3. 10 Time series of instantaneous wave elevation at att. pt 9 for WA

It is evident that the slow-varying surge and sway drift motions are present as shown in Figs 3.11 and 3.12. The lines tensions fluctuate about their pre-tension levels, since the mean offset due to steady wind and current are small. Furthermore, the effects of slow-drift motions are also present in the line tension.

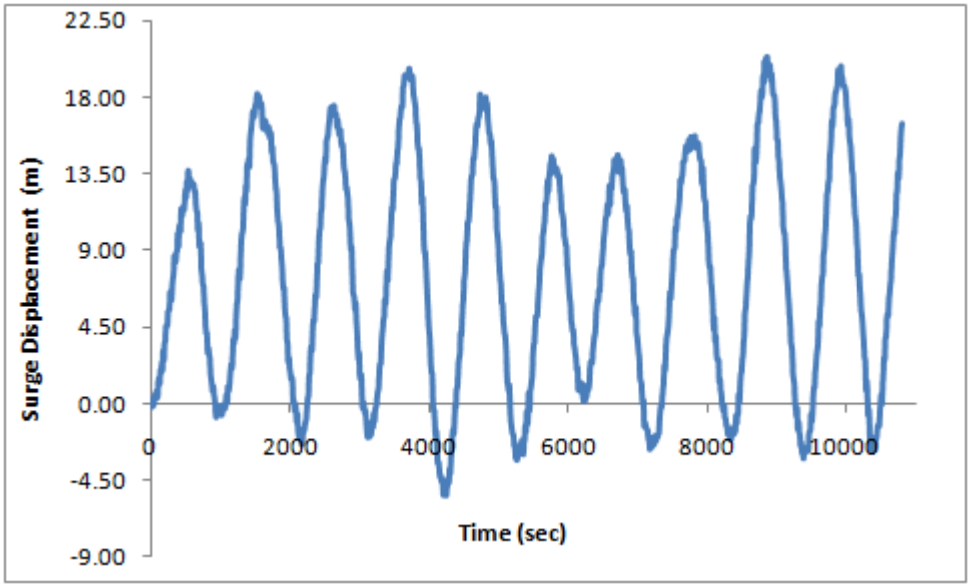

Fig. 3. 11 Time series of surge displacement at att. point 9 in the WA

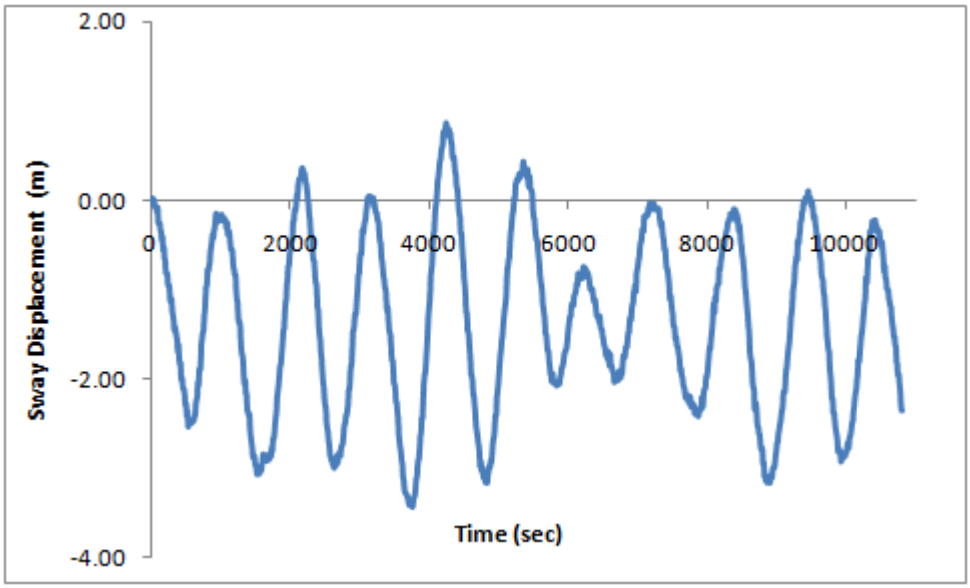

Fig. 3. 12 Time series of sway displacement at att. point 9 for WA

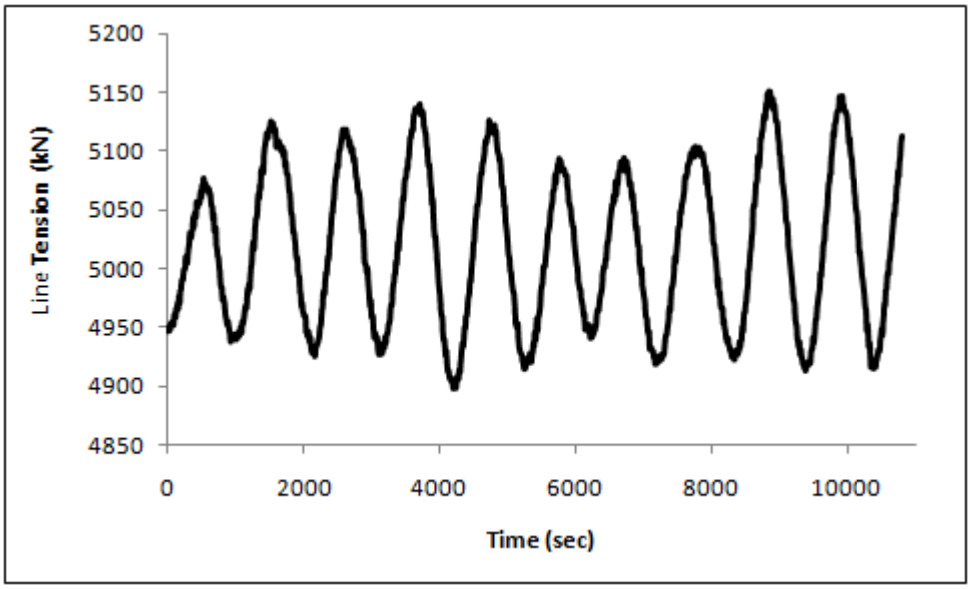

Fig. 3. 13m Time series of line tension in mooring line 9 for WA

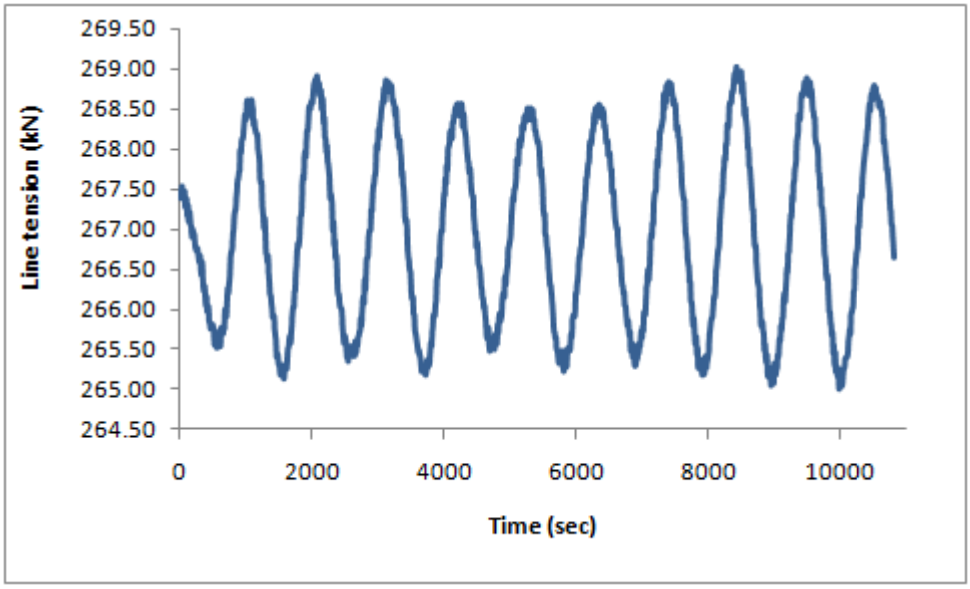

Fig. 3. 14 Time series of line tension in fluid line 8 for WA

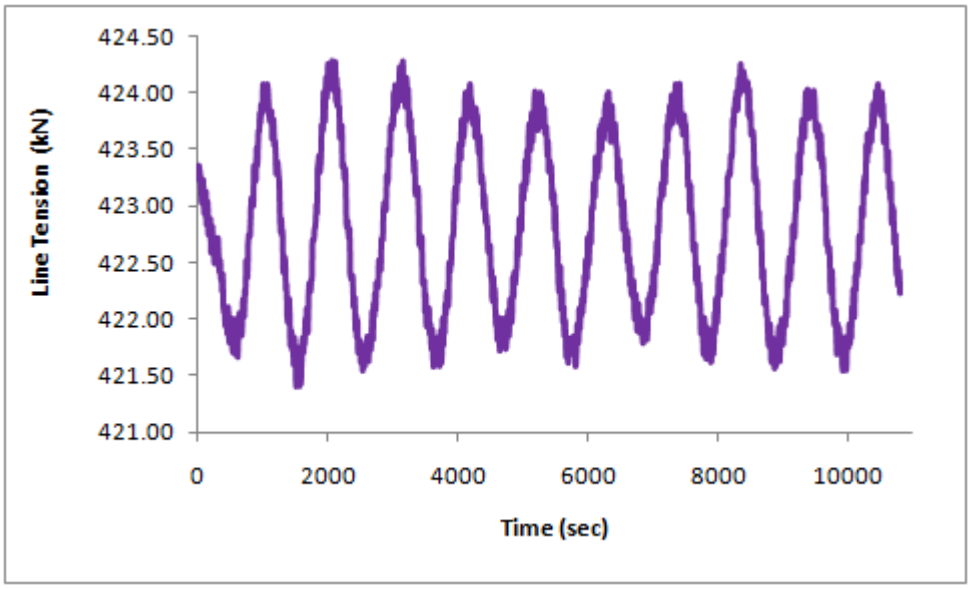

Fig. 3. 15 Time series of line tension in water line 4 for WA

The extreme vessel excursions in surge and sway for the West Africa condition are shown in Tables 3.10 and 3.11 respectively without and with the stiffness effect of SCRs, while Tables 3.12 and 3.13 summarise the resulting line tensions in the mooring and SCR lines and the bending stresses in the SCRs respectively.

Table 3. 10 Maximum Excursions X_j at attachment point 9 for WA: Mooring only

Parameter	Surge	Corresponding Sway	Sway	Corresponding Surge
$\xi_j^{(1)}$	0.446	-0.023	-0.016	0.285
$\xi_j^{(2)}$	19.96	-3.14	-3.42	19.02
ξ_j	**20.40**	**-3.17**	**-3.44**	**19.31**

Table 3. 11 Maximum Excursions X_j at attachment point 9 for WA: Mooring+SCRs

Parameter	Surge	Corresponding Sway	Sway	Corresponding Surge
$\xi_j^{(1)}$	0.088	-0.003	-0.006	0.17
$\xi_j^{(2)}$	33.54	-3.62	-5.36	27.88
$\tilde{\xi}_j$	**33.63**	**-3.62**	**-5.37**	**28.05**

Table 3. 12 Maximum mooring and SCR line tensions for WA

Line	**T (kN)**	**Case**
Mooring line 9	5150	Mooring only
Mooring line 9 Fluid line 8 Water line 4	5320 269 424	Mooring + SCR

Table 3. 13 Maximum bending stress at the touchdown point for WA

Description	σ_b (N/mm^2)	
	Pipe	Coating
Fluid line 8 Water line 4	43 42	13 N/A

It has been observed that the maximum tensions in the lines are caused by the maximum surge excursion because for the same reason given above in the case of the mooring lines. It is not readily evident from Tables 3.10 and 3.11 what contribution the presence of the SCRs make in limiting the excursions of the vessel since the maximum surge excursions as well as the maximum sway excursions have been seen to be higher when both mooring and SCRs were modeled. The reason for this is the fact that the seastate is random and therefore results cannot correlate if the same seastate is not maintained for the two analyses. The mooring line tensions have also been observed to

be different for the two cases, being higher when SCRs were considered. As with the frequency domain analysis, the first-order motions are quite small when compared to the slow-drift motions of the FPSO in the ARDO field.

Figs. 3.16 and 3.17 show the time series of the touchdown point (TDP) bending stresses in the SCR pipes and the coating where applicable for the West Africa condition. The maximum bending stress at the extreme fibres of both steel and concrete coating are found to be very small and within the expected limits as discussed above.

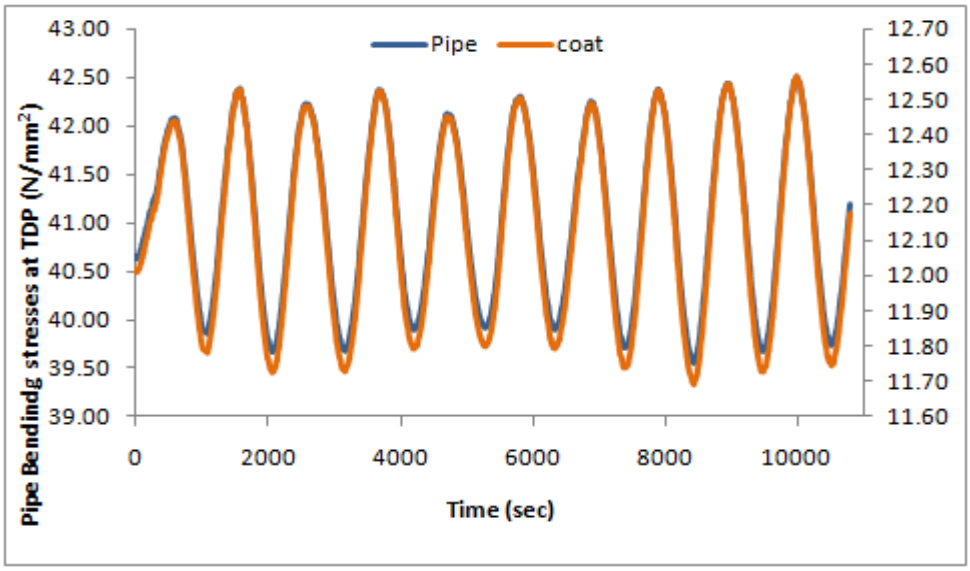

Fig. 3. 16 Time series of TDP stresses in fluid line 8 for WA

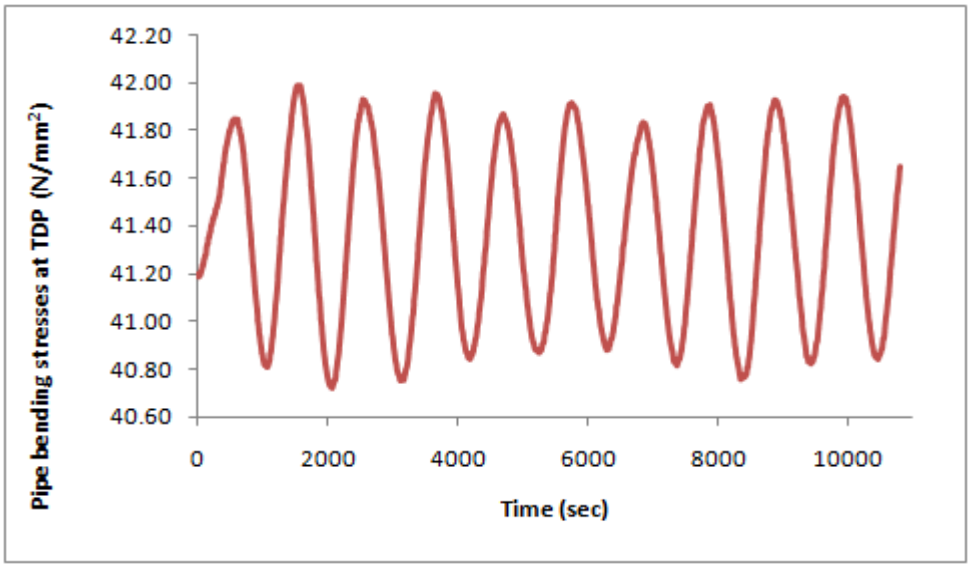

Fig. 3. 17 Time series of TDP stresses in water line 4 for WA

The weakness of using the catenary equations to compute the bending stress in the SCRs is that the bending stress is calculated using the equation of curvature only after the horizontal tension has been obtain assuming the SCRs to be perfectly flexible, that is, neglecting its bending stiffness. This is however a good approximation since in ultra deepwater, the diameter of the SCR is very small compared to its length (Hibbeler 1998).

3.6.1.2. *Gulf of Mexico (GoM) condition*

Fig. 3.18 demonstrates the time series of instantaneous wave elevation at attachment point 9 in the GoM condition and Figs. 3.19 and 3.20 show the corresponding time series of displacements in surge and sway respectively. Figs. 3.21 to 3.23 illustrate the time histories of the maximum mooring, steel catenary riser (fluid and water) lines tensions respectively for the GoM condition.

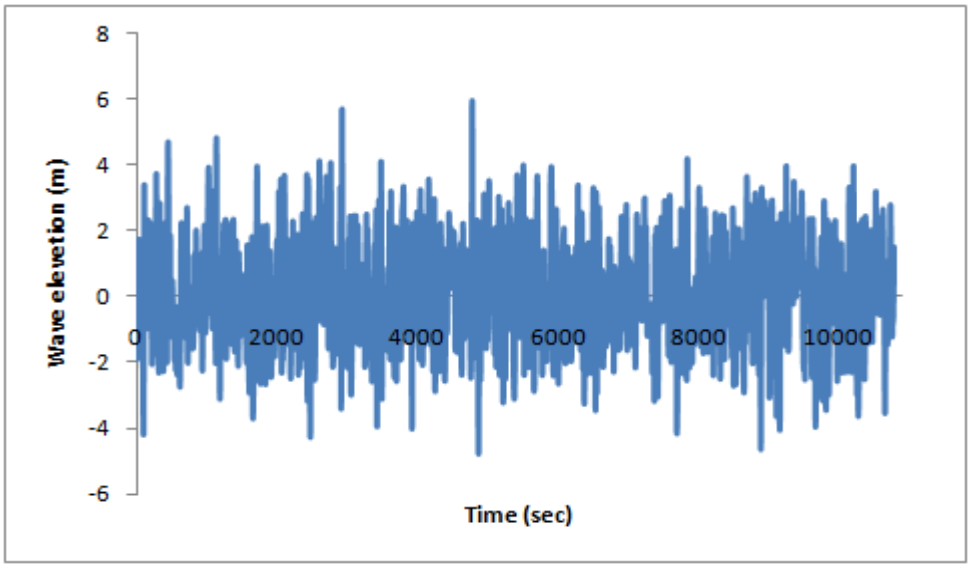

Fig. 3. 18 Time series of instantaneous wave elevation at att. pt 9 for GoM

Just like the WA condition it is evident that the slow-varying surge and sway drift motions are present as shown in Figs 3.19 and 3.20. The lines tensions fluctuate about their pre-tension levels, since the mean offset due to steady wind and current are small. Furthermore, the effects of slow-drift motions are also present in the line tension.

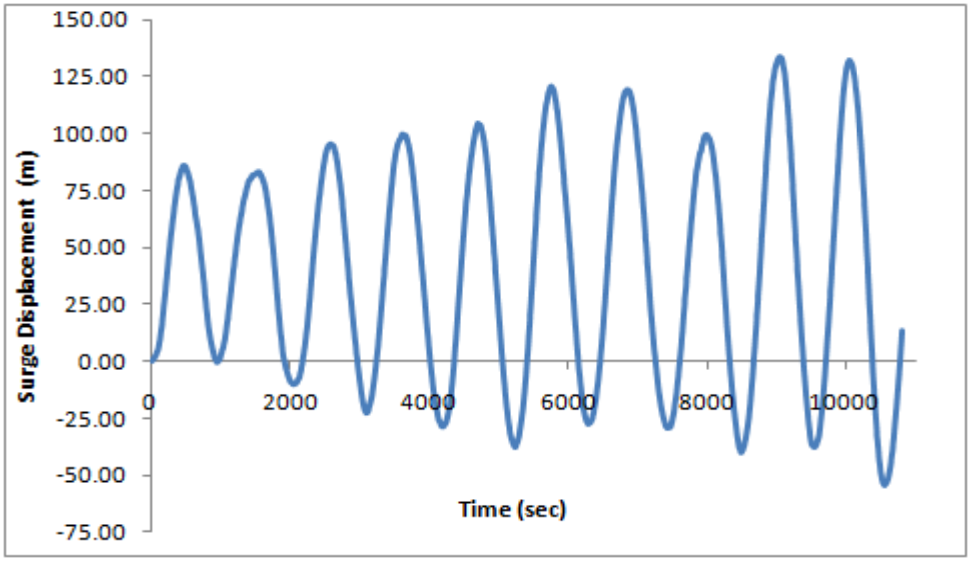

Fig. 3. 19 Time series of surge displacement at att. point 9 for GoM

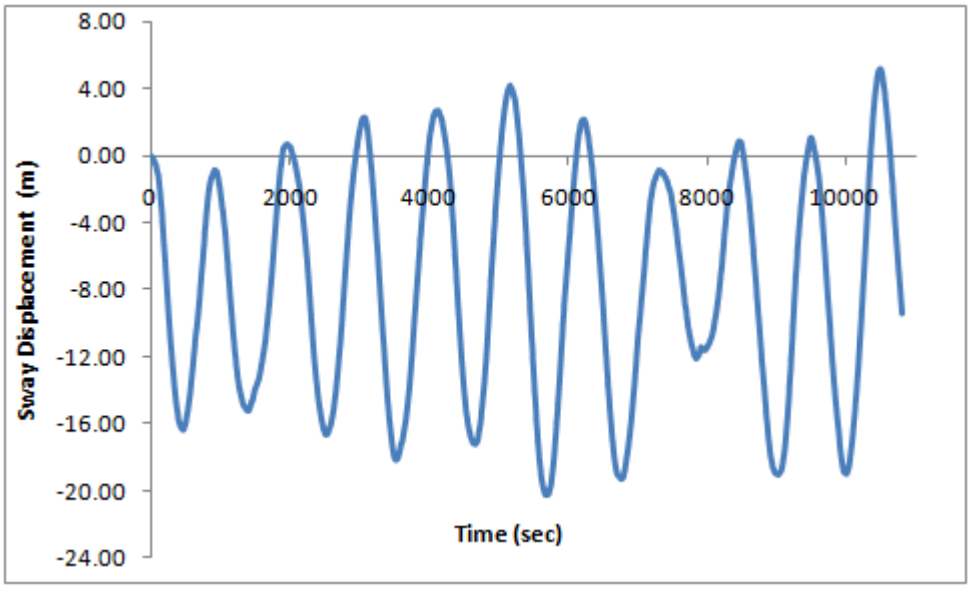

Fig. 3. 20 Time series of sway displacement at att. point 9 for GoM

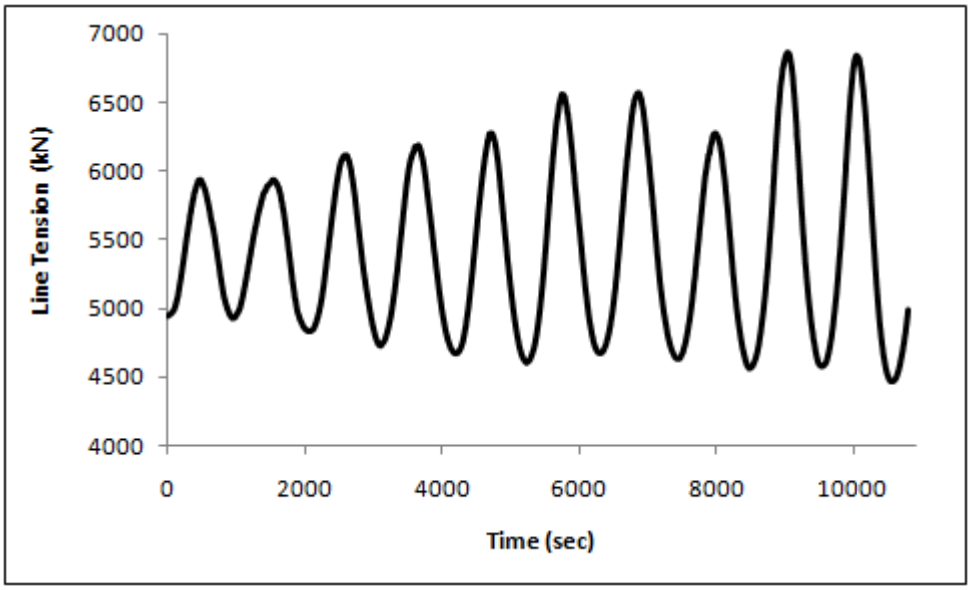

Fig. 3. 21 Time series of line tension in mooring line 9 for GoM

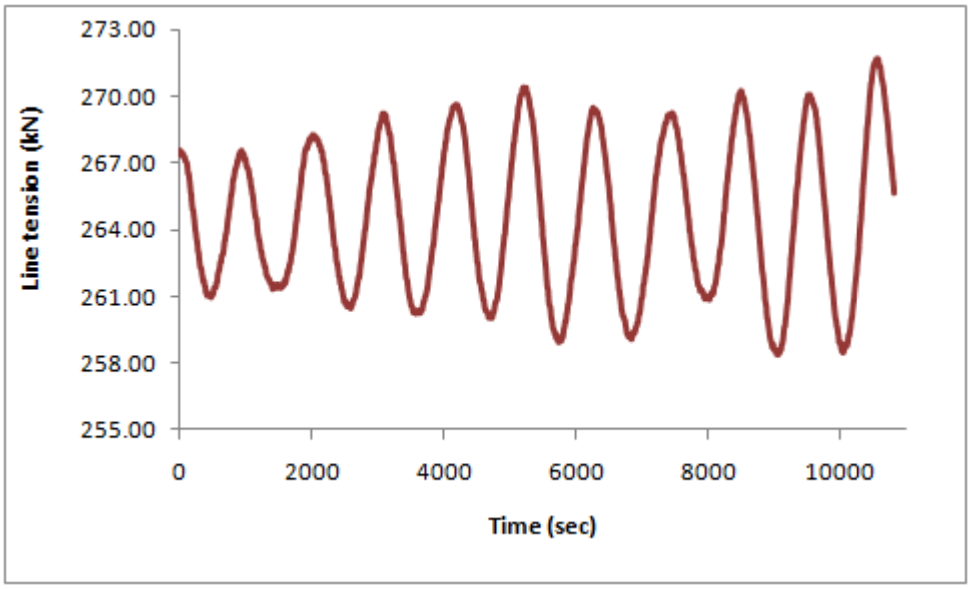

Fig. 3. 22 Time series of line tension in fluid line 8 for GoM

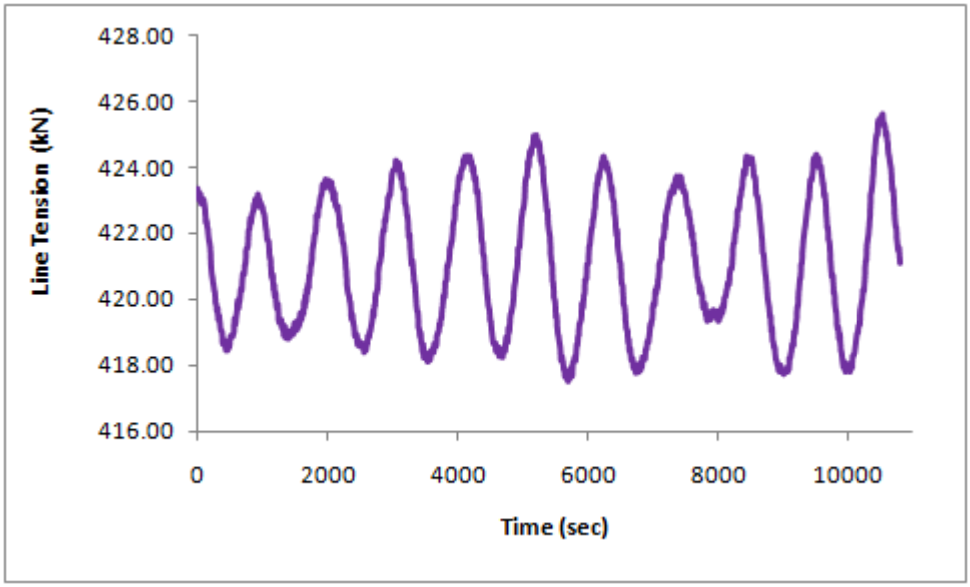

Fig. 3. 23 Time series of line tension in water line 4 for GoM

The extreme vessel excursions in surge and sway for the West Africa condition are shown in Tables 3.14 and 3.15 respectively without and with the stiffness effect of SCRs, while Tables 3.16 and 3.17 summarise the resulting line tensions in the mooring and SCR lines and the bending stresses in the SCRs respectively.

Table 3. 14 Maximum Excursions X_j at attachment point 9 for GoM: Mooring Only

Parameter	Surge	Corresponding Sway	Sway	Corresponding Surge
$\xi_j^{(1)}$	0.100	-0.019	0.008	-0.041
$\xi_j^{(2)}$	120.39	-24.86	-25.81	115.92
ξ_j	**120.49**	**-24.88**	**-25.80**	**115.88**

Table 3. 15 Maximum Excursions X_j at attachment point 9 for GoM: Mooring+SCRs

Parameter	Surge	Corresponding Sway	Sway	Corresponding Surge
$\xi_j^{(1)}$	0.258	-0.007	-0.021	-0.063
$\xi_j^{(2)}$	133.39	-18.88	-20.19	110.66
ξ_j	**133.65**	**-18.89**	**-20.21**	**110.59**

Table 3. 16 Maximum mooring and SCR line tensions for GoM

Line	**T (kN)**	**Case**
Mooring line 9	6454	Mooring only
Mooring line 9	6870	
Fluid line 8	272	Mooring + SCR
Water line 4	426	

Table 3. 17 Maximum bending stress at the touchdown point for GoM

Description	σ_b (N/mm2)	
	Pipe	Coating
Fluid line 8	49	14
Water line 4	44	N/A

It is observed that the maximum tensions in the lines are caused by the maximum surge excursion because for the same reason given above in the case of the mooring lines. Again just like the case of WA, here too it is not readily evident from Tables 3.14 and 3.16 what contribution the presence of the SCRs make in limiting the excursions of the vessel since the maximum surge excursions as well as the maximum sway excursions have been seen to be higher when both mooring and SCRs were modeled. The reason for this is the fact that the seastate is random and therefore results cannot correlate if the same seastate is not maintained for the two analyses. Similarly the mooring line tensions are also higher when both Mooring lines and SCRs are modeled. Most of the contribution to line excursions is due to slow-drift motions of the FPSO.

Figs. 3.24 and 3.25 show the time series of the touchdown point (TDP) bending stresses in the SCR pipes and the coating where applicable for the GoM condition. The maximum bending stress at the extreme fibres of both steel and concrete coating are found to be very small and within the expected limits as discussed in the previous sections.

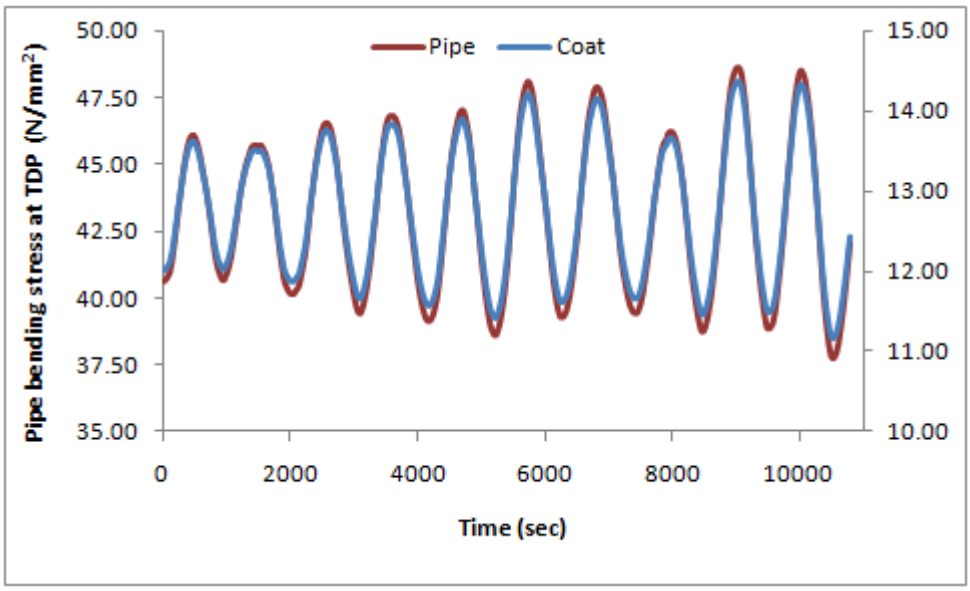

Fig. 3. 24 Time series of TDP stresses in fluid line 8 for GoM

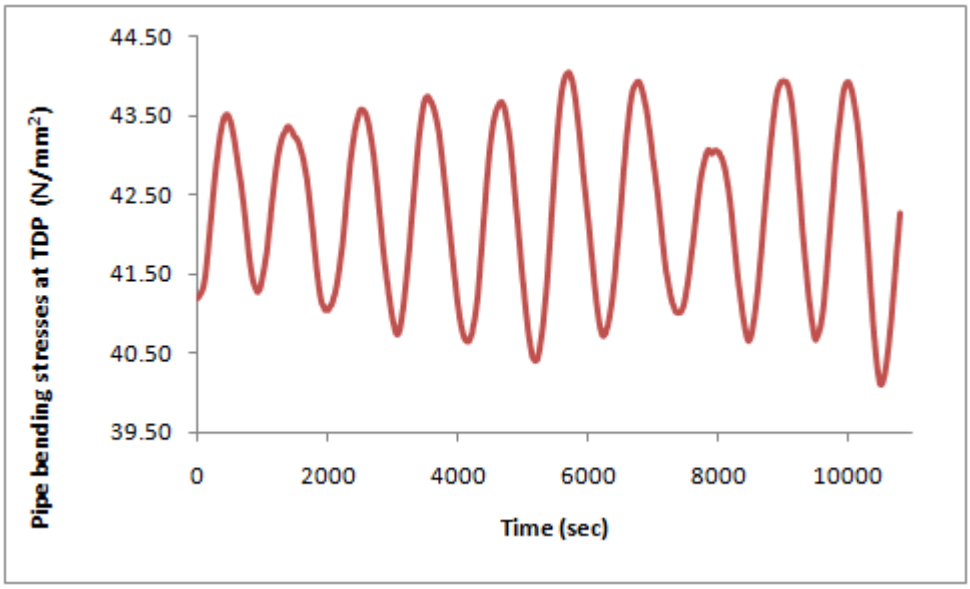

Fig. 3. 25 Time series of TDP stresses in water line 4 for GoM

3.7. Comparison between Frequency and Time Domain Results

The tables below summarises the maximum values of excursions at attachment points of the mooring and SCRs considered and the corresponding tensions and bending stresses.

3.7.1. Summary of Results for West Africa (WA) Condition

Table 3. 18 Moorings only summary of maximum excursions and tensions for WA

Description	Surge X_1 (m)	Corresponding Sway X_2 (m)	Sway X_2 (m)	Corresponding Surge X_1 (m)	Tension (kN)	Remarks
Frequency domain	47.58	N/A	5.72	N/A	5656	Moor. Line 9
Time domain	20.40	-3.17	-3.44	19.31	5320	Moor. Line 9

Table 3. 19 Mooring + SCRs Summary of maximum excursions and tensions for WA

Description	Surge X_1 (m)	Corresponding Sway X_2 (m)	Sway X_2 (m)	Corresponding Surge X_1 (m)	Tension (kN)	Remarks
Frequency domain	47.28	N/A	5.39	N/A	5644	Moor. Line 9
	47.5	N/A	5.40	N/A	265	Fluid line 8
	47.35	N/A	5.38	N/A	423	Water line 4
Time domain	33.63	-3.62	-5.34	28.05	5150	Moor. Line 9
	33.69	-4.04	-5.37	27.77	269	Fluid line 8
	33.69	-3.29	-5.38	27.77	424	Water line 4

Differences have been observed in the results from the two types of analyses as can be seen from Tables 3.18 and 3.19. The results from frequency domain analyses are more conservative in both cases, i.e. mooring lines modeled with and without SCRs. It is further observed that results from analyses whereby only mooring line were modeled tend to have higher values than when both mooring lines and SCRs were modeled for the same mooring lines. There was however no significant difference in maximum SCR tensions observed between frequency and time domain analysis results. Maximum SCR bending stresses at the touchdown point also remain practical the same between the two methods as shown in Table 3.20.

Table 3. 20 Summary of maximum SCR bending stress at the touchdown point for WA

Description	Frequency domain		Time domain	
	Pipe σ_b (N/mm^2)	Coating σ_b (N/mm^2)	Pipe σ_b (N/mm^2)	Coating σ_b (N/mm^2)
Fluid lines	43	12	43	13
Water lines	42	N/A	42	N/A

3.7.2. Summary of Results for Gulf of Mexico (GoM) Condition

The Gulf of Mexico is a more severe environment than the West Africa as is evident from Tables 3.21 and 3.22 with the resultant maximum excursions exceeding the allowable values in both cases for the frequency domain analysis.

Table 3. 21 Moorings only summary of maximum excursions and tensions for GoM

Description	Surge X_1 (m)	Corresponding Sway X_2 (m)	Sway X_2 (m)	Corresponding Surge X_1 (m)	Tension (kN)	Remarks
Frequency domain	279	N/A	35.26	N/A	7755*	Moor. Line 9
Time domain	120.5	-24.88	-25.80	115.88	6454	Moor. Line 9

Table 3. 22 Mooring + SCRs Summary of maximum excursions and tensions for GoM

Description	Surge X_1 (m)	Corresponding Sway X_2 (m)	Sway X_2 (m)	Corresponding Surge X_1 (m)	Tension (kN)	Remarks
Frequency domain	276	N/A	33.16	N/A	7755*	Moor. Line 9
	275		33.00		258*	Fluid line 8
	275		32.50		420*	Water line 4
Time domain	133.7	-18.89	-20.21	110.6	6870	Moor. Line 9
	133.6	-18.80	-20.22	114.34	272	Fluid line 8
	133.5	-18.87	-20.21	115.93	426	Water line 4

* Excursions exceeded the allowable, allowable values used in calculations

The same pattern of results as those of the West Africa environment has been observed with the results from frequency domain analyses being of higher values for the mooring lines. However, the values of SCR tensions have been observed to be higher in time domain. There is however no significant difference in maximum SCR tensions observed between frequency and time domain analysis results as shown in Table 3.23. Maximum SCR bending stresses at the touchdown point also remain practical the same between the two methods.

Table 3. 23 Summary of maximum SCR bending stress at the touchdown point for GoM

Description	Frequency domain		Time domain	
	Pipe σ_b (N/mm^2)	Coating σ_b (N/mm^2)	Pipe σ_b (N/mm^2)	Coating σ_b (N/mm^2)
Fluid lines	49	15	49	14
Water lines	43	N/A	44	N/A

3.8. Conclusions

Two methodologies have been presented for the quasi-static analysis of mooring line and steel catenary risers and subsequently used for the analysis of an FPSO mooring and steel catenary risers in two different environments: West Africa and the Gulf of Mexico. The analyses were performed both in frequency and time domain when only mooring lines were modeled as well as when both mooring and risers were modeled yielding practical results. The results for the various scenarios have been compared and discussed. The tensions and bending stresses in the lines were computed based catenary formulations developed in Chapter 2. The weakness of using the catenary equations to compute the bending stress in the SCRs is that the bending stress is calculated using the equation of curvature only after the horizontal tension has been obtain assuming the SCRs to be perfectly flexible, that is, neglecting its bending stiffness. This is however a good approximation since in ultra deepwater, the diameter of the SCR is very small compared to its length (Hibbeler 1998).

CHAPTER

4 DYNAMIC RISER/MOORING SYSTEM ANALYSIS METHODOLOGY

4.1. Introduction

In this chapter the dynamic analysis methodology for multi-component mooring and steel catenary risers is discussed in detail. A step by step algorithm for the implementation of the method has also been formulated. A FORTRAN program was then developed and used to solve a sample problem for comparison with results from a published paper on the same data.

4.2. Derivation of Dynamic Mooring System Equations

When the response of a moored FPSO is outside the natural mode frequency range of the mooring lines, quasi-static riser/mooring analysis can be used to address the dynamics of the system in a static manner. This kind of analysis however ignores the effects of riser/mooring line dynamics which in some cases can be a significant element in the dynamic analysis of a moored vessel (Ansari and Khan 1986). The dynamics of mooring cables and risers are important when the wavelength, L is much greater than the diameter, D of the lines, hence they can be modelled as slender structures (Triantafyllou 1999). Modelling of slender structures has been covered in detail by Bernitsas (1982), Garrett (1982), and Triantafyllou and Howell (1993) based on the finite element technique. When mooring lines and risers are modelled as catenaries, their bending stiffness under normal operating conditions are assumed to be negligible compared to the tension stiffness. To realistically predict the mooring system behaviour however, Khan and Ansari (1986) modelled each mooring line as a multi-segment discrete dynamic system using the lumped mass technique. By this arrangement, the mooring system is therefore a network of multi-component mooring lines, each of which is a combination of clumped weights, chains, and cables. Fig. 4.1 shows a typical multi-component mooring line. The mathematical model of each mooring line is a multi-degree of freedom system obtained from breaking up the line into a series of finite partitions or segments whose masses are lumped at appropriate nodes as shown in Fig. 4.2.

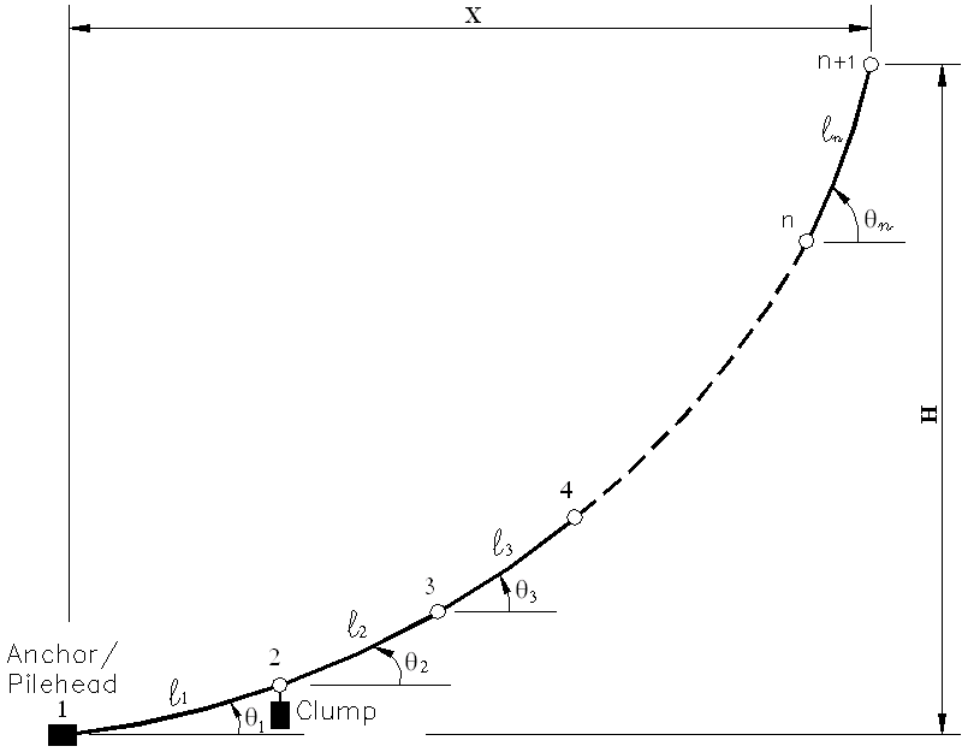

Fig. 4. 1 A typical multi-component mooring line

Each segment of the line between two lumped masses or nodes is treated as a massless, inextensible cylindrical link. This is justified for applications using chains and metal ropes. The number of nodes used should be large enough to model the basic motions of the mooring line but subject to the accuracy desired. Equations of motions are then formulated and numerically solved to obtain the tension-displacement characteristics and the nonlinear restoring force required for the dynamic analysis of the moored vessel.

The method used by Khan and Ansari 1986 applies the modified Lagrange's equations for cable motion permitting the use of holonomic constraints. The derivation of the modified Lagrange's equations from Hamilton's principle is summarised below.

4.3. Lagrange's Equations of Motion

Lagrange's equations can be derived from the principles of displacements (Langhaar 1962) or from Hamilton's principle (Craig 1981; Thomson 1993). It permits the use of scalar quantities such as work and kinetic energy, instead of vector quantities such as force and displacement required by Newton's laws and is therefore much simpler.

$$\delta\int_{t_1}^{t_2}(T-U)dt+\int_{t_1}^{t_2}\delta W_{nc}\,dt=0 \tag{4. 1}$$

where, T = the total kinetic energy of the system

U = the potential energy of the system

δW_{nc} = the virtual work of non-conservative forces acting on the system.

$\delta(\ )$= symbol denoting the first variation or virtual change in the quantity

t_1, t_2 = times at which the configuration of the system is known

For most mechanical and structural systems the kinetic energy can be expressed in terms of the generalised coordinates and their first derivatives, and the potential energy can be expressed in terms of the generalised coordinates alone. The virtual work of the non-conservative forces as they act through virtual displacements caused by arbitrary variations in the generalised coordinates can be expressed as a linear function of those variations. Thus,

$$\begin{aligned} T &= T\left(p_1, p_2, \ldots, p_N, \dot{p}_1, \dot{p}_2, \ldots, \dot{p}_N, t\right) \\ U &= U\left(p_1, p_2, \ldots, p_N, t\right) \\ \delta W_{nc} &= Q_1\delta p_1 + Q_2\delta p_2 + \ldots + Q_N\delta p_N \end{aligned} \tag{4. 2}$$

where, $Q_1, Q_2, \ldots, Q_N$ are called the generalised forces and have units such that each term $Q_i\delta p_i$ has the units of work. $p_1, p_2, \ldots, p_N$ are the generalised coordinates.

Generalised coordinates are defined as any set of N independent quantities which are sufficient to completely define the position of every point within an N-degrees-of-freedom (NDOF) system. Substituting Eq. 4.2 into Eq. 4.1 and integrating the terms involving $\delta\dot{p}_i$ by parts and neglecting the second derivative of T gives,

$$\int_{t_1}^{t_2}\left\{\sum_{i=1}^{N}\left[-\frac{d}{dt}\left(\frac{\partial T}{\partial \dot{p}_i}\right)+\frac{\partial T}{\partial p_i}-\frac{\partial U}{\partial p_i}+Q_i\right]\delta p_i\right\}dt=0 \tag{4. 3}$$

Eq. 4.3 can in general only be satisfied when the terms in the square brackets vanish for each value of i since the coordinates p_i and their variations $\delta p_i\left(i=1,2,...,N\right)$ must be independent. Thus,

$$\frac{d}{dt}\left(\frac{\partial T}{\partial \dot{p}_i}\right)-\frac{\partial T}{\partial p_i}+\frac{\partial U}{\partial p_i}=Q_i \quad \text{for } i=1,2,...,N \tag{4. 4}$$

Eq. 4.4 is known as the Lagrange's equation and is valid for both linear and non linear systems.

In real life situations, it is desirable or even necessary to employ a set of coordinates $q_1,q_2,...,q_M$ some of which may not be independent, i.e., constrained or superfluous, where $M>N$ (Thomson, 1993). The dependent or constraint coordinates must be associated with C constraint equations, where $C=M-N$. Constraints are said to be holonomic if the excess or superfluous coordinates can be eliminated through the equations of constraint (Thomson, 1993). These equations can be written in the form,

$$f_j\left(q_1,q_2,...,q_M\right)=0 \qquad \text{for } j=1,2,\ldots,C \tag{4. 5}$$

Let each coordinate q_i be given a variation δq_i then

$$\delta f_j = \frac{\partial f_j}{\partial q_1}\delta q_i + \frac{\partial f_j}{\partial q_2}\delta q_i + \ldots + \frac{\partial f_j}{\partial q_M}\delta q_M = \sum_{i=1}^{M}\frac{\partial f_j}{\partial q_i}\delta q_i \quad \text{for } j = 1, 2, \ldots, C \tag{4. 6}$$

Thus, the δqs are dependent, related by the C equations. Considering Eq. 4.6 with q coordinate instead of p gives the new Lagrange's equations as

$$\int_{t_1}^{t_2}\left\{\sum_{i=1}^{M}\left[-\frac{d}{dt}\left(\frac{\partial T}{\partial \dot{q}_i}\right)+\frac{\partial T}{\partial q_i}-\frac{\partial U}{\partial q_i}+Q_i\right]\delta q_i\right\}dt = 0 \tag{4. 7}$$

However, the expression in the square brackets cannot be set to zero as before since the δqs are not independent. By introducing and multiplying each of the C equations in 4.6 by an appropriate Lagrange multiplier, $\lambda_j(t)$ then the solution can be obtained by summing these up and substituting in into Eq. 4.7. Thus Eq. 4.6 becomes 4.8 and Eq. 4.7 becomes 4.9.

$$\sum_{j=1}^{C}\lambda_j\sum_{i=1}^{M}\frac{\partial f_j}{\partial q_i}\delta q_i = 0 \tag{4. 8}$$

$$\int_{t_1}^{t_2}\left\{\sum_{i=1}^{M}\left[-\frac{d}{dt}\left(\frac{\partial T}{\partial \dot{q}_i}\right)+\frac{\partial T}{\partial q_i}-\frac{\partial U}{\partial q_i}+Q_i+\sum_{j=1}^{C}\lambda_j\frac{\partial f_j}{\partial q_i}\right]\delta q_i\right\}dt = 0 \tag{4. 9}$$

While the δqs in Eq. 4.9 are still not independent, the Lagrange multipliers can be chosen such that the bracketed terms for $\delta q_i(i = 1,2,\ldots,C)$ equal to zero. Since the remaining $N = M - C$ coordinates are independent, the expression in the square brackets must also vanish for all $\delta q_i(i = C+1,\ldots,M)$. Hence, we have

$$\frac{d}{dt}\left(\frac{\partial T}{\partial \dot{q}_i}\right)-\frac{\partial T}{\partial q_i}+\frac{\partial U}{\partial q_i}-\sum_{j=1}^{C}\lambda_j\frac{\partial f_j}{\partial q_i} = Q_i \quad \text{for } i = 1,2,\ldots,M \tag{4. 10}$$

Eqs. 4.10 are the modified Lagrange's equations permitting the use of holonomic constraints.

4.4. Application of Lagrange's Equations of Motion to Mooring lines

Fig. 4.2 shows a mathematical lumped mass model of an n-segment multi-component mooring line. The coordinates of the anchor point is assumed to coincide with the origin of the coordinates system x_0, z_0. Coordinates x_i, z_i and θ_i, $(i = 1, 2, 3, ..., n)$ are chosen to describe the motion of the lumped masses $m_i (i = 0, 1, 2, 3, ..., n-1)$, where m_0 represents 50% of the mass of the segment attached to the anchor. If the anchor is not constrained, its mass must also be added to m_0. Similarly, m_n represents 50% of the mass of the nth segment plus the mass of the vessel if modelled together with the lines. The $\theta_i s$ are generalised coordinates and hence independent while x_i, z_i are dependent coordinates which are related to the $\theta_i s$ through constraint equations. For this model, the number of such constraint equations will be $2n$, i.e. one equation for each dependent coordinate, as shown in Eq. 4.11. Because of line motion in surrounding fluid, the mooring line would be subjected to drag as well as damping. The added mass effect from acceleration of the fluid around a link can be included in the form of a fractional mass added to each lumped mass as suggested by Khan and Ansari (1986).

$$
\begin{aligned}
f_1 &= x_1 - x_0 - l_1 \cos\theta_1 = 0 \\
f_2 &= z_1 - z_0 - l_1 \sin\theta_1 = \\
f_3 &= x_2 - x_1 - l_2 \cos\theta_2 = 0 \\
f_4 &= z_2 - z_1 - l_2 \sin\theta_2 = 0 \\
f_5 &= x_3 - x_2 - l_3 \cos\theta_3 = 0 \\
f_6 &= z_3 - z_2 - l_3 \sin\theta_3 = 0 \\
&\vdots \\
f_{2n-1} &= x_n - x_{n-1} - l_n \cos\theta_n = 0 \\
f_{2n} &= z_n - z_{n-1} - l_n \sin\theta_n = 0
\end{aligned}
\qquad (4.\ 11)
$$

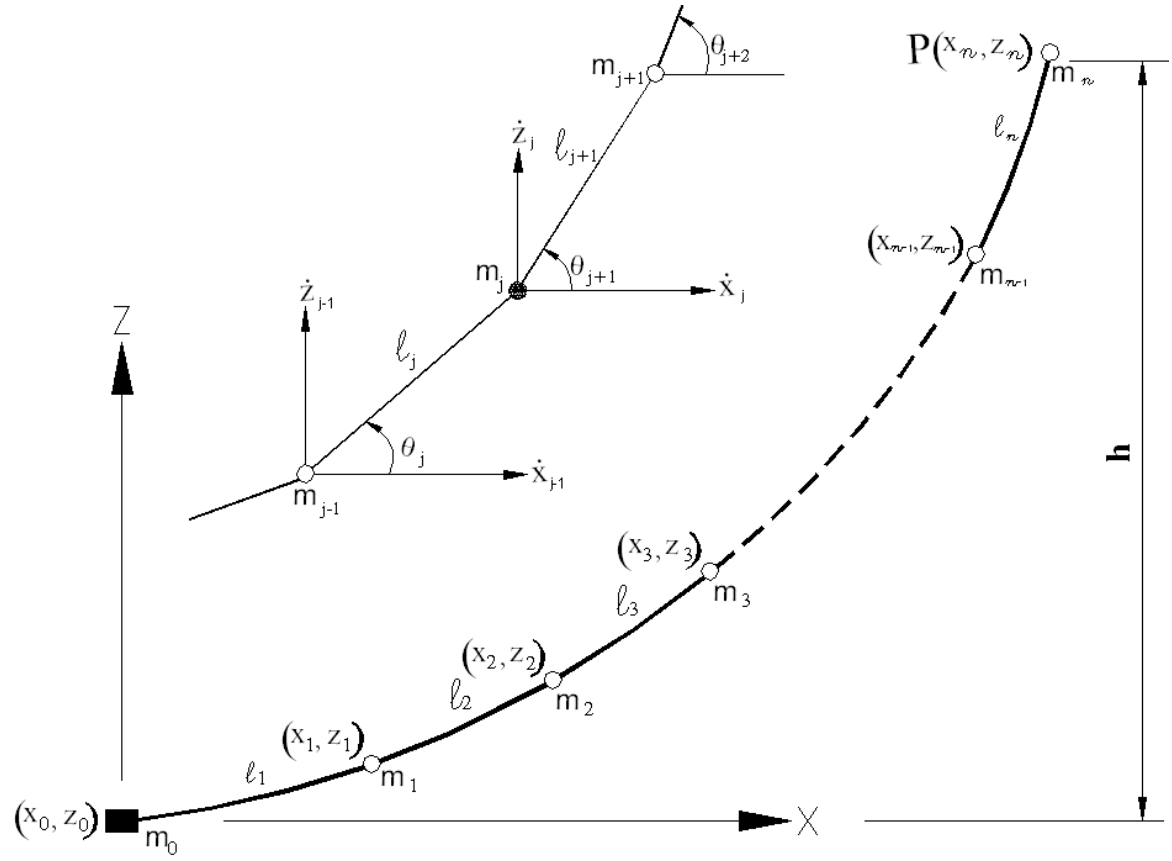

Fig. 4. 2 Mathematical model of an n-segment mooring line

For the n-segments mooring line shown in Fig. 4.2, there are a total of 3n+2 coordinates q_1 to q_{3n+2} as shown:

$$q_1 = x_0,\ q_2 = z_0,\ q_{2i+1} = x_i,\ q_{2i+2} = z_i, \ldots, q_{2n+1} = x_{n,}\ q_{2n+2} = z_n$$
$$q_{2n+2+i} = \theta_i, \ldots, q_{3n+2} = \theta_n \quad \text{for } i = 1,2,\ldots .n \tag{4. 12}$$

The kinetic energy expression is

$$T = \frac{1}{2} m_0 v_0^2 + \frac{1}{2} m_1 v_1^2 + \frac{1}{2} m_2 v_2^2 + \frac{1}{2} m_3 v_3^2 + \ldots + \frac{1}{2} m_n v_n^2 \tag{4. 13}$$

$$T = \frac{1}{2} m_0 \left(\dot{x}_0^2 + \dot{z}_0^2\right) + \frac{1}{2} m_1 \left(\dot{x}_1^2 + \dot{z}_1^2\right) + \frac{1}{2} m_2 \left(\dot{x}_2^2 + \dot{z}_2^2\right) + \ldots + \frac{1}{2} m_n \left(\dot{x}_n^2 + \dot{z}_n^2\right) \tag{4. 14}$$

Similarly, the potential energy of the lumped masses can be expressed as

$$U = m_0 g z_0 + m_1 g z_1 + m_2 g z_2 + m_3 g z_3 + \ldots + m_n g z_n \tag{4. 15}$$

It can be shown from Eq. 4.11 that the coordinates of the nodes are related with each other as follows:

$$x_k = x_n - \sum_{i=k+1}^{n} l_i \cos\theta_i$$
$$z_k = z_n - \sum_{i=k+1}^{n} l_i \sin\theta_i \qquad \text{for } k = 0,1, \ldots, n-1 \tag{4.16}$$

Hence, the nodal velocities are given by

$$\dot{x}_k = \dot{x}_n + \sum_{i=k+1}^{n} l_i \dot{\theta}_i \sin\theta_i$$
$$\dot{z}_k = \dot{z}_n - \sum_{i=k+1}^{n} l_i \dot{\theta}_i \cos\theta_i \qquad \text{for } k = 0,1, \ldots, n-1 \tag{ 4.17}$$

and their accelerations are given by

$$\ddot{x}_k = \ddot{x}_n + \sum_{i=k+1}^{n} l_i \ddot{\theta}_i \sin\theta_i + \sum_{i=k+1}^{n} l_i \dot{\theta}_i^2 \cos\theta_i$$
$$\ddot{z}_k = \ddot{z}_n - \sum_{i=k+1}^{n} l_i \ddot{\theta}_i \cos\theta_i + \sum_{i=k+1}^{n} l_i \dot{\theta}_i^2 \sin\theta_i \qquad \text{for } k = 0,1, \ldots, n-1 \tag{4. 18}$$

Applying Eq. 4.10 to Eq. 4.11- 4.15 results into $3n+2$ equations to be derived as indicated below. The first 2 equations representing the anchor motions are given by:

$$m_0\ddot{x}_0 + \lambda_1 = Q_{x_0} \tag{4. 19}$$

$$m_0\ddot{z}_0 + m_0 g + \lambda_2 = Q_{z_0} \tag{4. 20}$$

The next $3n$ equations representing the motion of the mooring line lumped massed and their interactions are given by:

$$m_i\ddot{x}_i - \lambda_{2i-1} + \lambda_{2i+1} = Q_{x_i} \qquad \text{for } i = 1, 2, \ldots, n-1 \tag{4. 21}$$

$$m_i\ddot{z}_i + m_i g - \lambda_{2i} + \lambda_{2i+2} = Q_{z_i} \qquad \text{for } i = 1, 2, \ldots, n-1 \tag{4. 22}$$

$$m_n\ddot{x}_n - \lambda_{2n-1} = Q_{x_n} \tag{4. 23}$$

$$m_n\ddot{z}_n + m_n g - \lambda_{2n} = Q_{z_n} \tag{4. 24}$$

$$\lambda_{2i} = \lambda_{2i-1}\tan\theta_i \qquad \text{for } i = 1, 2, \ldots, n \tag{4. 25}$$

It is noted that, for a catenary line, the generalised force $Q_{\theta_i} = 0$; $i = 1, 2, \ldots, n$. By eliminating the λs using the interaction equations generated from Eq. 4.25, Eqns. 4.19 to 4.24 will result into the following $n+1$ equations:

$$\begin{aligned}\sum_{k=1}^{i} m_{k-1}\ddot{x}_{k-1}\sin\theta_i - \sum_{k=1}^{i} m_{k-1}\ddot{z}_{k-1}\cos\theta_i - \sum_{k=1}^{i} m_{k-1} g\cos\theta_i \\ = \sum_{k=1}^{i} Q_{x_{k-1}}\sin\theta_i - \sum_{k=1}^{i} Q_{z_{k-1}}\cos\theta_i\end{aligned} \qquad \text{for } i = 1, 2, 3, \ldots, n \tag{4. 26}$$

$$\text{and } m_n\ddot{x}_n\sin\theta_n - m_n\ddot{z}_n\cos\theta_n = m_n g\cos\theta_n + Q_{x_n}\sin\theta_n - Q_{z_n}\cos\theta_n \tag{4. 27}$$

Relevant parts of Eqns. 4.18 are then substituted into Eqns. 4.26 in order to reduce the number of variables in the resulting equations to $n+2$ independent coordinates $x_n,\ z_n, \theta_i;\ i = 1, 2, \ldots n$. Thus the first *n* equations are given by

$$\sum_{k=1}^{i} m_{k-1} \sin\theta_i \ddot{x}_n - \sum_{k=1}^{i} m_{k-1} \cos\theta_i \ddot{z}_n + \sum_{j=1}^{n}\sum_{k=1}^{i} m_{k-1} l_j \cos(\theta_j - \theta_i)\ddot{\theta}_j +$$
$$\sum_{j=1}^{n}\sum_{k=1}^{i} m_{k-1} l_j \sin(\theta_j - \theta_i)\dot{\theta}_j^2 = \sum_{k=1}^{i} m_{k-1} g \cos\theta_i + \sum_{k=1}^{i} Q_{x_{k-1}} \sin\theta_i - \quad \text{for } i = 1, 2, \ldots, n \qquad (4.28)$$
$$\sum_{k=1}^{i} Q_{z_{k-1}} \cos\theta_i$$

The last two are dynamic equilibrium equations which are derived from Eqns. 4.19 to 4.24 by eliminating the λs and are given by

$$\sum_{k=1}^{n+1} m_{k-1} \ddot{x}_{k-1} = \sum_{k=1}^{n+1} Q_{x_{k-1}}$$
$$\sum_{k=1}^{n+1} m_{k-1} \ddot{z}_{k-1} = -\sum_{k=1}^{n+1} m_{k-1} g + \sum_{k=1}^{n+1} Q_{z_{k-1}} \qquad (4.29)$$

The foregoing two equations can be expanded to

$$\sum_{k=1}^{n+1} m_{k-1} \ddot{x}_n + \sum_{j=1}^{n}\sum_{k=1}^{j} m_{k-1} l_j \ddot{\theta}_j \sin\theta_j + \sum_{j=1}^{n}\sum_{k=1}^{j} m_{k-1} l_j \dot{\theta}_j^2 \cos\theta_j = \sum_{k=1}^{n+1} Q_{x_{k-1}}$$
$$\sum_{k=1}^{n+1} m_{k-1} \ddot{z}_n - \sum_{j=1}^{n}\sum_{k=1}^{j} m_{k-1} l_j \ddot{\theta}_j \cos\theta_j + \sum_{j=1}^{n}\sum_{k=1}^{j} m_{k-1} l_j \dot{\theta}_j^2 \sin\theta_j = -\sum_{k=1}^{n+1} m_{k-1} g + \sum_{k=1}^{n+1} Q_{z_{k-1}} \qquad (4.30)$$

The resulting equations 4.28 and 4.30 are coupled and nonlinear for a dynamic analysis of a mooring/SCR line with *n* number of segments and *n*+2 independent coordinates $x_n,\ z_n, \theta_i;\ i = 1,2,\ldots n$. Note that the dependent coordinates $x_i,\ z_i;\ i = 0,1,\ldots n-1$ and their velocities and accelerations can be found from Eqns 4.16 to 4.18 respectively after the independent coordinates are solved from Eqns. 4.28 and 4.30.

The number of equations to be solved from the dynamic motion equations given by Eqns. 4.28 and 4.30 for line dynamic analysis depend on whether or not the anchor point at (x_0, z_0) and/or the attachment point at (x_n, z_n) motions are prescribed. In general, the attachment point will be displaced by the vessel motions, and the anchor

point will be fixed if it has sufficient holding capacity. When the anchor fails to hold the sea bed, the anchor point will be displaced due to the large vessel motion induced on the mooring line.

It follows from the above discussions that as long as the kinematic properties at the attachment point such as $\ddot{x}_n$, $\ddot{z}_n$, $\dot{x}_n$, $\dot{z}_n$, x_n,and z_n are prescribed, two possible cases in the application of the dynamic motion equations given by Eqns. 4.28 and 4.30 for line dynamic analysis need to be considered as follows:

1. Free anchor and attachment points

   Eq. 4.28 can be directly used to solve $\ddot{\theta}_i$ for $i = 1,2,\ldots n$. Then Eq. 4.30 is used to calculate the unknown Q_{x_n} and Q_{z_n}, and Eqns 4.16 to 4.18 are employed to calculate the dependent coordinates x_i, z_i; $i = 0,1,\ldots n-1$ and their velocities and accelerations respectively.

2. Fixed anchor point but free attachment point

   The number of equations in Eq. 4.28 is reduced to $n-1$ as shown below.

$$\sum_{k=2}^{i} m_{k-1} \sin\theta_i \ddot{x}_n - \sum_{k=2}^{i} m_{k-1} \cos\theta_i \ddot{z}_n + \sum_{j=2}^{n}\sum_{k=2}^{i} m_{k-1} l_j \cos(\theta_i - \theta_j)\ddot{\theta}_j + \sum_{j=2}^{n}\sum_{k=2}^{i} m_{k-1} l_j \sin(\theta_i - \theta_j)\dot{\theta}_j^2 = \sum_{k=1}^{i} m_{k-1} g \cos\theta_i + \sum_{k=1}^{i} Q_{x_{k-1}} \sin\theta_i - \sum_{k=1}^{i} Q_{z_{k-1}} \cos\theta_i \quad \text{for } i = 2,3,\ldots,n \tag{4.31}$$

While Eq. 4.30 becomes

$$\begin{aligned} &\sum_{k=2}^{n+1} m_{k-1} \ddot{x}_n + \sum_{j=2}^{n}\sum_{k=2}^{j} m_{k-1} l_j \ddot{\theta}_j \sin\theta_j + \sum_{j=2}^{n}\sum_{k=2}^{j} m_{k-1} l_j \dot{\theta}_j^2 \cos\theta_j = \sum_{k=1}^{n+1} Q_{x_{k-1}} \\ &\sum_{k=2}^{n+1} m_{k-1} \ddot{z}_n - \sum_{j=2}^{n}\sum_{k=2}^{j} m_{k-1} l_j \ddot{\theta}_j \cos\theta_j + \sum_{j=2}^{n}\sum_{k=2}^{j} m_{k-1} l_j \dot{\theta}_j^2 \sin\theta_j = -\sum_{k=1}^{n+1} m_{k-1} g + \sum_{k=1}^{n+1} Q_{z_{k-1}} \end{aligned} \tag{4. 32}$$

Eliminating the unknown reactions Q_{x_0} and Q_{z_0} in Eq. 4.32 yields

$$\sum_{k=2}^{n+1} m_{k-1}\ddot{x}_n \sin\theta_1 + \sum_{j=2}^{n}\sum_{k=2}^{j} m_{k-1} l_j \ddot{\theta}_j \cos(\theta_j - \theta_1) - \sum_{j=2}^{n}\sum_{k=2}^{j} m_{k-1} l_j \dot{\theta}_j^2 \sin(\theta_j - \theta_1) -$$
$$\sum_{k=2}^{n+1} m_{k-1}\ddot{z}_n \cos\theta_1 = \sum_{k=2}^{n+1} Q_{x_{k-1}} \sin\theta_1 + \left(\sum_{k=2}^{n+1} m_{k-1} g - \sum_{k=2}^{n+1} Q_{z_{k-1}}\right)\cos\theta_1 \quad (4.33)$$

Eqns. 4.27 and 4.33 can be used to express the unknown generalised forces Q_{x_n} and Q_{z_n} in terms of θs and their derivatives as follows:

$$\begin{Bmatrix} Q_{x_n} \\ Q_{z_n} \end{Bmatrix} = \frac{1}{sin(\theta_n - \theta_1)} \begin{bmatrix} -\cos\theta_n & \cos\theta_1 \\ -\sin\theta_n & \sin\theta_1 \end{bmatrix} \begin{Bmatrix} B_1 \\ B_2 \end{Bmatrix} \quad (4.34)$$

where

$$B_1 = \left(\sum_{k=2}^{n+1} m_{k-1}\ddot{x}_n - \sum_{k=2}^{n} Q_{x_{k-1}}\right)\sin\theta_1 - \left(\sum_{k=2}^{n+1} m_{k-1}(\ddot{z}_n + g) - \sum_{k=2}^{n} Q_{z_{k-1}}\right)\cos\theta_1$$
$$+ \sum_{j=2}^{n}\sum_{k=2}^{j} m_{k-1} l_j \ddot{\theta}_j \cos(\theta_j - \theta_1) - \sum_{j=2}^{n}\sum_{k=2}^{j} m_{k-1} l_j \dot{\theta}_j^2 \sin(\theta_j - \theta_1)$$

$$B_2 = m_n \ddot{x}_n \sin\theta_n - m_n(\ddot{z}_n + g)\cos\theta_n$$

Eq. 4.31 is then used to solve $\ddot{\theta}_i$ for $i = 2,3\ldots n$ after which Eq. 4.34 is used to calculate the unknown Q_{x_n} and Q_{z_n} as before while Eqns 4.16 to 4.18 are employed to calculate the dependent coordinates x_i, z_i; $i = 0,1,\ldots n-1$ and their velocities and accelerations respectively as well as the values of θ_1 and its first and second time derivatives at the fixed anchor point.

4.5. Equations of Motion for a 3-Segment Line

Having derived the equations of motion for an n-segment mooring line as detailed above, a three segment mooring line will now be used to demonstrate how it works. For a three segments mooring line, there will be a total of three equations to be generated from Eqns. 4.28 when both anchor and attachment points are displaced:

$$\begin{aligned} &m_0 l_1 \cos(\theta_1-\theta_1)\ddot{\theta}_1 + m_0 l_2 \cos(\theta_2-\theta_1)\ddot{\theta}_2 + m_0 l_3 \cos(\theta_3-\theta_1)\ddot{\theta}_3 + m_0 \sin\theta_1 \ddot{x}_3 \\ &- m_0 \cos\theta_1 \ddot{z}_3 - m_0 l_1 \sin(\theta_1-\theta_1)\dot{\theta}_1^2 - m_0 l_2 \sin(\theta_2-\theta_1)\dot{\theta}_2^2 - m_0 l_3 \sin(\theta_3-\theta_1)\dot{\theta}_3^2 = \\ &m_0 g \cos\theta_1 + Q_{x_0} \sin\theta_1 - Q_{z_0} \cos\theta_1 \end{aligned} \quad (4.35)$$

$$\begin{aligned} &m_0 l_1 \cos(\theta_1-\theta_2)\ddot{\theta}_1 + (m_0+m_1) l_2 \cos(\theta_2-\theta_2)\ddot{\theta}_2 + (m_0+m_1) l_3 \cos(\theta_3-\theta_2)\ddot{\theta}_3 + \\ &(m_0+m_1)\sin\theta_2 \ddot{x}_3 - (m_0+m_1)\cos\theta_2 \ddot{z}_3 - m_0 l_1 \sin(\theta_1-\theta_2)\dot{\theta}_1^2 - \\ &(m_0+m_1) l_2 \sin(\theta_2-\theta_2)\dot{\theta}_2^2 - (m_0+m_1) l_3 \sin(\theta_3-\theta_2)\dot{\theta}_3^2 = (m_0+m_1) g \cos\theta_2 + \\ &(Q_{x_0}+Q_{x_1})\sin\theta_2 - (Q_{z_0}+Q_{z_1})\cos\theta_2 \end{aligned} \quad (4.36$$

$$\begin{aligned} &m_0 l_1 \cos(\theta_1-\theta_3)\ddot{\theta}_1 + (m_0+m_1) l_2 \cos(\theta_2-\theta_3)\ddot{\theta}_2 + (m_0+m_1+m_2) l_3 \cos(\theta_3-\theta_3)\ddot{\theta}_3 \\ &+ (m_0+m_1+m_2)\sin\theta_3 \ddot{x}_3 - (m_0+m_1+m_2)\cos\theta_3 \ddot{z}_3 \\ &- m_0 l_1 \sin(\theta_1-\theta_3)\dot{\theta}_1^2 - (m_0+m_1) l_2 \sin(\theta_2-\theta_3)\dot{\theta}_2^2 - (m_0+m_1+m_2) l_3 \sin(\theta_3-\theta_3)\dot{\theta}_3^2 \\ &= (m_0+m_1+m_2) g \cos\theta_3 + (Q_{x_0}+Q_{x_1}+Q_{x_2})\sin\theta_3 - (Q_{z_0}+Q_{z_1}+Q_{z_2})\cos\theta_3 \end{aligned} \quad (4.37$$

Eqns. 4.35 to 4.37 could be further simplified into the standard matrix form as:

$$[A]\{\ddot{q}\} + [B]\{\dot{q}^2\} = \{F_1\} + \{F_2\} + \{F_3\} \quad (4.38$$

where

$$[A] = \begin{bmatrix} m_0 l_1 \cos(\theta_1-\theta_1) & m_0 l_2 \cos(\theta_2-\theta_1) & m_0 l_3 \cos(\theta_3-\theta_1) \\ m_0 l_1 \cos(\theta_1-\theta_2) & (m_0+m_1) l_2 \cos(\theta_2-\theta_2) & (m_0+m_1) l_3 \cos(\theta_3-\theta_2) \\ m_0 l_1 \cos(\theta_1-\theta_3) & (m_0+m_1) l_2 \cos(\theta_2-\theta_3) & (m_0+m_1+m_2) l_3 \cos(\theta_3-\theta_3) \end{bmatrix},$$

$$[B] = \begin{bmatrix} -m_0 l_1 \sin(\theta_1-\theta_1) & -m_0 l_2 \sin(\theta_2-\theta_1) & -m_0 l_3 \sin(\theta_3-\theta_1) \\ -m_0 l_1 \sin(\theta_1-\theta_2) & -(m_0+m_1) l_2 \sin(\theta_2-\theta_2) & -(m_0+m_1) l_3 \sin(\theta_3-\theta_2) \\ -m_0 l_1 \sin(\theta_1-\theta_3) & -(m_0+m_1) l_2 \sin(\theta_2-\theta_3) & -(m_0+m_1+m_2) l_3 \sin(\theta_3-\theta_3) \end{bmatrix}$$

$$\{\ddot{q}\}=\begin{Bmatrix}\ddot{\theta}_1\\ \ddot{\theta}_2\\ \ddot{\theta}_3\end{Bmatrix},\ \{\dot{q}^2\}=\begin{Bmatrix}\dot{\theta}_1^2\\ \dot{\theta}_2^2\\ \dot{\theta}_3^2\end{Bmatrix},\ \{F_1\}=\begin{Bmatrix} m_0\left((\ddot{z}_3+g)\cos\theta_1-\ddot{x}_3\sin\theta_1\right)\\ (m_0+m_1)\left((\ddot{z}_3+g)\cos\theta_2-\ddot{x}_3\sin\theta_2\right)\\ (m_0+m_1+m_2)\left((\ddot{z}_3+g)\cos\theta_3-\ddot{x}_3\sin\theta_3\right)\end{Bmatrix},$$

$$,\ \{F_2\}=\begin{Bmatrix} Q_{X_0}\sin\theta_1\\ \left(Q_{X_0}+Q_{X_1}\right)\sin\theta_2\\ \left(Q_{X_0}+Q_{X_1}+Q_{X_2}\right)\sin\theta_3\end{Bmatrix},\ \{F_3\}=\begin{Bmatrix} -Q_{Z_0}\cos\theta_1\\ -\left(Q_{Z_0}+Q_{Z_1}\right)\cos\theta_2\\ -\left(Q_{Z_0}+Q_{Z_1}+Q_{Z_1}\right)\cos\theta_3\end{Bmatrix}$$

Solving Eq. 4.38 yields $\ddot{\theta}_i$ and integrating them gets $\dot{\theta}_i$ and θ_i for $i=1,2,3$. Using Eq. 4.30, the unknown generalised forces Q_{x_3} and Q_{z_3} at the attachment point can be respectively determined by

$$\begin{aligned}Q_{x_3}&=(m_0+m_1+m_2+m_3)\ddot{x}_3-Q_{x_0}-Q_{x_1}-Q_{x_2}\\&\quad+m_0l_1\sin\theta_1\ddot{\theta}_1+(m_0+m_1)l_2\sin\theta_2\ddot{\theta}_2+(m_0+m_1+m_2)l_3\sin\theta_3\ddot{\theta}_3\\&\quad+m_0l_1\cos\theta_1\dot{\theta}_1^2+(m_0+m_1)l_2\cos\theta_2\dot{\theta}_2^2+(m_0+m_1+m_2)l_3\cos\theta_3\dot{\theta}_3^2\end{aligned}$$

$$\begin{aligned}Q_{z_3}&=(m_0+m_1+m_2+m_3)(\ddot{z}_3+g)-Q_{z_0}-Q_{z_1}-Q_{z_2}\\&\quad-m_0l_1\cos\theta_1\ddot{\theta}_1-(m_0+m_1)l_2\cos\theta_2\ddot{\theta}_2-(m_0+m_1+m_2)l_3\cos\theta_3\ddot{\theta}_3\\&\quad+m_0l_1\sin\theta_1\dot{\theta}_1^2+(m_0+m_1)l_2\sin\theta_2\dot{\theta}_2^2+(m_0+m_1+m_2)l_3\sin\theta_3\dot{\theta}_3^2\end{aligned}$$

With sufficient anchor holding capacity, the anchor point cannot move, so that the number of motion equations can be reduced to *n*–1. Hence, making use of Eq. 4.31, the matrices $[A],\{\ddot{q}\},[B],\{\dot{q}^2\},\{F_1\},\{F_2\},and\ \{F_3\}$ for the 3 segment line with a fixed anchor point and displaced attachment point become:

$$[A]=\begin{bmatrix} m_1l_2\cos(\theta_2-\theta_2) & m_1l_3\cos(\theta_3-\theta_2)\\ m_1l_2\cos(\theta_2-\theta_3) & (m_1+m_2)l_3\cos(\theta_3-\theta_3)\end{bmatrix},\{\ddot{q}\}=\begin{Bmatrix}\ddot{\theta}_2\\ \ddot{\theta}_3\end{Bmatrix}$$

$$[B]=\begin{bmatrix} -m_1l_2\sin(\theta_2-\theta_2) & -m_1l_3\sin(\theta_3-\theta_2)\\ -m_1l_2\sin(\theta_2-\theta_3) & -(m_1+m_2)l_3\sin(\theta_3-\theta_3)\end{bmatrix},\{\dot{q}^2\}=\begin{Bmatrix}\dot{\theta}_2^2\\ \dot{\theta}_3^2\end{Bmatrix},$$

$$\{F_1\}=\begin{Bmatrix}(m_0+m_1)((\ddot{z}_3+g)\cos\theta_2-\ddot{x}_3\sin\theta_2)\\(m_0+m_1+m_2)((\ddot{z}_3+g)\cos\theta_3-\ddot{x}_3\sin\theta_3)\end{Bmatrix}\quad,\quad \{F_2\}=\begin{Bmatrix}(Q_{x_0}+Q_{x_1})\sin\theta_2\\(Q_{x_0}+Q_{x_1}+Q_{x_2})\sin\theta_3\end{Bmatrix},$$

$$\{F_3\}=\begin{Bmatrix}-(Q_{z_0}+Q_{z_1})\cos\theta_2\\-(Q_{z_0}+Q_{z_1}+Q_{z_2})\cos\theta_3\end{Bmatrix}$$

The unknown Q_{x_3} and Q_{z_3} at the displaced attachment point are determined from Eqns. 4.34.

4.6. Matrix Form of Equations of Motion

Although the equations for the dynamic analysis of a mooring of SCR line with any number of segments can be derived completely using Eqns. 4.27 to 4.29, a better way of achieving the same result which is more suitable for numerical analysis is to use Eq. 4.38. By using Eq. 4.38 it is noted that the elements of the mass matrices $[A]$ and $[B]$, and those of the force matrices $\{F_1\}$, $\{F_2\}$ and $\{F_3\}$ can be derived easily as detailed below.

4.6.1. Elements of matrix [A]

When both ends on the line are completely unrestrained, the elements of matrix [A] of order $n\times n$ for an $n-$ segment line can be derived as follows:

$$A_{ij}=\sum_{k=1}^{i}m_{k-1}l_j\cos(\theta_j-\theta_i)\quad for\ i=1,2,\ldots n\ and\ j>i$$
$$A_{ij}=\sum_{k=1}^{j}m_{k-1}l_j\cos(\theta_j-\theta_i)\quad for\ i=1,2,\ldots n\ and\ j\le i \qquad (4.39$$

4.6.2. Elements of matrix [B]

The elements of the matrix [B] of order $n \times n$ can be derived as follows:

$$B_{i,j} = -\sum_{k=1}^{i} m_{k-1} l_j \sin(\theta_j - \theta_i) \quad for \;\; i = 1, 2, \ldots n \;\; and \;\; j > i$$
$$B_{ij} = -\sum_{k=1}^{j} m_{k-1} l_j \sin(\theta_j - \theta_i) \quad for \;\; j = 1, 2, \ldots n \;\; and \;\; j \le i \tag{4.40}$$

4.6.3. Elements of matrix $\{F_1\}$

The elements of the matrix $\{F_1\}$ of order n for an n-segment mooring line can be written as follows:

$$F_{1i} = \sum_{k=1}^{i} m_{k-1} \left[(\ddot{z}_3 + g) \cos\theta_i - \ddot{x}_3 \sin\theta_i \right] \quad for \; i = 1, 2, \ldots n \tag{4.41}$$

4.6.4. Elements of matrix $\{F_2\}$

The elements of the matrix $\{F_2\}$ of order n for an n-segment mooring line can similarly be written as follows:

$$F_{2i} = \sum_{k=1}^{i} Q_{x_{k-1}} \sin\theta_i \quad for \; i = 1, 2, \ldots n \tag{4.42}$$

4.6.5. Elements of matrix $\{F_3\}$

The elements of the matrix $\{F_3\}$ of order n for an n-segment mooring line can be written as:

$$F_{3i} = -\sum_{k=1}^{i} Q_{z_{k-1}} \cos\theta_i \quad for\ i = 1,2,\ldots n \tag{4.43}$$

By simple modification of Eqns. 4.39 through 4.41 the matrices of Eq. 4.38 for a fixed anchor point and displaced attachment point could also be derived. It is noted that the masse m_0 represents the sum of the anchor mass and half of the mass of the first segment of the line and m_n represents half of the mass of the nth segment of the line where these are applicable.

4.7. Calculation of the Generalised Forces

The generalised forces represent the external forces acting at the nodes in the specified degree-of-freedom. For a mooring line, these are the x-components and z-components of the external loads acting at the nodes. The sources of these external loads are wind, waves and current forces on the line and FPSO which can be constant or time dependent. For the mooring lines, wind and wave loads will not be considered due to the fact that they are assumed to be completely submerged and substantially lie below wave zone. Therefore, this study will only be concerned with current forces due to steady flow. The force per unit length of the mooring line cable can be computed from Morison's equation below.

$$f = \frac{1}{2}\rho_w C_D A_p V|V| + \rho_w C_m \left(\frac{\pi}{4}\right) D^2 \left(\frac{\partial u}{\partial t}\right) \tag{4.44}$$

where ρ_w is the density of seawater

C_D, C_m are the drag and added mass coefficients respectively which are functions of the Reynolds number R_e and the Keulega-Carpenter number k_c,.

D is the mooring line diameter

$V = (u - \dot{x})$ is the relative mooring line segment velocity

A_p is the projected area of the line segment

u is the current velocity which in the case studies in this thesis is assumed to be negligible

$\dot{x}$ is the velocity of the member

Eq. 4.44 has two parts; the drag or frictional part and the inertia or added mass part. The added mass part is already included in the inertia force computation. Hence, the virtual mass of a segment to be lumped at its nodes is given by,

$$m = \left(m_{sub} + \rho_w C_m \left(\frac{\pi}{4} \right) D^2 \right) \cdot l \tag{4.45}$$

where m_{sub} is the mass per unit length of the segment

l is the mooring line segment length

Since the flow is steady there is no Froude-Krylov term, hence $C_m = C_a$ (Downie, 2005). The value of $C_m = 2.0$ has been used. Contribution to fluid damping due to unsteady motion has been assumed to be negligible in the case studies and therefore not considered.

The external force due to steady current acting at the nodes therefore is due only to the drag or frictional part of Eq. 4.44. Since the mooring lines are considered to be cylindrical, the projected area of the line segments $A_p = D$, therefore;

$$f_D = \frac{1}{2}\rho_w C_D D \cdot V|V| \tag{4.46}$$

The drag force as given by Eq. 4.46 can be split into two components; the normal and the tangential components of the mooring line as shown in Fig. 4.2 to give Eqn. 4.47.

$$\begin{aligned} F_j^N &= -\frac{1}{2}\rho_w D_j l_j \cdot C_{Dj}^N \cdot V_j^N \left|V_J^N\right| \\ F_j^T &= -\frac{1}{2}\rho_w D_j l_j \cdot C_{Dj}^T \cdot V_j^T \left|V_J^T\right| \end{aligned} \quad \text{for } j = 1,2,3,\ldots,n \tag{4.47}$$

If the normal and tangential velocity components V_j^N and V_j^T are assumed to be the average of those acting at its opposite ends as shown in Fig. 4.3 then the expressions for these can be shown from Eq. 4.17 to be as given in Eqns 4.48 and 4.49.

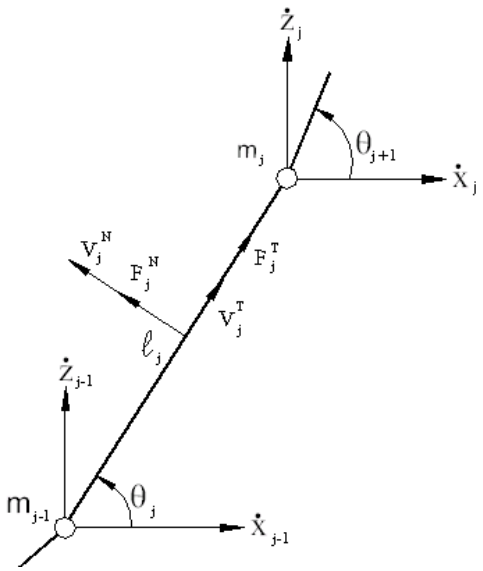

Fig. 4. 3 Average velocities and drag forces normal and tangential to a line segment

$$\begin{aligned} V_j^N &= -\dot{x}_n \sin\theta_j + \dot{z}_n \cos\theta_j - \frac{1}{2} l_j \dot{\theta}_j - \sum_{i=j+1}^{n} l_i \dot{\theta}_i \cos\left(\theta_i - \theta_j\right) \\ V_n^N &= -\dot{x}_n \sin\theta_n + \dot{z}_n \cos\theta_n - \frac{1}{2} l_n \dot{\theta}_n \end{aligned} \quad \text{for } j = 1,2,\ldots,n-1 \tag{4.48}$$

$$V_j^T = \dot{x}_n \cos\theta_j + \dot{z}_j \sin\theta_j + \sum_{i=j+1}^{n} l_i \dot{\theta}_i \sin\left(\theta_i - \theta_j\right) \qquad \text{for } j = 1, 2, \ldots, n-1$$
$$V_n^T = \dot{x}_n \cos\theta_n + \dot{z}_n \sin\theta_n \tag{4.49}$$

The forces on the line segments in x and z directions can be obtained by resolving the normal and tangential forces as follows

$$F_j^x = -F_j^N \sin\theta_j + F_j^T \cos\theta_j$$
$$F_j^z = F_j^N \cos\theta_j + F_j^T \sin\theta_j \qquad \text{for } j = 1, 2, 3, \ldots, n \tag{4.50}$$

For a displaced anchor, the normal and tangential drag forces on the anchor are given by

$$F_A^N = -\frac{1}{2}\rho_w A_x C_D^N \cdot \dot{x}_0 \left|\dot{x}_0\right|$$
$$F_A^T = -\frac{1}{2}\rho_w A_z C_D^T \cdot \dot{z}_0 \left|\dot{z}_0\right| \tag{4.51}$$

where the superscripts N and T refer to the normal and tangential component of the parameters, A_x and A_z are the projected areas of the anchor in x and z directions respectively. Khan and Ansari (1976) suggested the use of the normal and tangential coefficients C_D^N and C_D^T recommended by (Casarella and Parsons 1970). However, suitable values from other sources can be used as well. In this study, the values of $C_D^N = 1.2$ and $C_D^T = 0.015$ for rough surfaces at $\mathrm{Re} = 2\mathrm{x}10^3$ suggested by Berteaux (1970) were used.

If there is sufficient anchor holding capacity then $\dot{x}_0 = \dot{z}_0 = 0$ and the external forces F_A^T and F_A^N on the anchor are zero. On the other hand, the external forces at the attachment point x_n, z_n are F_a^x and F_a^z in x and z directions respectively.

Hence, the generalised forces Q_x and Q_z acting at the nodes are given by;

$$
\begin{aligned}
Q_{x_0} &= F_A^N + \frac{1}{2}F_1^x \\
Q_{z_0} &= F_A^T + \frac{1}{2}F_1^z \\
Q_{x_j} &= \frac{1}{2}\left(F_j^x + F_{j+1}^x\right) \\
Q_{z_j} &= \frac{1}{2}\left(F_j^z + F_{j+1}^z\right) \\
Q_{x_n} &= \frac{1}{2}F_n^x + F_a^x \\
Q_{z_n} &= \frac{1}{2}F_n^z + F_a^z
\end{aligned}
\qquad j = 1,\ 2,\ 3,\ \ldots,\ n-1 \qquad (4.52)
$$

4.8. Dynamic Line Tensions

The dynamic line tensions at the centres of the individual lumped masses of the mooring line can be calculated from the equilibrium of forces at those points as shown in Fig. 4.4

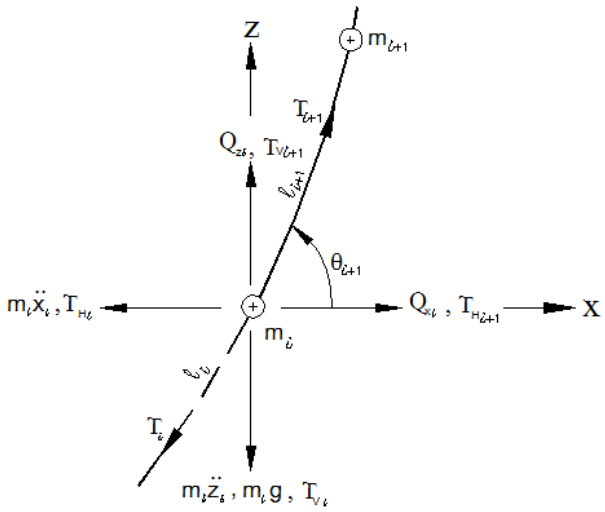

Fig. 4. 4 Forces acting on a mooring line lumped mass

Taking the summation of forces acting in x- and z-directions gives:

$$
\begin{aligned}
T_{H_i} &= Q_{x_i} - m_i\ddot{x}_i + T_{H_{i+1}} \\
T_{V_i} &= Q_{z_i} - m_i g - m_i\ddot{z}_i + T_{V_{i+1}} \quad for\ i = 0,1,\ldots n-1
\end{aligned}
\qquad (4.53)
$$

where Q_x and Q_z are the external forces acting at the points in the horizontal and vertical directions respectively. T_H and T_V are the horizontal and vertical tension components of the line at the points. $\ddot{x}$, $\ddot{z}$ are the accelerations of the lumped mass in x- and z-directions as defined in Eq. 4.17.

4.9. Numerical Solution for Uncoupled System

The equations of dynamic motions of a mooring/SCR line have been developed for n-segments mooring line using Lagrange's equations of motion and the lumped mass technique.

The relevant equations to solve the dynamic motions of a mooring/SCR line can be generated automatically from Eqns. 4.38 to 4.43 once the number of segments is known. The equations so generated are coupled non-linear differential equations, which can then be solved numerically. The number of equations generated depends on the number of independent coordinates or the boundary conditions of the model.

In an uncoupled analysis, the oscillation $\xi_j(x, y, \mathrm{z}, t)$ of the attachment point $P(x_n, \mathrm{y_n}, \mathrm{z_n})$ of mooring or SCR is assumed to start from rest and gradually approach a sinusoidal motion (Nakajima and Fujino, 1982). For horizontal excursion the (x_n, z_n) coordinate of the attachment point is given by:

$$\begin{aligned} x_n^{p+1} &= x_n^0 + \left(1.0 - e^{-\nu t}\right)\left[\xi_1(x, y, z, t)\cos\alpha + \xi_2(x, y, z, t)\sin\alpha\right] \\ z_n^{p+1} &= z_n^0 + \left(1.0 - e^{-\nu t}\right)\xi_3(x, y, z, t) \end{aligned} \tag{4.54}$$

Where α is the angle between the global *x*-axis of the vessel and the local *x*-axis of the line. $1.0 - e^{-\nu t}$ is a ramp function, ν is a chosen parameter, $t = (p+1)\Delta t$; $p =$

0,1,2,3 … is the analysis time step, $\left(x_n^0, z_n^0\right)$ are the coordinates of initial equilibrium position of the attachment point, $\xi_j(x, y, z, t)$ for j = 1,2,3 is the resultant displacement due to first order motion $\xi_j^{(1)}(x, y, z, t)$ and the slowly varying drift motion $\xi_j^{(2)}(t)$ of the vessel as discussed in Section 3.6 of Chapter 3.

As a starting point for the solution process, the initial conditions can be assumed to be the static equilibrium condition in which the values of the variables x_i, z_i and θ_i for $i = 0,1, \ldots, n$ are known and their first time derivatives are zero. Then $\ddot{x}_n$, $\ddot{z}_n$ can be calculated from 4.54 and $\ddot{\theta}_i$ for $i = 1,2, \ldots, n$ can be obtained by solving Eq. 4.38 simultaneously using either the Gauss elimination method or the LU decomposition. Once the values of all the variables are known the equations can then be solved iteratively at each time step using the Runge-Kutta method for solving second-order system of differential equations. A brief discussion of the method is presented in Thomson (1993). This procedure is popular because it is self starting and results in good accuracy. In this thesis, a FORTRAN program was developed using Runge-Kutta subroutines published in Numerical Recipes in Fortran 90 (Press, et al. 1996) customised to suit. At the end of the each time step of the analysis, the values of displacement, velocity and acceleration of the lumped masses at will be obtained.

A method of obtaining the static configuration of the multi-component mooring system was developed in chapter two. This could be used to obtain the required starting mooring lines configurations.

Having obtained the displacements, accelerations and the tensions at the individual lumped masses positions in the line from section 4.6 and 4.7, it is possible to plot time series curves of horizontal tensions and displacements of the mooring lines. A step by step implementation of the methodology developed here is shown in Fig. 4.5.

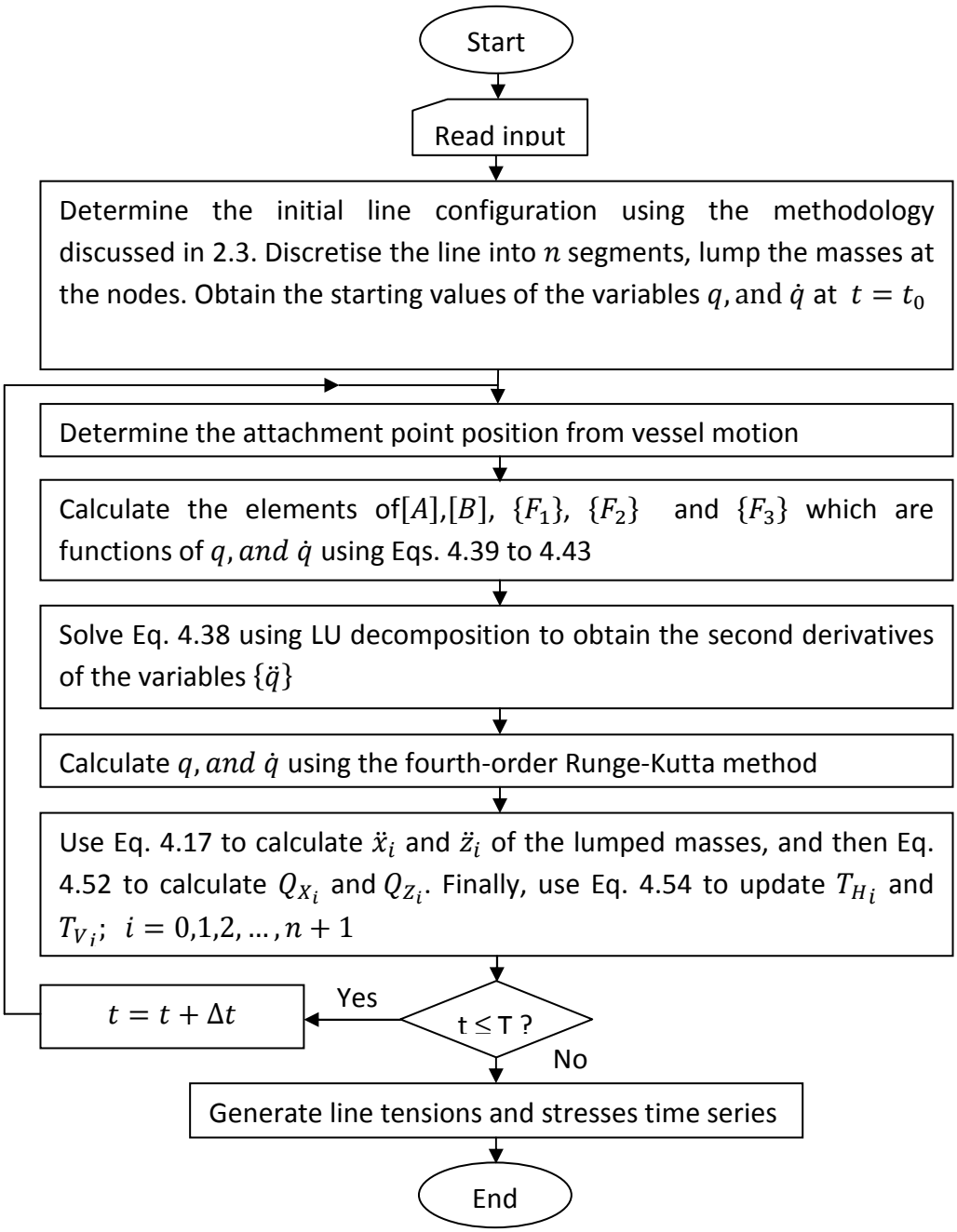

Fig. 4.5 Algorithm for a step by step implementation of line dynamics analysis

4.10. Comparison of Results obtained with those from other Publications

To compare the results obtained using the methodology developed here a numerical calculation of the dynamic behaviour of a multi-component mooring line represented by 16 segments was performed. The line is made of steel chain without studs and the principal particulars of the chain are shown in Table 4.1. The clump weight is made up of lead having a submerged unit weight of 1.823kg. The anchor point is fixed to the seabed and coincides with origin of the line while the attachment is assumed to lie on the free surface.

Table 4. 1 Principal Particulars of Chain (Nakajima and Fujino, 1982)

Weight per Length in water	0.1938 kg/m
Weight per Length in air	0.222 kg/m
Equivalent Diameter	0.599 cm
Volume per Length	28.2 cm^3/m
Modulus of elasticity	2.15 x 10^6 kg/cm^2

The water depth is 3.0m above the seabed which is considered to be flat and the total horizontal excursion of the attachment point at the position of static equilibrium is 17.56m. Fig. 4.6 shows the static configuration of the line obtained using the methodology developed in Chapter 2 for the analysis of multi-component mooring and still catenary riser systems. Also shown in the figure is the static configuration of the line given in Nakajima and Fujino (1982). The two configuration lines agree reasonably.

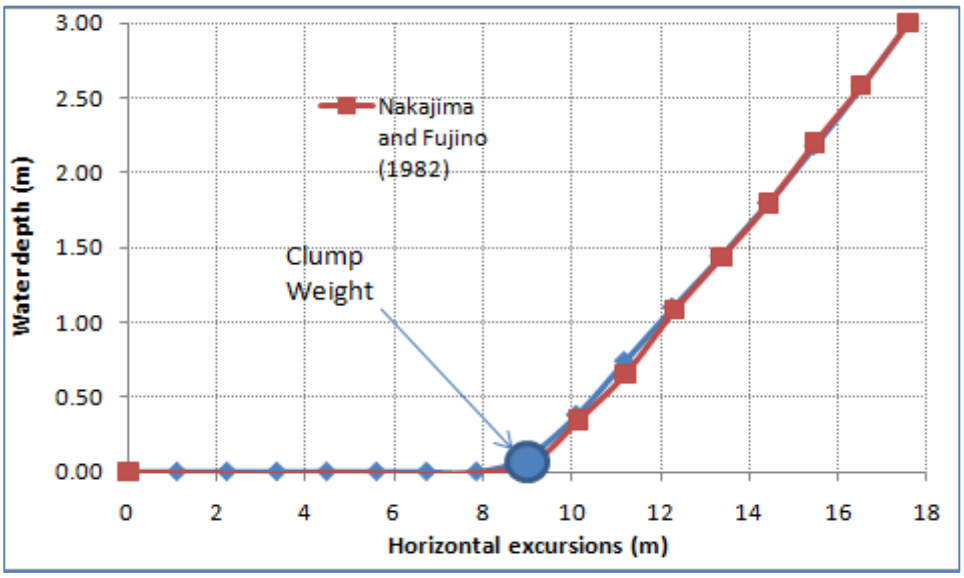

Fig. 4.6 Static configuration of the mooring line with clump weight

A time-domain simulation of the mooring chain with clump weight was then carried out using the methodology developed in this Chapter. The maximum amplitude of horizontal motion at the attachment point is 5cm. The added mass, normal and tangential drag coefficients of the line are 1.98, 2.18 and 0.17 respectively. Figs. 4.7, 4.8 and 4.9 show plots of the horizontal displacement of the attachment point, and the resulting dynamic tensions in the horizontal and vertical directions respectively.

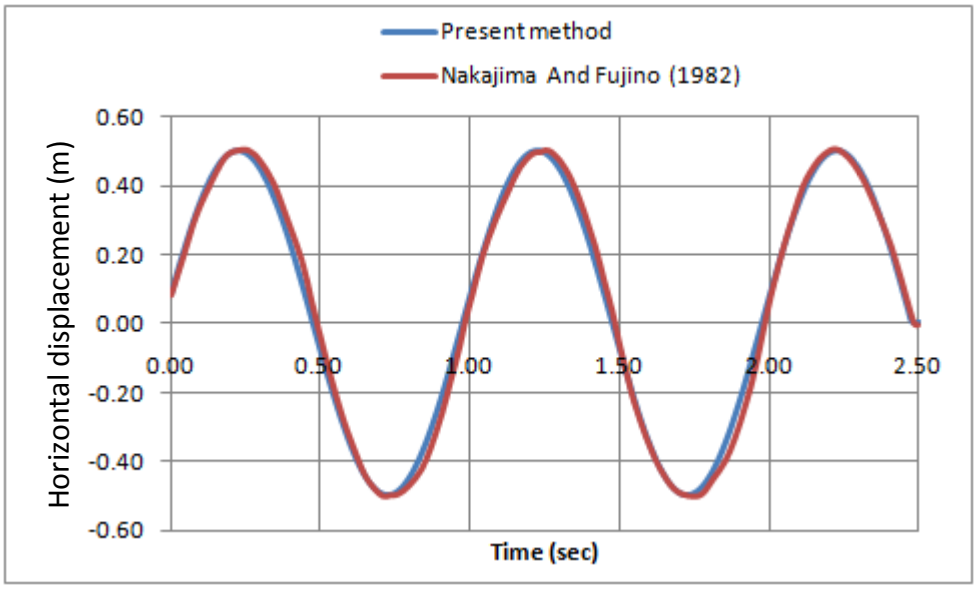

Fig. 4.7 Hoizontal displacement of the attachment point (m)

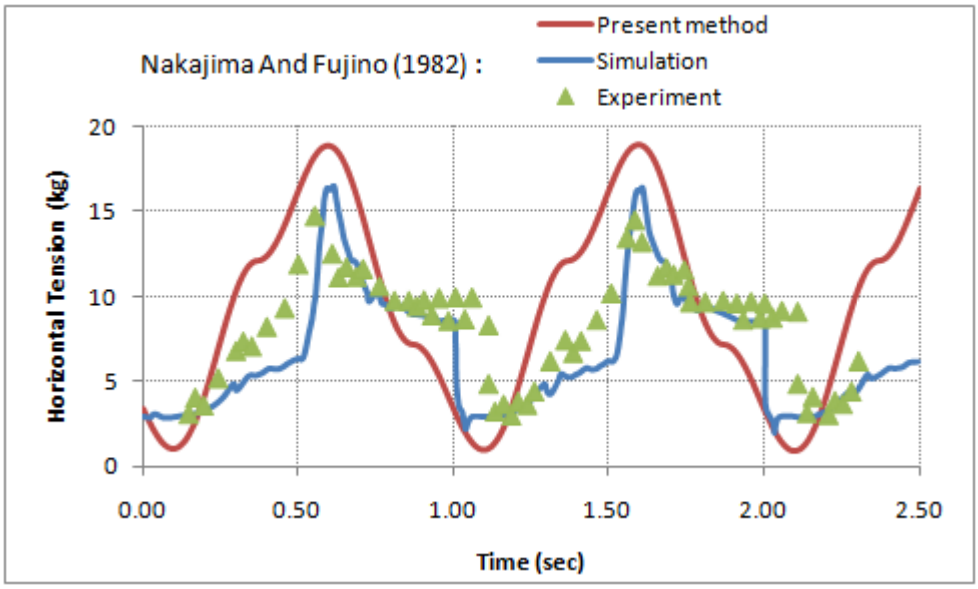

Fig. 4.8 Dynamic horizontal tension at the attachment point (kg)

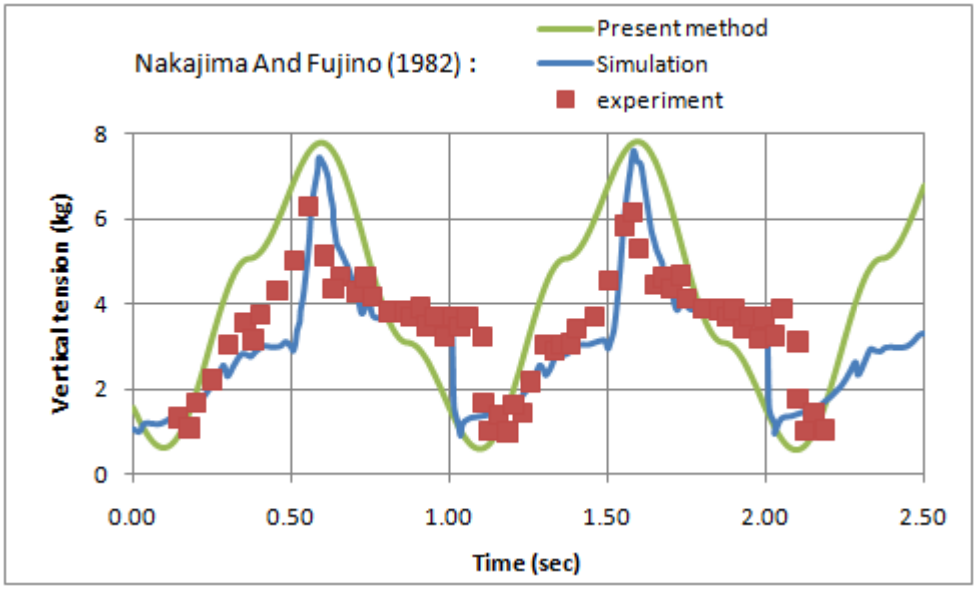

Fig. 4.9 Dynamic vertical tension at the attachment point (kg)

Again, there was some agreement between the results obtained using the current methodologies as compared to those of Nakajima and Fujino (1982) in both experiment and simulation particularly at the peaks and troughs. The differences can be due to the fact that the current methodology does not allow for elastic deformation of the mooring lines. Also, while the current method uses the modified Lagrange's equations, the latter uses finite difference technique in conjunction with Newton-Ralphson method to solve

for the non-linear differential equations. The time steps are also different, in this method a 0.01s step was used while, Nakajima and Fujino used a 0.02s. All the results show the impact load on the chain when the clump weight is lifted up from the bottom of the seabed, while a drastic change of tension occurs whenever the clump weight hit the seabed again. These points are indicated by a sudden change in slope in the graphs of Figs. 4.8 and 4.9.

4.11. Conclusions

A methodology has been developed based on the modified Lagrange's method for the effective modelling and analysis of any mooring and riser system once the number of segments is known. The method can be used for both coupled and uncoupled analysis of mobile or fixed mooring and SCR systems in any water depth.

Comparison with other similar works carried out yielded results which compared quite reasonably with those of experiment as well as simulations based on the same data.

An attempt is being made to use this methodology for the dynamic analysis of mooring lines and steel catenary risers for an FSPO operating in ultra deepwater in Offshore West Africa and the Gulf of Mexico. Because of shortage of time and resources, this has not yet been completed.

CHAPTER

5 CONCLUSIONS AND RECOMMENDATIONS FOR FUTHER STUDY

5.1. Conclusions

With the gradual depletion of oil and gas resources onshore as well as shallow offshore waters, oil exploration is gradually moving deeper into the seas. Floating Production Storage and offloading (FPSO) system are one of the major means of oil exploration at such locations. Because of the harsh environmental conditions prevailing at such locations effective mooring system analysis is critical to the overall success of any project.

There are several methods available which are well tested for the analysis of systems operating in shallow to deepwater using catenary or finite element approach in both frequency and time domain. Most of these methods currently in use are based on research done in extremely harsh environments such as the Gulf of Mexico (GOM) and the North Sea being the pioneer areas of oil and gas exploration. Using these methods

for the analysis of mooring systems and risers in ultra deepwater and benign environments such as West Africa may therefore be unrealistic.

Thus, the main objective of the present study has been to develop a methodology for the analysis of mooring and steel catenary risers in ultra deepwater which can be applied for the analysis of mooring systems in benign environments. To achieve this, methodologies for the quasi-static and dynamic analyses of single and multi-component mooring and steel catenary riser systems in ultra deepwater have been developed as discussed in Chapters 2 and 4 respectively. Though some of the formulations are not entirely new, these have been enhanced and solved in a way that has not been done before. This resulted in algorithms that are both easier as well as faster to implement.

For the implementation of the methodologies developed herein, a FORTRAN program MOOSA has been developed which contains three modules. Module one is for computing mooring and SCR pretensions based on the methodology developed in Chapter 2. Module two is for computing the FPSO first and second-order motions as outlined in Chapter 3. The third module is for the mooring system analysis including line dynamics based on the methodology developed in Chapter 4.

The first methodology developed is for the static analysis of multi-component mooring lines and steel catenary risers for any number of line components and clump weights including an algorithm for implementation in Chapter 2. A four component mooring line has been used to demonstrate how the basic catenary equations for the different components can be combined into one or two nonlinear equations depending on the instantaneous configuration of the line. These equations where solved simultaneously using the highly efficient iterative techniques of Newton-Ralpson method combined with Line Search to give the horizontal tension and the restoring coefficients at the

attachment points of the lines. These are then used as inputs into Motion 3D program to determine the motion response characteristics of the FPSO.

Comparison of results from the static methodology to results from similar published works has been carried out using the multi-component mooring line in a shallow water depth of 15.24m. The total length of the mooring line is 500 ft (152.4 m) length. It is a chain 2-1/8 in (54 mm) in diameter with a 10 kip (44.4 kN) clump weight positioned 150 ft (45.7 m) from an anchor pile. The chain forward of the clump weight was broken up into two equal segments of 53.35m each. The analysis was carried out at incremental horizontal distance of 0.01m. The horizontal tension-displacement characteristics obtained compared reasonably well with those of Ansari (1980) based on the same data.

Application of the methodology was the subject of Chapter 3 in which quasi-static analysis of a multi-component mooring and steel catenary risers in 2500m deep water in West Africa and the Gulf of Mexico environments was carried out successfully both in frequency and time domain. The results of the analyses were compared and conclusions drawn. Quasi-static analysis is usually employed when the motion response of a moored vessel is outside the wave exciting frequency range of the mooring system. This means that the dynamic behaviour of the lines is negligible and the mooring lines will only respond statically to the motions of the vessel. The dynamic motion responses of the vessel coupled with the static catenary riser/mooring system can then be used to find the resulting maximum line. The weakness of this method is that the effects of line dynamics which may be significant if the line inertia is important are ignored.

In order to account for the effects of line dynamics, a second methodology has been developed based on the modified Lagrange's method. Using this technique, the relevant equations to solve the dynamic motions of a mooring/SCR line can be generated automatically once the number of segments is known. The equations so generated are coupled non-linear differential equations, which can then be solved numerically using the fourth order Runge-Kutta method. The number of equations generated depends on the number of independent coordinates and the boundary conditions of the model. In an uncoupled analysis, the oscillation of the attachment point of mooring or SCR is assumed to start from rest and gradually approach a sinusoidal motion. The starting point for the solution process can be assumed to be the static equilibrium.

To compare the results obtained using the methodology to those obtained using other methods, a numerical calculation of the dynamic behaviour of a multi-component mooring line represented by 16 segments was performed. The line is made of steel without studs and a clump weight made up of lead. The anchor point is fixed to the seabed and coincides with the origin of the line while the attachment is assumed to lie on the free surface. The water depth is 3.0m above the seabed which is considered to be flat. The initial configuration of the line obtained using the methodology developed in Chapter 2 for the analysis of multi-component mooring and still catenary riser systems. There was a good agreement between the results obtained using the current methodology as compared to those of Nakajima and Fujino (1982) in both experiment and simulation based on the same data. Efforts to apply this technique to the analysis of an FPSO mooring system in a 2500m water offshore Nigeria and the Gulf of Mexico is

currently underway. However, because of shortage of time and resources, this has not been concluded.

5.2. Recommendations

Some of the major constrains of this research has been that of limited funds and shortage of time. These constraints meant that it has not been possible to exhaustively investigate all areas of interest in this study. Another constraint has been the difficulty of getting precise data on FPSO, mooring and risers system for the application of the various methodologies developed. This necessitated the adoption of simplifying assumptions regarding the vessel, number, pattern, and particulars of the mooring lines and risers which in turn can impact on the accuracy of the case study results.

The application of the proposed methodologies has so far been limited to computations of the first and second-order motion amplitudes of the attachment point and the evaluation of the tension/bending stress-displacement characteristics of the mooring lines and SCRs with and without line dynamics in frequency and time domain. The mooring lines and the SCRs are assumed to be inelastic and perfectly flexible so that they behave like common catenaries. Thus, the bending stress in the lines has been calculated using the equation of curvature. This can significantly underestimate the bending stress particularly in the SCRs. It is therefore recommended that the current methodologies be extended to take into account the elasticity as well as rigidity of the lines.

Furthermore, mooring system and SCRs analysis is incomplete without fatigue life assessment. Fatigue sources include: first and second-order vessel motions due to wave and wind loading, thermal and pressure induced stresses, line motions due to direct wave loading, vortex induced vibration (VIV) of risers due to current loading, residual stresses from fabrication, and installation loads, etc. Fatigue prone areas of the SCRs are mostly the touchdown region, the section around top connection and other joints and connections in between. Fatigue life calculations should take into account all the relevant associated uncertainties including the statistical distribution of the S-N curve, eccentricities induced during welding, modelling errors leading to errors in stress calculations, uncertainties in the cumulative damage calculation using Miner's rule, etc. Therefore, recommendation for further work to extend the application of the current techniques to include fatigue life assessment and/or reliability analysis of the mooring line and steel catenary risers cannot be overemphasised.

AUTHOR'S PUBLICATIONS

Ba, U. m. and H.-S. Chan (2010). Analysis of a multi-component mooring and steel catenaryrisers system in ultra deepwater. 11th International symposium on practical design of ships and other floating structures. Rio de Janeiro, COPPE/UFRJ: 285-294.

Ba, U. m. and H.-S. Chan (2011). Time domain analysis of a multi-component mooring and steel catenary risers system in ultra deepwater. Proceedings of the ASME 30th International Conference on Ocean, Offshore and Arctic Engineering, OMAE2011, 2011, Rotterdam, The Netherlands.

CHAPTER

6 REFERENCES

Ansari, K. A. (1979). "How to design a multicomponent mooring system." Ocean Ind. ; Vol/Issue: 14:3: Pages: 60-68.

Ansari, K. A. and N. U. Khan (1986). "The effect of cable dynamics on the station-keeping response of a moored offshore vessel." J. Energy Resour. Technol. ; Vol/Issue: 108:1: Pages: 52-58.

Bamforth, P., Chisholm, D. et al. (2008). Properties of Concrete for use in Eurocode 2. Camberley, Surrey, The Concrete Centre. CCIP-029: 59.

Barltrop, N. D. P., Centre for Marine and Petroleum Technology. (1998). Floating structures: a guide for design and analysis, Oilfield Publications Limited.

Barltrop, N. D. P. and A. J. Adams (1991). Dynamics of fixed marine structures, Butterworth-Heinemann.

Bernitsas, M. M. (1982). "A Three-Dimensional, Nonlinear, Large Deflection Model for Dynamic Behavior of Risers, Pipelines and Cables." Journal of Ship Research **Vol. 26**(No. 1): pp. 59-64.

Berteaux, H. O. (1970). "Design of deep-sea mooring lines." Marine Technology Society Journal 4(3): 33-46.

Braskoro, S., T. D. T. Dronkers, et al. (2004). "From Shallow to Deep Implications for Offshore Pipeline Design." Journal of the Indonesian Oil and Gas Community: 1-9.

Broughton, P. and P. Ndumbaro (1994). Analysis of Cable and Catenary Structures. London, Thomas Telford Services Ltd, Thomas Telford house, 1 Heron Quay, E14 4JD.

Casarella, M. J. and M. Parsons (1970). "Cable System Under Hydrodynamic Loading." Marine Technology Society Journal 4(4): 27-44.

Chai, Y. T., K. S. Varyani, and Barltrop, N. D. P. (2002). "Three-dimensional Lump-Mass formulation of a catenary riser with bending, torsion and irregular seabed interaction effect." Ocean Engineering 29(12): 1503-1525.

Chakrabarti, S. K. (1990). Nonlinear Methods in Offshore Engineering. Amsterdam, Elsevier Science Publishing Company INC.

Chan, H.-S. (1992). "Dynamic Structural Response of a Mono-hull Vessel to Regular Waves." Interna-tional Shipbuilding progr, 39, 287-315.

Chan, H.-S. and T. P. Ha (2008). Numerical Methods for the Analysis of Mooring Systems in Deep Water. Proceedings of the eighteenth (2008) International Offshore and Polar Engineering Conference. Vancouver, BC, Canada: 185-191.

Chaudhury, G. (2001). A new method for coupled dynamic analysis of platforms. Proceedings of the International Offshore and Polar Engineering Conference. Stavanger, Norway: 444-448.

Childers, M. A. (1973). "Mooring systems for hostile waters." Petroleum engineer 45(5): 58-70.

Childers, M. A. (1974a). "Deep water mooring - part I: Environmental factors control station keeping methods." Petroleum engineer 46(10): 36-58.

Childers, M. A. (1974b). "Deep water mooring - part II: The utradeep water spread mooring system." Petroleum engineer 2(October): 108-118.

Childers, M. A. (1975). "Deep water mooring - part III: Equipment for handling the ultradeep water spread mooring system." Petroleum engineer **5**(May): 114-132.

Clauss, G., E. Lehmann, et al. (1992). Offshore structures. London; New York, Springer-Verlag.

Connaire, A., K. Kavanagh, Ahilan, R. V., Goodwin, Paul (1999). Integrated mooring & riser design: analysis methodology. Proceedings of the Annual Offshore Technology Conference, Houston, TX, USA: 1-14

Craig, R. R. J. (1981). Mathematical Models of Multi-degrees-of-freedom Systems. Structural Dynamics: An Introduction to Computer Methods chichester, John Wiley and Sons.

Cronin, D. J., Godfrey, P. S., Hook, P. M., and Wyatt, T. A. (1976). "Spectral Fatigue Analysis, for Offshore Structures." Numerical Methods in Offshore Engineering, 281 - 316.

Dingwall, J. R. (1997). The Design of a Deep Water Catenary Riser. Naval architecture and Ocean Engineering. Glasgow, University of Glasgow. **PhD**.

DNV. (1996). "Position Mooring (POSMOOR), Rules for classification of mobile offshore units." D. N. Veritas, ed.

Downie, M (2005). “Lecture notes in Advanced offshore structures”

Faltinsen, O. M. (1990). Sea Loads on Ships and Offshore Structures. Cambridge, Cambridge University Press.

Garrett, D. L. (1982). "Dynamic analysi of slender rods." 104(4): 302-306.

Garrett, D. L. (2005). "Coupled analysis of floating production systems." Ocean Engineering 32(7 SPEC ISS): 802-816.

Garrett, D. L., R. B. Gordon, et al. (2002). Mooring-and riser-induced damping in fatigue seastates, Oslo, Norway, American Society of Mechanical Engineers.

Hess, J. L., and Smith, A. M. O. (1962). "Calculation of non-lifting potential flow about arbitrary three-dimensional bodies." Es40622, Douglas Air-craft Company.

Hibbeler, R. C. (1998). Structural Analysis. New Jersey, Prentice -Hall, Inc.

Hogg, B., A. M. Harte, and Grealish, Frank (2004). "A Combined Riser Mooring System for Deepwater Applications." Journal of Offshore Mechanics and Arctic Engineering, 2004 126: 273 - 279.

Huang, K. (2000). "Mooring System Design Considerations for FPSOs." N/A, access online at http://www.scribd.com/doc/23714622/Mooring-System-Design-Considerations-for-FPSOs: 1-6.

Hugh, H. (1995) "Advances in Stell Catenary Riser Design.", DEEPTEC '95, Aberdeen,UK: 1-5

Jun-Bumn, R., A. K. Alexander, Jong-Jun, J.,Hyun-Soo, S., and Woo-Seob, L. (2007). "Coupled Analysis of Deepwater Floating System Including VIV in Time Domain." Proceedings of the 26th International Conference on Offshore Mechanics and Arctic Engineering, OMAE2007,June 10-15, 2007, San Diego, California, USA, Copyright © 20xx by ASME.

Khan, N. U. and K. A. Ansari (1986). "On the dynamics of a multicomponent mooring line." Computers and Structures 22(3): 311-334.

Kim, M. H., B. J. Koo, Mercier, R. M., and Ward, E. G. (2005). "Vessel/mooring/riser coupled dynamic analysis of a turret-moored FPSO compared with OTRC experiment." Ocean Engineering 32(14-15): 1780-1802.

Liang, H. (2009). “Review or research on interactionds between deepwater steel catenary risers and soft clay seabeds.” Journal of Marine Science and Application,. **8**: p. 163-167.

Low, Y. M. and R. S. Langley (2006a). A comparison of time domain and frequency domain approaches for the fully coupled analysis of deepwater floating systems, Hamburg, Germany, American Society of Mechanical Engineers, New York, NY 10016-5990, United States.

Low, Y. M. and R. S. Langley (2006b). "Time and frequency domain coupled analysis of deepwater floating production systems." Applied Ocean Research 28(6): 371-385.

Low, Y. M. and R. S. Langley (2007). A Comparison of Methods for the Coupled Analysis of Floating Structures. 26th International Conference on Offshore Mechanics and Arctic Engineering, OMAE2007. San Diego, California, USA, ASME.

Mansour, G., P. Jukes, et al. (2007). Deepwater Riser Design, Fatigue Life and Standards Study Report Houston, TX, USA**:** 1-98.

Maruo, H. (1960). "The Drift , a Body floating on Waves." Journal of ship Research, 4, 1-10.

Nakajima, T., S. Motora, et al. (1982). On the dynamic analysis of multi-component mooring lines. OTC. Houston, Texas, 14th Annual offshore technology conference: 105-110.

Newman, J. N. (1967). "The Drift Force and Moment on Ships in Waves." Journal of Ship Research, 11, 51-60.

Newman, J. N. (1993)."Wave-drift damping of floating bodies." J. Fluid Mech. 249, 241–259

O'Brien, T. and Francis, A. J. "Cable movements under two dimensional loads." J. Structural Div. ASCE 89-123 (1964).

Ormberg, H. and K. Larsenb (1998). "Coupled analysis of floater motion and mooring dynamics a turret-moored ship." Applied Ocean Research(20): 55-67.

Ormberg, H., H. Lie, and Stansberg, C.T (2005). Coupled analysis of offshore floating systems. Numerical Models in Fluid-Structure Interaction. S. K. Chakrabarti. Plainfield, USA, Offshore Structure Analysis Inc.: 389 - 426.

Pennwell, C. (2007). Offshore West Africa conference preview Offshore. 66.

Pevrot, A. H. and A. M. Goulois (1979). "Analysis of cable structures." Computers and Structures 10(5): 805-813.

Pinkster, J. A. (1979). "mean and Low Frequency Wave Drifting Forces on Floating Structures." Ocean Engineering, 6, 593-615.

Press, W. H., S. A. Teukolsky, et al. (1996). Numerical Recipes in Fortran 90: The Art of Parallel Scientific Computing, University of Cambridge.

Schellin, T. E., Scharrer, M., and Mathies, H. G. (1982). "Analysis of Vessel Moored in Shallow Unpro-tected Waters." Offshore technology Confe-rence.

Skop, R. A. and G. J. O'Hara (1970). "The method of imaginary reactions, a new technique for analyzing structural cable systems." Marine Technology Society Journal 4: 21-30.

Tahar, A. and M. H. Kim (2003). "Hull/mooring/riser coupled dynamic analysis and sensitivity study of a tanker-based FPSO." Applied Ocean Research 25(6): 367-382.

Thomson, W. T. (1993). Theory of Viibration with Applications. Padstow, Cornwall, Prentice Hall.

Triantafyllou, M. S. (1999). Cable Dynamics For Offshore Applications. Developments in Offshore Engineering. J. B. Herbich. Houston, Texas, Gulf Publishing Company**:** 256-294.

Triantafyllou, M. S. and C. T. Howell (1993). "Non-linear Unstable Response Of Hanging Chains." Journal of Sound and Vibration **162**(2): 263-280.

Van den Boom, H. J. J. (1985). Dynamic behaviour of mooring lines. Behaviour of Offshore Structures, Proceedings of the 4th International Conference., Delft, Neth, Elsevier Science Publishers BV (Developments in Marine Technology, v 2).

Wichers, J. E. W. (1982). "On the low frequency surge motions of vessels moored in high seas." Annual Offshore Technology Conference, 4, 711 -734

Wichers, J. E. W. and P. V. Devlin (2001). Effect of coupling of mooring lines and risers on the design values for a turret moored FPSO in deep water of the Gulf of Mexico Proceedings of the International Offshore and Polar Engineering Conference. Stavanger, Norway: 480-487.

CHAPTER

7 BIBLIOGRAPHY

1. Bradford, M.A., *Elastic analysis of straight members at elevated temperatures.* Advances in Structural Engineering, 2006. **9**(5): p. 611-618.
2. Cella, P., *Methodology for exact solution of catenary.* Journal of Structural Engineering, 1999. **125**(12): p. 1451-1453.
3. Chakrabarti, S.K., *Hydrodynamics of Offshore Structures*. 2001, southampton: WIT Press, Ashurst, Southampto, UK. 439.
4. Chan, H.-S., *Dynamic Structural Response of a Mono-hull Vessel to Regular Waves.* International Shipbuilding progr, 1992. **39**: p. 287-315.
5. Craig, R.R.J., *Mathematical Models of Multi-degrees-of-freedom Systems*, in *Structural Dynamics: An Introduction to Computer Methods* 1981, John Wiley and Sons: chichester.
6. Ellermann, K., *Techniques for the Analysis of the Stochastic Dynamics of Offshore Systems*, in *26th International Conference on Offshore Machanics and Arctic Engineering, OMAE2007*. 2007, ASME: San Diego, California, USA.
7. Han, S. and M. Grosenbaugh, *Modeling of seabed interaction of oceanographic moorings in the frequency domain.* Journal of Waterway, Port, Coastal and Ocean Engineering, 2006. **132**(6): p. 450-456.

8. Hatton, S.A. and N. Willis, *Steel catenary risers for deepwater environments*, in *Offshore technology conference*. 1998: Houston, TX, USA. p. 1-9.

9. Hess, J.L. and A.M.O. Smith, *Calculation of non-lifting potential flow about arbitrary three-dimensional bodies*. 1962, Douglas Aircraft Company.

10. Heurtier, J.M., et al. *Coupled dynamic response of moored FPSO with risers*. 2001. Stavanger: International Society of Offshore and Polar Engineers.

11. Huang, C.-C. and J.-Y. Pan, *Mooring line fatigue: A risk analysis for an SPM cage system.* Aquacultural Engineering. **42**(1): p. 8-16.

12. Huang, K., *Mooring System Design Considerations for FPSOs.* N/A, 2000: p. 1-6.

13. Huang, K. and M.-Y. Lee. *Experiences in classification of deepwater mooring systems for floating installations*. 1998.

14. Jayaraman, H.B. and W.C. Knudson, *CURVED ELEMENT FOR THE ANALYSIS OF CABLE STRUCTURES.* Computers and Structures, 1981. **14**(3-4): p. 325-333.

15. Karoumi, R., *Some modeling aspects in the nonlinear finite element analysis of cable supported bridges.* Computers and Structures, 1999. **71**(4): p. 397-412.

16. Lang, D.W., et al. *Advances in frequency and time domain coupled analysis for floating production and offloading systems*. 2005. Halkidiki, Greece: American Society of Mechanical Engineers, New York, NY 10016-5990, United States.

17. Liang, H., *Review or research on interactionds between deepwater steel catenary risers and soft clay seabeds.* Journal of Marine Science and Application, 2009. **8**: p. 163-167.

18. Luo, Y. and S. Baudic. *Predicting FPSO responses using model tests and numerical analysis*. 2003. Honolulu, HI, United States: International Society of Offshore and Polar Engineers.

19. Ma, W., et al., *On the design and installation of an innovative deepwater taut-leg mooring system.* Proceedings of the Annual Offshore Technology Conference, 1999. **3**: p. 145-153.

20. Mansour, G., P. Jukes, and J. Skinner, *Deepwater Riser Design, Fatigue Life and Standards Study Report* 2007: Houston, TX, USA. p. 1-98.

21. Mercier, R., et al. *Hull/mooring/riser coupled dynamic analysis of a turret-moored FPSO compared with OTRC experiment*. 2003. Houston, TX, United States: American Society of Civil Engineers.

22. Pugsley, A., *The Theory of Suspension Bridges*. Second edition ed. 1968, London: Edward Arnold (Publishers) Ltd. 155.

23. Raman-Nair, W. and R.E. Baddour, *Three-dimensional coupled dynamics of a buoy and multiple mooring lines: Formulation and algorithm.* Quarterly Journal of Mechanics and Applied Mathematics, 2002. **55**(2): p. 179-207.

24. Raman-Nair, W. and R.E. Baddour, *Three-dimensional dynamics of a flexible marine riser undergoing large elastic deformations.* Multibody System Dynamics, 2003. **10**(4): p. 393-423.

25. Rawlins, C.B., *Effect of non-linearity in free large oscillations of a shallow catenary.* Journal of Sound and Vibration, 2004. **273**(4-5): p. 857-874.

26. Rosales, M.B. and C.P. Filipich, *Full modeling of the mooring non-linearity in a two-dimensional floating structure.* International Journal of Non-Linear Mechanics, 2006. **41**(1): p. 1-17.

27. Ryu, S., et al. *Coupled analysis of deepwater oil offloading buoy and experimental verification*. 2005. Seoul, South Korea: International Society of Offshore and Polar Engineers, Cupertino, CA 95015-0189, United States.

28. Sen, T.K., *Probability of fatigue failure in steel catenary risers in deepwater.* Journal of Engineering Mechanics, 2006. **132**(9): p. 1001-1006.

29. Stump, D.M. and G.H.M. Van Der Heijden, *Matched asymptotic expansions for bent and twisted rods: Applications for cable and pipeline laying.* Journal of Engineering Mathematics, 2000. **38**(1): p. 13-31.

30. Tahar, A. and M.H. Kim, *Hull/mooring/riser coupled dynamic analysis and sensitivity study of a tanker-based FPSO.* Applied Ocean Research, 2003. **25**(6): p. 367-382.

31. Tirant, P.L. and J. Meunier, eds. *Design Guides for Offshore Structures*. Anchoring of Floating Structures. Vol. 2. 1990, Science and Technical Information Limited: Oxford. 236.

32. Valiente, A., *Symmetric catenary of a uniform elastic cable of neo-Hookean material.* Journal of Engineering Mechanics, 2006. **132**(7): p. 747-753.

33. Vaz, M.A. and M.H. Patel, *Three-dimensional behaviour of elastic marine cables in sheared currents.* Applied Ocean Research, 2000. **22**(1): p. 45-53.

34. Veers, P.S., *Fatigue crack growth due to random loading*, in *Other Information: Portions of this document are illegible in microfiche products. Original copy available until stock is exhausted*. 1987. p. Medium: X; Size: Pages: 163.

35. Wang, C., et al., *A new catenary cable element.* International Journal of Space Structures, 2003. **18**(4): p. 269-275.

36. Wang, C.Y. and L.T. Watson, *ELASTIC CATENARY.* International Journal of Mechanical Sciences, 1982. **24**(6): p. 349-357.

37. Webster, R.L., *NONLINEAR STATIC AND DYNAMIC RESPONSE OF UNDERWATER CABLE STRUCTURES USING THE FINITE ELEMENT METHOD.* 1975(Compendex): p. 753-764.

38. Wichers, J.E.W. and P.V. Devlin. *Effect of coupling of mooring lines and risers on the design values for a turret moored FPSO in deep water of the Gulf of Mexico*. 2001. Stavanger: International Society of Offshore and Polar Engineers.

39. Wirsching, P.H. and A.M. Shehata, *Fatigue under wide band random stresses using the rainflow method.* Journal of Engineering Materials and Technology, Transactions of the ASME, 1977. **99 Ser H**(3): p. 205-211.

40. Wirsching, P.M. and M.C. Light, *Fatigue under wide band random stresses.* ASCE J Struct Div, 1980. **106**(7): p. 1593-1607.

41. Wren, T., J.N. Fawcett, and J.S. Burdess, *Application of extensible catenary theory to determine the displacement of a moored ship.* Mechanism & Machine Theory, 1989. **24**(3): p. 207-212.

42. Wu, S., *Adaptive dynamic relaxation technique for static analysis of catenary mooring.* Marine Structures, 1995. **8**(5): p. 585-599.

APPENDIX

A RESTORING COEFFICIENTS

The following sections present the restoring coefficients k_{11} and k_{33} for various configurations of the mooring and steel catenary riser lines. The coefficients are obtained from differentiation the catenary equations in Chapter two using Matlab R2008a.

A. 1 Restoring Coefficients for Mooring line Configuration two

$$k_{11} = 1./(-1.(/SQRT(1.+2.*(TH/W(2))/H2))/W(2) + 1./W(2) * ACOSH(1.+H2/TH*W(2)) - 1./TH * (H2/SQRT(H2/TH*W(2)))/SQRT(2.+H2/TH*W(2)) + 1./W(3) * (ASINH(L(3)/TH * W(3) + H2*SQRT(1.+2.*(TH/W(2))/H2)/TH*W(2)) - SINH(H2*SQRT(1.+2. * (TH/W(2))/H2)/TH*W(2))) + TH/W(3) * ((-L(3)/TH**2*W(3)+1.(/SQRT(1.+2. * (TH/W(2))/H2))/TH - H2*SQRT(1.+2.*(TH/W(2))/H2)/TH**2 * W(2))/SQRT((L(3)/TH*W(3)+H2*SQRT(1.+2.*(TH/W(2))/H2)/TH*W(2))**2 + 1.) - (1.(/SQRT(1.+2.*(TH/W(2))/H2))/TH - H2*SQRT(1.+2. * (TH/W(2))/H2)/TH**2*W(2))/SQRT(H2**2*(1.+2.*(TH/W(2))/H2)/TH**2 * W(2)**2 + 1.)))$$

$$k_{33} = (W(2) * SQRT(1.+2.* TH/H2/W(2)) - 1./H2/SQRT(1.+2.* TH/H2/W(2)) * TH)/(1.+TH/W(3)$$
$$* (1./SQRT((L(3)/TH * W(3) + H2 * SQRT(1.+2.* TH/H2/W(2))/TH * W(2)) ** 2 + 1.)$$
$$* (L(3)/TH * W(3) + H2 * SQRT(1.+2.* TH/H2/W(2))/TH * W(2)) * (SQRT(1.+2.$$
$$* TH/H2/W(2))/TH * W(2) - 1./H2/SQRT(1.+2.* TH/H2/W(2))) - 1./2./SQRT(H2 ** 2$$
$$* (1.+2.* TH/H2/W(2))/TH ** 2 * W(2) ** 2 + 1.) * (2.* H2 * (1.+2.* TH/H2/W(2))/TH *$$
$$* 2 * W(2) ** 2 - 2./TH * W(2))))$$

A. 2 Restoring Coefficients for Mooring line Configuration three

$$k_{11} = 1./(1./W(2) * (ASINH(L(2)/TH * W(2) + TAN(\theta 2)) - ASINH(TAN(\theta 2))) - 1./TH$$
$$* L(2)/SQRT((L(2)/TH * W(2) + TAN(\theta 2)) ** 2 + 1.) + 1./W(3) * (ASINH(L(3)/TH$$
$$* W(3) + L(2)/TH * W(2) + TAN(\theta 2)) - ASINH(L(2)/TH * W(2) + TAN(\theta 2)))$$
$$+ TH/W(3) * ((-L(3)/TH ** 2 * W(3) - L(2)/TH ** 2 * W(2))/SQRT((L(3)/TH * W(3)$$
$$+ L(2)/TH * W(2) + TAN(\theta 2)) ** 2 + 1.) + L(2)/TH ** 2 * W(2)/SQRT((L(2)/TH * W(2)$$
$$+ TAN(\theta 2)) ** 2 + 1.)))$$

$$k_{33} = TH * (TAN(\theta 2) ** 2 + 1.)/(TH/W(2) * (1./SQRT((L(2)/TH * W(2) + TAN(\theta 2)) ** 2 + 1.) * (L(2)/TH$$
$$* W(2) + TAN(\theta 2)) * (TAN(\theta 2) ** 2 + 1.) - SQRT(TAN(\theta 2) ** 2 + 1.) * TAN(\theta 2))$$
$$+ TH/W(3) * (1./SQRT((L(3)/TH * W(3) + L(2)/TH * W(2) + TAN(\theta 2)) ** 2 + 1.)$$
$$* (L(3)/TH * W(3) + L(2)/TH * W(2) + TAN(\theta 2)) * (TAN(\theta 2) ** 2 + 1.)$$
$$- 1./SQRT((L(2)/TH * W(2) + TAN(\theta 2)) ** 2 + 1.) * (L(2)/TH * W(2) + TAN(\theta 2))$$
$$* (TAN(\theta 2) ** 2 + 1.))T_H)$$

A. 3 Restoring Coefficients for Mooring line Configuration four

$$k_{11} = 1./(-1./SQRT(1.+2.*TH/W(1)/H1)/W(1)+1./W(1)*ACOSH(1.+H1/TH*W(1))-1./TH*H1/SQRT(H1/TH*W(1))/SQRT(2.+H1/TH*W(1))+1./W(2)*(ASINH(L(2)/TH*W(2)+WC/TH+H1*SQRT(1.+2.*TH/W(1)/H1)/TH*W(1))-ASINH(WC/TH+H1*SQRT(1.+2.*TH/W(1)/H1)/TH*W(1)))+TH/W(2)*((-L(2)/TH**2*W(2)-WC/TH**2+1./SQRT(1.+2.*TH/W(1)/H1)/TH-H1*SQRT(1.+2.*TH/W(1)/H1)/TH**2*W(1))/SQRT((L(2)/TH*W(2)+WC/TH+H1*SQRT(1.+2.*TH/W(1)/H1)/TH*W(1))**2+1.)-(-WC/TH**2+1./SQRT(1.+2.*TH/W(1)/H1)/TH-H1*SQRT(1.+2.*TH/W(1)/H1)/TH**2*W(1))/SQRT((WC/TH+H1*SQRT(1.+2.*TH/W(1)/H1)/TH*W(1))**2+1.))+1./W(3)*(ASINH(L(3)/TH*W(3)+L(2)/TH*W(2)+WC/TH+H1*SQRT(1.+2.*TH/W(1)/H1)/TH*W(1))-ASINH(L(2)/TH*W(2)+WC/TH+H1*SQRT(1.+2.*TH/W(1)/H1)/TH*W(1)))+TH/W(3)*((-L(3)/TH**2*W(3)-L(2)/TH**2*W(2)-WC/TH**2+1./SQRT(1.+2.*TH/W(1)/H1)/TH-H1*SQRT(1.+2.*TH/W(1)/H1)/TH**2*W(1))/SQRT((L(3)/TH*W(3)+L(2)/TH*W(2)+WC/TH+H1*SQRT(1.+2.*TH/W(1)/H1)/TH*W(1))**2+1.)-(-L(2)/TH**2*W(2)-WC/TH**2+1./SQRT(1.+2.*TH/W(1)/H1)/TH-H1*SQRT(1.+2.*TH/W(1)/H1)/TH**2*W(1))/SQRT((L(2)/TH*W(2)+WC/TH+H1*SQRT(1.+2.*TH/W(1)/H1)/TH*W(1))**2+1.)))$$

$$k_{33} = (W(1)*SQRT(1.+2.*TH/H1/W(1))-1./H1/SQRT(1.+2.*TH/H1/W(1))*TH)/(1.+TH/W(2)*(1./SQRT((L(2)/TH*W(2)+WC/TH+H1*SQRT(1.+2.*TH/H1/W(1))/TH*W(1))**2+1.)*(L(2)/TH*W(2)+WC/TH+H1*SQRT(1.+2.*TH/H1/W(1))/TH*W(1))*(SQRT(1.+2.*TH/H1/W(1))/TH*W(1)-1./H1/SQRT(1.+2.*TH/H1/W(1)))-1./SQRT((WC/TH+H1*SQRT(1.+2.*TH/H1/W(1))/TH*W(1))**2+1.)*(WC/TH+H1*SQRT(1.+2.*TH/H1/W(1))/TH*W(1))*(SQRT(1.+2.*TH/H1/W(1))/TH*W(1)-1./H1/SQRT(1.+2.*TH/H1/W(1))))+TH/W(3)*(1./SQRT((L(3)/TH*W(3)+L(2)/TH*W(2)+WC/TH+H1*SQRT(1.+2.*TH/H1/W(1))/TH*W(1))**2+1.)*(L(3)/TH*W(3)+L(2)/TH*W(2)+WC/TH+H1*SQRT(1.+2.*TH/H1/W(1))/TH*W(1))*(SQRT(1.+2.*TH/H1/W(1))/TH*W(1)-1./H1/SQRT(1.+2.*TH/H1/W(1)))-1./SQRT((L(2)/TH*W(2)+WC/TH+H1*SQRT(1.+2.*TH/H1/W(1))/TH*W(1))**2+1.)*(L(2)/TH*W(2)+WC/TH+H1*SQRT(1.+2.*TH/H1/W(1))/TH*W(1))*(SQRT(1.+2.*TH/H1/W(1))/TH*W(1)-1./H1/SQRT(1.+2.*TH/H1/W(1)))))$$

A. 4 Restoring Coefficients for Mooring line Configuration five

$$k_{11} = 1./(1./W(1) * (ASINH(L(1)/TH * W(1) + TAN(\theta 1)) - ASINH(TAN(\theta 1))) - 1./TH * L(1)/SQRT((L(1)/TH * W(1) + TAN(\theta 1)) ** 2 + 1.) + 1./W(2) * (ASINH(L(2)/TH * W(2) + WC/TH + L(1)/TH * W(1) + TAN(\theta 1)) - ASINH(WC/TH + L(1)/TH * W(1) + TAN(\theta 1))) + TH/W(2) * ((-L(2)/TH ** 2 * W(2) - WC/TH ** 2 - L(1)/TH ** 2 * W(1))/SQRT((L(2)/TH * W(2) + WC/TH + L(1)/TH * W(1) + TAN(\theta 1)) ** 2 + 1.) - (-WC/TH ** 2 - L(1)/TH ** 2 * W(1))/SQRT((WC/TH + L(1)/TH * W(1) + TAN(\theta 1)) * * 2 + 1.)) + 1./W(3) * (ASINH(L(3)/TH * W(3) + L(2)/TH * W(2) + WC/TH + L(1)/TH * W(1) + TAN(\theta 1)) - ASINH(L(2)/TH * W(2) + WC/TH + L(1)/TH * W(1) + TAN(\theta 1))) + TH/W(3) * ((-L(3)/TH ** 2 * W(3) - L(2)/TH ** 2 * W(2) - WC/TH ** 2 - L(1)/TH * * 2 * W(1))/SQRT((L(3)/TH * W(3) + L(2)/TH * W(2) + WC/TH + L(1)/TH * W(1) + TAN(\theta 1)) ** 2 + 1.) - (-L(2)/TH ** 2 * W(2) - WC/TH ** 2 - L(1)/TH ** 2 * W(1))/SQRT((L(2)/TH * W(2) + WC/TH + L(1)/TH * W(1) + TAN(\theta 1)) ** 2 + 1.)))$$

$$k_{33} = TH * (TAN(\theta 1) ** 2 + 1.)/(TH/W(1) * (1./SQRT((L(1)/TH * W(1) + TAN(\theta 1)) ** 2 + 1.) * (L(1)/TH * W(1) + TAN(\theta 1)) * (TAN(\theta 1) ** 2 + 1.) - SQRT(TAN(\theta 1) ** 2 + 1.) * TAN(\theta 1)) + TH/W(2) * (1./SQRT((L(2)/TH * W(2) + WC/TH + L(1)/TH * W(1) + TAN(\theta 1)) ** 2 + 1.) * (L(2)/TH * W(2) + WC/TH + L(1)/TH * W(1) + TAN(\theta 1)) * (TAN(\theta 1) ** 2 + 1.) - 1./SQRT((WC/TH + L(1)/TH * W(1) + TAN(\theta 1)) ** 2 + 1.) * (WC/TH + L(1)/TH * W(1) + TAN(\theta 1)) * (TAN(\theta 1) ** 2 + 1.)) + TH/W(3) * (1./SQRT((L(3)/TH * W(3) + L(2)/TH * W(2) + WC/TH + L(1)/TH * W(1) + TAN(\theta 1)) ** 2 + 1.) * (L(3)/TH * W(3) + L(2)/TH * W(2) + WC/TH + L(1)/TH * W(1) + TAN(\theta 1)) * (TAN(\theta 1) ** 2 + 1.) - 1./SQRT((L(2)/TH * W(2) + WC/TH + L(1)/TH * W(1) + TAN(\theta 1)) ** 2 + 1.) * (L(2)/TH * W(2) + WC/TH + L(1)/TH * W(1) + TAN(\theta 1)) * (TAN(\theta 1) ** 2 + 1.)))$$

where

TH is the horizontal tension

$W(i)$) for i=1,2,3 is the submerged unit weight of line component i

$H2/H1$ are vertical projection of components two and one respectively

$L(i)$for i=1,2,3 is length of component i

$\theta 1$ is the angle made by the line and the horizontal seabed at the anchor joint

$\theta 2$ is the angle made by the line and the horizontal seabed at the clump weight joint

A. 5 Restoring Coefficients for Steel Catenary Risers Configuration two

$$k_{11} = 1./((ASINH(TAN(\theta 1) + 1./TH * L(1) * W(1)) - ASINH(TAN(\theta 1)))/W(1) - L(1)/(TH * SQRT((TAN(\theta 1) + (L(1) * W(1))/TH) ** 2 + 1.)))$$

$$k_{33} = (TAN(\theta 1) ** 2 + 1.) * W(1)/(1./SQRT((L(1)/TH * W(1) + TAN(\theta 1)) ** 2 + 1.) * (L(1)/TH * W(1) + TAN(\theta 1)) * (TAN(\theta 1) ** 2 + 1.) - SQRT(TAN(\theta 1) ** 2 + 1.) * TAN(\theta 1))$$